NEURON MODELS OF THE GENERIC BIFURCATION TYPE: NETWORK ANALYSIS AND DATA MODELING

PAR

Enno DE LANGE

M. Sc. in electrical engineering, Technische Universiteit Delft, Delft, Pays-Bas
de nationalité néerlandaise

EPFL

ÉCOLE POLYTECHNIQUE
FÉDÉRALE DE LAUSANNE

Lausanne, EPFL
2006

ABSTRACT

Minimal nonlinear dynamic neuron models of the generic bifurcation type may provide the middle way between the detailed models favored by experimentalists and the simplified threshold and rate model of computational neuroscientists. This thesis investigates to which extent generic bifurcation type models grasp the essential dynamical features that may turn out play a role in cooperative neural behavior. The thesis considers two neuron models, of increasing complexity, and one model of synaptic interactions.

The FitzHugh-Nagumo model is a simple two-dimensional model capable only of spiking behavior, and the Hindmarsh-Rose model is a three-dimensional model capable of more complex dynamics such as bursting and chaos. The model for synaptic interactions is a memory-less nonlinear function, known as fast threshold modulation (FTM). By means of a combination of nonlinear system theory and bifurcation analysis the dynamical features of the two models are extracted. The most important feature of the FitzHugh-Nagumo model is its dynamic threshold: the spike threshold does not only depend on the absolute value, but also on the amplitude of changes in the membrane potential. Part of the very complex, intriguing bifurcation structure of the Hindmarsh-Rose model is revealed.

By considering basic networks of FTM-coupled FitzHugh-Nagumo (spiking) or Hindmarsh-Rose (bursting) neurons, two main cooperative phenomena, synchronization and coincidence detections, are addressed. In both cases it is illustrated that pulse coupling in combination with the intrinsic dynamics of the models provides robustness.

In large scale networks of FTM-coupled bursting neurons, the stability of complete synchrony is independent from the network topology and depends only on the number of inputs to each neuron. The analytical results are obtained under very restrictive and biologically implausible hypotheses, but simulations show that the theoretical predictions hold in more realistic cases as well.

Finally, the realism of the models is put to a test by identification of their parameters from in vitro measurements. The identification problem is addressed by resorting to standard techniques combined with heuristics based on the results of the reported mathematical analysis and on a priori knowledge from neuroscience.

The FitzHugh-Nagumo model is only able to model pyramidal neurons and even then performs worse than simple threshold models; it should be used only when the advantages of the more realistic threshold mechanism are prevalent. The Hindmarsh-Rose model can model much of the diversity of neocortical neurons; it can be used as a model in the study of heterogeneous networks and as a realistic model of a pyramidal neuron.

Keywords: neuronal modeling, generic bifurcation models, Hindmarsh-Rose model, FitzHugh-Nagumo model, nonlinear dynamics, synaptic interaction, synchronization, neocortical diversity.

VERSION ABRÉGÉE

Des modèles de neurones non linéaires dynamiques minimaux du type *bifurcation générique* se trouvent entre les modèles détaillés favorisés par les expérimentalistes et les modèles simplifiés, qu'ils soient à seuil ou de fréquence, utilisés par les computationalistes. Cette thèse investigue à quel point les modèles à bifurcations génériques saisissent les traits dynamiques essentiels qui pourraient jouer un rôle dans le comportement coopératif des neurones. La thèse considère deux modèles de complexité différente et un modèle d'interaction synaptique.

Le modèle FitzHugh-Nagumo (FN) est un modèle simple à deux dimensions. Il est capable seulement de simuler un comportement périodique dit « spiking » (émission continue de potentiels d'action). Le modèle Hindmarsh-Rose (HR), quant à lui, est un modèle à trois dimensions, capable de comportements plus complexes tel que le « bursting » et le chaos. Enfin, le modèle d'interaction synaptique, connu sous le nom « fast threshold modulation » (FTM) est une fonction non linéaire sans mémoire.

En combinant la théorie de systèmes non linéaires et l'analyse de bifurcations, les traits dynamiques des deux modèles sont extraits. L'élément le plus important du modèle FN est le seuil dynamique : le seuil d'initiation des potentiels d'action ne dépend pas seulement de la valeur absolue du potentiel de la membrane, mais aussi de l'amplitude de changement de ce dernier. Une partie de la structure de bifurcation complexe et intrigante du modèle HR est dévoilée. En considérant des réseaux de base de neurones FN ou HR couplés avec FTM, on adresse deux phénomènes de coopération principaux. Dans les deux cas il est montré que le couplage à pulses en combinaison avec la dynamique intrinsèque des modèles rend les configurations robuste.

Dans des réseaux à grande échelle de neurones bursting couplés FTM, la synchronisation complète est indépendante de la topologie du réseau et dépend uniquement du nombre d'entrées de chaque neurone. Les résultats analytiques sont obtenus sous des hypothèses très restrictives et biologiquement peu probables. Néanmoins des simulations montrent que les prédictions théoriques s'appliquent également dans des cas plus réalistes.

Finalement, le niveau de réalisme des modèles est testé par l'identification des paramètres sur des mesures in vitro. Le problème d'identification est attaqué en utilisant des techniques standards combinées avec des heuristiques basés sur les résultats de l'analyse mathématique rapportée et sur la connaissance à priori de la neuroscience. Le modèle FN n'est capable de modéliser que les neurones pyramidaux et sa performance est inférieure à celle des modèles à seuil simples ; il devrait donc être utilisé uniquement si le mécanisme de seuil est un élément plus important que la précision des résultats. Le modèle HR peut modéliser une grande partie de la diversité des neurones néocorticaux ; il peut être utilisé comme modèle dans l'étude des réseaux hétérogènes ainsi que comme modèle réaliste d'un neurone pyramidal.

Liste de mots-clés : modèles de neurones, détection de coïncidences, synchronisation, diversité néocorticale, interaction synaptique, fast threshold modulation, generic bifurcation models, FitzHugh-Nagumo, Hindmarsh-Rose.

CONTENTS

ACKNOWLEDGEMENTS

Although sometimes writing a thesis can be a lonely task, it is certainly not one that can be accomplished by the doctoral candidate alone. Everywhere in this work where my views, opinions interpretations and the results of my research are presented, the influence of many people surrounding me directly and indirectly is inevitably present. This is of course the place where I thank all these people from the bottom of my heart. Without you this thesis would not be.

Prof. Martin Hasler who has been, and still is, one of the most important influences in my scientific career, starting with the decision he made in October 2000 to give a course on nonlinear phenomena, even though only two students were present, and who all along allowed me great freedom in the interpretation of my subject and the directions I chose in my research.

Oscar De Feo has always encouraged my work and transmitted his enthusiasm for engineering, but most of all he has been a great friend all along the way.

Igor Belykh has not only taught me a lot, but also given me a peek into the mind of a mathematician, sometimes illustrated by wonderful examples of approaches a mathematician has to everyday problems such as opening windows and reading emails.

The scientific contact with Prof. Wulfram Gerstner and with people from his group and Prof. Henry Markram's group, especially Dr. Maria Toledo and Dr. Renaud Jolivet, were of great help in my entering the complex field of neuroscience. Dr. Hugh Robinson and Dr. Patrick Thiran, as members of my thesis jury, provided me with great feedback on my work.

Essential in the successful accomplishment of my thesis was also the great atmosphere at LANOS throughout the years. I was especially lucky in sharing an office with Norman Baier, with whom I spent numerous hours on more and less scientific discussions as diverse as the correct kernel configuration, the presence or not of corn in Dutch beer, baking bread and equal opportunities (why are men not encouraged to study psychology?), to name a few. Cristian Carmeli also became a wonderful friend, who often faced the same problems I did and with whom it was always refreshing to be able to talk about what bothered me. Joseph was always ready to lend a hand with many different things. I thank Cristianne and Erika for having coped with incredible efficiency with some of the administrative matters. And, less specifically, but not less gratefully: Thomas, Bertrand, Francesco, Kumiko, Jugoslava, Slobodan, Mehdi, thank you for the great time I had at LANOS in the last four years!

I want to thank all friends who have supplied me with advice and moral support throughout the years. Especially my girlfriend Sandra, who had to cope with my craze in the last half year, thank you for not running away screaming. And finally, most importantly, all this would never have been possible without the eternal support of my parents. Thank you.

INTRODUCTION

Neurons, the building blocks of the central nervous system, are highly complex dynamical systems. To understand the way neurons interact, simplified mathematical models are used, which aim to capture the essence of their underlying dynamics. Generic bifurcation models fall into this class of simplified neuron models. They aim to describe the underlying dynamics of the neuron by systems of ordinary differential equations. When these models are used in networks, techniques from the field of nonlinear dynamics can be applied to study phenomena of synchronization and pattern emergence.

The essence of mathematical modeling is to find the right trade off between accuracy and simplicity. One of the most important questions in computational neuroscience is therefore which features of the complex dynamics observed in biological neurons form the essence of the specific tasks fulfilled by that neuron. Generic bifurcation models might provide a promising middle way between detailed models used by experimentalists and the more simple threshold and rate models used by computational neuroscientists.

This thesis investigates to which extent two generic bifurcation models of different complexity grasp the essential dynamical features that play a role in cooperative neural behavior.

1.1   CONTEXT

Most neurons react on injection of a current by a quick, short depolarization of their membrane potential, which is negative in rest. This is known as an action potential, or spike. The activity of neurons observed in vivo consists of these spikes, alternated by long periods of low activity around rest potential. These series of pulses are known as spike trains and they are considered to carry (an important part of) the information transmitted by neurons.

In vitro, not all neurons react with the same firing pattern on sustained current injection; especially neurons in the mammalian neocortex, which is believed to support the complex cognitive functions that distinguish mammals from other animals, show a rich diversity of electrical behavior [Connors & Gutnick, 1990; Llinás, 1988; Markram *et al.*, 2004]. Stoop *et al.* [2000] show that, from a computational point of view, local chaos can indeed lead to chaos on a macroscopical scale in neocortical networks, but experimentally, whether this complex behavior manifests itself on a larger scale is a question that is

very hard to address due to the difficulties of isolating the behavior of single neurons in vivo. There have been reports that this diversity does indeed occur in vivo. Examples include non-random components found in neuronal activity, [Faure & Korn, 1997], that spike-timing is essential to learning [Markram *et al.*, 1997] and information processing [Chechik, 2003] and that the diversity of electrical properties influences the firing rate [Robinson, 2004]. On the other hand, it seems that neocortical cell classes, i.e., types of neurons exhibiting different kinds of behavior in vitro, are not as clearly defined in wakeful animals in vivo: firing patterns can be transformed from one type into another [Steriade, 2004].

So, although the electrical behavior of neurons observed in vitro should not be taken as the final word on the way the neuron behaves in the intact brain, it does show how the neuron *could* behave. One way to address the question how this behavior can propagate theoretically is to apply dynamical models that capture the diversity in input-output behavior in small networks and to study the influence on properties such as synchronization and pattern emergence.

During the last twenty years, the study of the dynamics of coupled nonlinear dynamical systems has attracted a rapidly growing interest. Many studies were done on synchronization in limit cycle systems and, more recently, chaotic systems; for a review, see Pikovsky *et al.* [2001]. Models of the generic bifurcation type have been employed in many studies on synchronization in networks [Ermentrout & Kopell, 1986; Izhikevich, 2001b; Rubin & Terman, 2002b, for instance]. In most of these studies, the coupling between the elements in the network was assumed to be electrical meaning that the influence of the coupling system on the coupled system is via a (constant) conductance. In the brain however the coupling between neurons is often not this simple; neurons are coupled via synapses. Although there exist synapses that behave like electrical coupling, the majority are chemical synapses [Koch, 1999]. In contrast to the proportional coupling electrical synapses provide, chemical synapses show an all or nothing-like behavior. The *fast threshold modulation* (FTM), proposed by Somers & Kopell [1993], is a simple mathematical model that approaches better this kind of coupling.

Since the introduction of the Hodgkin-Huxley model [Hodgkin & Huxley, 1952], many simplified spiking neuron models have been proposed. The most popular include the Integrate-and-fire [Knight, 1972; Lapique, 1907; Tuckwel, 1988], the Morris-Lecar model [Morris & Lecar, 1981], the FitzHugh-Nagumo model [FitzHugh, 1961; Nagumo *et al.*, 1962] and the Hindmarsh-Rose model [Hindmarsh & Rose, 1984]. Of these models, the latter three belong to the class of generic bifurcation models, whereas the integrate-and-fire is of the threshold type, meaning it incorporates a discontinuity and a reset condition.

Hodgkin-Huxley like models are often very accurate in representing neuronal activity in many different situations. The flexibility of the Hodgkin-Huxley framework allows addition of new specific features such as different ion channels and compartments. They are very effective in the study of properties of single neurons but their disadvantage is that the great number of variables and parameters obscures the underlying dynamics.

Integrate-and-fire-type models are commonly employed in the analysis of pattern emergence in networks of neurons [Gerstner *et al.*, 1996b; Golomb & Rinzel, 1993]. Recently proposed models, such as the quadratic model with adaptation proposed by Izhikevich [2003] and the adaptive exponential integrate-and-fire model proposed by Brette & Gerstner [2005], can mimic a wide variety of discharge patterns observed in real neurons [Izhikevich, 2004]. Their drawback is that, because of the discontinuity in their threshold,

many analytical tools cannot be applied for their theoretical analysis in networks.

Generic bifurcation models aim on a phenomenological representation of neuronal activity, thus avoiding the complex nonlinearities and many parameters that follow from the physiological modeling approach that leads to Hodgkin-Huxleytype models. They are outperformed in accuracy by Hodgkin-Huxley models and in simulation speed by Integrate-and-Fire models, although even in some simulation studies of intermediate sized networks they could be the right trade-off between speed and accuracy, but their great strength lies in the possibilities to combine techniques from nonlinear dynamics and bifurcation theory to study analytically the mathematical principles of neuronal activity, both in single neurons and in networks. It is in this context that this thesis aims to contribute.

1.2 GOALS

The aim of this thesis is to investigate the way two neuron models of the generic bifurcation type – the FitzHugh-Nagumo model [FitzHugh, 1961; Nagumo *et al.*, 1962] and the Hindmarsh-Rose model [Hindmarsh & Rose, 1984] – model the essential dynamical features of real neurons in vitro and how these dynamical features might play a role in cooperative neural behavior.

This goal is to be attained through several different sub-goals. First, the models in question are analyzed using techniques from nonlinear dynamics [Ott, 1993; Strogatz, 2001] and bifurcation theory [Kuznetsov, 1995] with the aim to provide basic tools for the rest of the study. Next, the study of basic network configurations using both FitzHugh-Nagumo and Hindmarsh-Rose neurons coupled with the FTM model for chemical synapses permits the assessment of the way the dynamics of the models, and the special form if the FTM coupling, influence two main cooperative phenomena: synchronization and coincidence detection.

These results are then extended to one special case of a large-scale network: where the goal is to study synchronization in a regular network of bursting Hindmarsh-Rose neurons. We use a duly constructed Lyapunov function [Zwillinger, 1998] to study the way the stability conditions for synchronization depend on the network topology.

Finally, an important goal is to put the models to a test using data from in vitro experiments. To this extent an approach has to be developed to identify the parameters of the generic bifurcation models, which have no quantitative relation to the measurements, from the data. Also, criteria have to be defined to assess the quality of the fits to the data. This leads to the last goal, which is to assess the capacities of the models to grasp the different dynamical features present in the experimental data.

1.3 STRUCTURE OF THE THESIS

This thesis consists of two parts. The first part, Chaps. 2, 3 and 4 concern theoretical, analytical and numerical, studies of the FitzHugh-Nagumo and Hindmarsh-Rose models and their application in small networks with FTM coupling.

Chapter 2 has two purposes. First it serves as a general introduction on neuronal modeling and as a review of the neuron models, the models for connectivity, and the measures for evaluation of the performance of neuron models used. Second it presents an analytical and numerical treatment as well as an evaluation of the possibilities and limitations of both generic bifurcation models – the FitzHugh-Nagumo and Hindmarsh-Rose model – used in this work.

Chapter 3 considers pairs and triplets of synaptically coupled generic bifurcation models. The mechanisms behind synchronization and coincidence detection in these configurations are outlined. The FitzHugh-Nagumo coincidence detector is applied in a case study on a realistic model of coincidence detector in the barn owl's auditory pathway.

Chapter 4 contains a study on the synchronization properties of large-scale networks of pulse-coupled Hindmarsh-Rose neurons. This is an adapted version of the article by Belykh *et al.* [2005b].

The second part of the thesis – Chap. 5 – puts the reality of the neuron models to a test by identification of their parameters from in vitro measurements. The analytical and numerical treatment presented in Chap. 2 is combined with techniques from nonlinear system identification to design an approach to around difficulties posed by the complex bifurcation of the models.

NEURONAL MODELING

Brief — The models studied and used in this thesis are introduced in this chapter. Two neuron models of different mathematical complexity – the 2D FitzHugh-Nagumo model and the 3D Hindmarsh-Rose model – and one model for synaptic interaction – the FTM model – are used. Using a combination of nonlinear system theory and bifurcation analysis the dynamical features of the models are extracted. For the Hindmarsh-Rose model part of the very complex bifurcation structure is revealed by simulation and numerical continuation.

Personal Contribution — Most of the material in this chapter is a literature review. The discussion on the dynamic threshold in the FitzHugh-Nagumo model contains new material as well as the numeric bifurcation analysis of the Hindmarsh-Rose model, which was done in collaboration with Dr. Oscar De Feo.

Since Hodgkin & Huxley [1952] first gave a mathematical description of the dynamical behavior of excitable cell membrane, this description has become a paradigm for neuronal behavior in general and many different models based on this framework have been proposed in literature; some giving even more detail, approximating the behavior of (some specific type of) real neurons even better, and some simplifying the Hodgkin-Huxley model to make it analytically more tractable, or computationally less expensive.

Models for single neurons range from units that only model the spike rate (*rate models*), via simple integrators up to models consisting of many differential equations with dozens of parameters that model every ionic current known in a detailed way and account for dendritic structure. Roughly the different single neuron models can be separated in four categories: conductance based models, generic bifurcation models, threshold-type models and the aforementioned rate models. These different models all correspond to different levels of detail in the modeling of the neuronal behavior. Each kind of model has its own field of application and its own limitations.

Conductance-based models are complex systems of ordinary, or partial differential equations, that describe neuronal behavior in great detail, but are slow to solve numerically and near to impossible to treat analytically. They can be used in studies of the details

of behavior of single neurons and, as computers get faster, to simulate small networks of neurons. (One of the largest networks currently considered; the recently started *Bluebrain project*[1], is with 10'000 neurons is still a "small" network compared to the number of neurons in the cerebral cortex of even the simplest intelligent animals – for instance around 21 million in the rat.)

Generic bifurcation models, unlike conductance-based models, do not aim to model neuronal behavior quantitatively, but rather focus on imitating the qualitative essence of neuronal behavior, using ordinary differential equations. In terms of computational complexity, as well as detail of modeling, they can be situated between threshold models and conductance-based models, although on the side of the threshold models this separation is not that simple; some generic bifurcation models (like the FitzHugh-Nagumo model, that is introduced below), are simpler than some of the more complex threshold-type models like the recent models proposed by Izhikevich [2003] and Brette & Gerstner [2005].

Threshold models consider neurons as series of spike trains. A current injected into the neuron, or a synaptic input, changes the membrane potential, which is modeled explicitly, until a certain threshold is reached at which point the model is stopped and reset and the time recorded. This gives a series of pulses known as a *spike train*. The assumption in threshold models is that no information is contained in the form or height of spikes, but only in their timing. Gerstner & Kistler [2002] give an exhaustive review of threshold-based models.

Finally, *rate models* go one step further and even discard this timing information to only model the spike rate, or frequency. They are often used in artificial neural networks [Hopfield, 1984; Knight, 1972].

As the modeling of single neurons evolved into maturity, the modeling of the interaction between neurons has more recently gained in popularity. The interaction through chemical synapses is the most complex and yet the most abundant in the brain [Gibson & Connors, 2002], and their specific characteristics, such as a threshold-type behavior, might determine the dynamics of networks of neurons [Belykh *et al.*, 2005b]. Recent work shows however that electrical synapses, though rare in occurrence, might be essential for synchronization properties in networks of inhibitory cells [Kopell & Ermentrout, 2004]. In this work we focus on coupling through a model for chemical synapses which consists of an instantaneous nonlinear function, ignoring synaptic dynamics. This model is called fast threshold modulation (FTM) [Somers & Kopell, 1993].

Section 2.1 first introduces the Hodgkin-Huxley framework, mainly to show the ideas behind the reductions that lead to simplified models. Also, to mark off the other side of the domain occupied by generic bifurcation models, a brief section is dedicated to threshold models, especially introducing the more complex ones that can compete in the level of modeling, with generic bifurcation models.

Sections 2.3 and 2.4 present an extensive review of the two generic bifurcation models considered in this work, giving some novel results on the Hindmarsh-Rose model and Sect. 2.5 introduces the FTM model used for chemical synapses in Chaps. 3 and 4.

Finally, section 2.6 presents some considerations about the assessment of the quality of the prediction of neuron models along with the measure used in this work.

---

[1]http://bluebrain.epfl.ch

2.1 Conductance based neuron models and reduction to simpler models

The principle behind the Hodgkin-Huxley framework is the observation that voltage across the cell membrane is caused by different ionic current components:

$$C\frac{\mathrm{d}V}{\mathrm{d}t} = -\sum_k I_k(t) + I_{ext}(t) \tag{2.1}$$

where C is the membrane capacitance and I_k are the ionic currents. I_{ext} is an external current applied to the patch.

In (2.1) the time-dependence of the currents is made explicit, but at this point it should be mentioned that from here on we will adopt the convention not to mention time-dependence in dynamical systems explicitly, when this is clear from the context. Also we will henceforth use the dot operator for time derivative. Finally we will use V for the membrane potential in models with qualitative values and real units, like the Hodgkin-Huxley model and more complex extensions, and to designate the membrane potential in experimental data. In the case of qualitative models like threshold models and generic bifurcation models we will use u for the membrane potential instead to stress the fact that this is a unit-less variable with only a qualitative relation to real membrane potential.

An ion current as it is understood in the Hodgkin-Huxley model is the current due to the net flow of ions through the membrane. Ions are transported through the membrane by ion channels. These ion channels have a certain probability of opening and closing, which is modulated by the potential difference over the membrane. This means that in reality the ion currents are stochastic with a mean modulated by the membrane potential. The approximation made in the Hodgkin-Huxley framework is that on a patch of membrane usually the number of individual ion channels is so large that this modulated probability can be seen as a deterministic voltage-dependent current. The error made in this approximation is usually small, but explains for instance (at least partially) the unreliability of spike generation in vitro [White *et al.*, 2001].

In the original Hodgkin-Huxley model, two ion currents were modeled: the sodium and potassium currents. The opening and closing of ion flow, is modeled by gating variables. The two ion currents together are governed by three of these gating variables which each have a time constant associated to them, which gives a four dimensional model when added to 2.1. The variables of the original Hodgkin-Huxley model being the membrane potential, V, and the three gating variables: m and h govern the fast opening and slow closing of the sodium channels and n governs the potassium channels.

The different time-constants of the gating variables give rise to movement on different time-scales. The principal behind reduction of the Hodgkin-Huxley model to simpler models is to lump different ion currents with similar time-scales together to be modeled by one dynamic variable. The variable pair (V, m) represents excitability and rapid change, whereas the pair (h, n) cause accommodation and refractoriness by their relatively slow change [FitzHugh, 1960].

The reduction is based on the observation that, during the action potential, the curves of n and $-h$ versus t have similar shapes and can therefore be represented by their average $w = 0.5(n-h)$. This will only cause a loss in the description of the action potential shape and not of any essential physiological properties. Geometrically speaking the evolution of the system in the (n, h) plane concentrates along the line $h + n = 0.85$. A reduction without too much loss of essential features can therefore be obtained by projecting onto this line of constant w.

Similarly, points in the (V, m) plane are projected onto the line $u = V - 36m$, although this approximation is less accurate, since the evolution does not concentrate around this line as much as for the (n, h) case [FitzHugh, 1961].

We are then left with two distinct time and voltage scales: slow, subthreshold movements and quick spiking behavior. In the past decades two different approaches have become popular to capture these two distinct movements in a system of differential equations. The first is by only modeling the slow movement of the membrane potential explicitly, with a single differential equation, and introducing a static threshold where the computation is stopped and the membrane potential reset to some pre-defined reset value. These are called *threshold-type models*, the integrate-and-fire model is the oldest and simplest. The second approach is by using two-dimensional *slow-fast* dynamical systems, which model the sub-threshold activity, as well as the fast super-threshold movement thus giving a continuous model.

2.2 THRESHOLD TYPE MODELS

Threshold-type neuron models are based on the hypothesis that the essence of neuronal behavior can be captured by modeling the subthreshold behavior. The entire process of fast sodium activation followed by inactivation, leading to the generation of action potentials, i.e., the spiking behavior, is modeled by a hard threshold. When the membrane potential of a threshold model reaches this pre-defined threshold, which, in more advanced versions, can be time and/or state dependent, the state of the system is reset to some pre-defined reset value, which, again, can be state and time dependent.

The simplest threshold model is the *Integrate and Fire* model [Lapique, 1907; Stein, 1967; Tuckwel, 1988]. The integrate-and-fire model is the typical and oldest example of a threshold model, where nowadays usually the leaky integrate-and-fire model is meant, when referring to the integrate-and-fire model, where the addition "leaky" refers to the addition of a leak current that makes the rest potential a stable equilibrium. The model is linear and integrates an input current or synaptic input until it reaches a threshold θ; then the membrane potential is reset to a reset voltage u_r and the process starts over. The integration is described by the following differential equation:

$$\tau_m \frac{\mathrm{d}u}{\mathrm{d}t} = -u + s$$
$$\text{if} \quad u > \theta \wedge \frac{\mathrm{d}u}{\mathrm{d}t} > 0, \quad \text{then} \quad u = u_r < \theta \tag{2.2}$$

where u is the membrane potential, s is the input signal, which is either RI; the current injected into the soma multiplied by the membrane resistance, or a synaptic input, and τ_m is the time-constant, which is equal to the product of the membrane resistance and the membrane capacitance.

In real neurons the onset of a spike is not sudden, like in the leaky integrate-and-fire model, but starts gradually with an increase of sodium conductance, which leads to an avalanche effect through positive feedback. To model this smooth spike onset, a logical extension to the leaky integrate-and-fire model is to generalize it with a nonlinear function of the membrane potential [Abbott & van Vreeswijk, 1993; Gerstner & Kistler, 2002]:

$$\tau \frac{\mathrm{d}u}{\mathrm{d}t} = F(u) + G(u)I \tag{2.3}$$

Different functions have been proposed for the nonlinear function $F(u)$. Ermentrout [1996] and Feng [2001] propose a quadratic function, whereas Fourcaud-Trocme *et al.* [2003] argue that an exponential function would describe the spike generation mechanism better.

Two-dimensional integrate-and-fire models are an extension in a different direction than the nonlinear models. Whereas the nonlinear extensions principally aim to alter the threshold behavior, the extension to two dimensions alters the dynamics. If in addition the model is nonlinear, complex behavior is possible, such as bursting and chaos [Izhikevich, 2004].

The idea is to model the influence of slow-varying ion currents that are responsible for adaptation by means of a voltage-dependent adaptation current w. Ermentrout & Kopell [1986] were amongst the first authors to propose two-dimensional nonlinear integrate-and-fire models. Recently, the quadratic integrate-and-fire model proposed by Izhikevich [2003] has become popular. Based on the observations of Fourcaud-Trocme *et al.* [2003], Brette & Gerstner [2005] propose an adaptive model with exponential threshold given by the following equations:

$$\begin{cases} C\dfrac{\mathrm{d}u}{\mathrm{d}t} = f(u) - w + I \\[2mm] \tau_w\dfrac{\mathrm{d}w}{\mathrm{d}t} = a\,(u - E_L) - w \\[2mm] f(u) = -g_L\,(u - E_L) + g_L\Delta_T \exp\left(\dfrac{u - u_T}{\Delta_T}\right) \end{cases} \tag{2.4}$$

with reset condition:

$$\text{if } u > \theta \begin{cases} u \to E_L \\ w \to w + b \end{cases} \tag{2.5}$$

The threshold is fixed at $\theta = 20\,\mathrm{mV}$, although Brette & Gerstner [2005] argue that this value is not important because it "only shifts the spike times by a fraction of milliseconds", which can easily be seen by calculating the derivative $\dot{u}$ for values around $u = u_T$.

The second variable in (2.4), w, is the slow adaptation current, that models subthreshold resonances and adaptation [Richardson *et al.*, 2003]. Furthermore, the model exhibits spike-triggered adaptation; the slow variable w is not reset to a fixed value after a spike, but to a value that depends on the value of w before the spike. This model is meant to be a quantitative model that can be fit to data and, at the same time, has the advantages of the two-dimensional threshold models as shown by Izhikevich [2004].

The principal problem when simulating neuronal activity is the rapidity of the spikes, which requires a high resolution on the time scale. Integrate-and-fire-like models get around this problem by not simulating spikes at all; this makes them orders of magnitudes faster in simulation than models without a threshold. The obvious down-side is that the spikes are not simulated and thus any possible input-induced diversity in spike form and length is lost.

The great advantage of the linear leaky integrate-and-fire model is that an analytical solution exists. Nonlinear versions loose that advantage, but gain in a more faithful modeling of the behavior around threshold, which seems to be important for the reproduction of spike timing [Brette & Gerstner, 2005; Jolivet, 2005].

Another effect that could be of importance for modeling the dynamical behavior around threshold, and thus spike timing, is adaptation. In (2.4) the second state variable is a

slow evolving current. This current has implications both on dynamic behavior below threshold, but it also causes a variable threshold, which results in the typical spike-frequency adaptation observed in some real neurons.

2.3   THE FITZHUGH-NAGUMO MODEL

The FitzHugh-Nagumo model originates from the Van der Pol oscillator [Van der Pol, 1928b], which is a relaxation oscillator stemming from electronics, but often used in biology – even before FitzHugh's work – for instance as a model for cardiac activity [Van der Pol, 1928a] or intestinal activity [Linkens, 1979]. To avoid confusion it should be mentioned that here the temporal Bonhoeffer-Van der Pol model presented by FitzHugh [1961] is meant, and not the spatio-temporal traveling wave model described by Nagumo *et al.* [1962], which sometimes goes under the same name.

The use of the Bonhoeffer-Van der Pol model for neuronal activity is motivated by FitzHugh [1961] by the derivation presented in Sect. 2.1. The reduction was obtained while looking at the evolution of spike trains. Other kinds of behavior that have since then be observed in vitro and reproduced with the Hodgkin-Huxley equations, such as bursting, have trajectories that diverge more from the two straight lines.

The FitzHugh-Nagumo model consists of two dynamic (state) variables, u and w, and is given by the following differential equations:

$$
\begin{cases}
\dot{u} = u - \dfrac{u^3}{3} - w + I, \\
\dot{w} = \phi \left(u + a - bw \right),
\end{cases}
\tag{2.6}
$$

with a, b and ϕ positive constants. Variable u represents the membrane potential and variable w the slow currents, therefore ϕ, the slow parameter, is chosen (much) smaller than unity. Parameters a and b are fitting, or physiological parameters, and I is the input current, although dimensionless, as is variable u. The parameters are often fixed at the standard values given by FitzHugh [1961], which are

$$
a = 0.7, \quad b = 0.8, \quad \phi = 0.08.
\tag{2.7}
$$

In chapter 3 we will use these default values, whereas in chapter 5 and below all are free within bounds given below.

2.3.1   BIFURCATIONS IN THE AUTONOMOUS SYSTEM

In this section we review the properties of the autonomous FitzHugh-Nagumo model. Methods from nonlinear dynamics and bifurcation theory are applied to extract the influence of the different parameters on the qualitative behavior. The focus is on properties that can be usefully applied in neuronal modeling. For a complete bifurcation analysis, see Rocsoreanu *et al.* [2000] and Kostova *et al.* [2004].

In the static situation, the external input is considered as a parameter (i.e., with $\dot{I} = 0$ in (2.6)). The influence of I is then equivalent to that of $-a/b$, meaning that for any constant I, the model can always be transformed into a topologically equivalent one with $I = 0$ by adapting the value of a accordingly. In accordance with what is usual in bifurcation analysis we will look at parameter a, rather than I, but the results can easily be converted for I.

For the bifurcation analysis it is instructive to study the system graphically in the *phase plane* (u, w) [Strogatz, 1994, pp. 145–160]. The equilibrium points of the system are given by the intersections of the curves $\dot{u} = 0$ and $\dot{w} = 0$; the so-called *nullclines*. The two nullclines can be solved for w, thus obtaining two functions f and g in state space:

$$\dot{u} = 0 \quad \Leftrightarrow \quad w = f(u) = u - \frac{u^3}{3} + I,$$
$$\dot{w} = 0 \quad \Leftrightarrow \quad w = g(u) = (u + a)/b. \tag{2.8}$$

The nullclines are sketched in Fig. 2.1. The existence of the equilibrium points and the
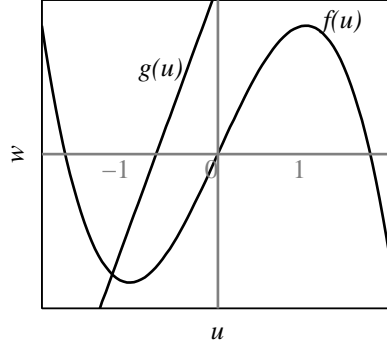

FIGURE 2.1: The nullclines of the FitzHugh-Nagumo model for $I = 0$.

asymptotic behavior of the system is entirely determined by parameters a and b, parameter ϕ having vanished in (2.8). First we will study the influence of a and b graphically from Fig. 2.1 before studying in more detail the bifurcation that is of interest for the FitzHugh-Nagumo system as a neuron model and finally we will explain the influence of ϕ using singular perturbation theory [Rubin & Terman, 2002a]. This study will give bounds on the parameters of the model as well as insight in the qualitative behavior which we need in later chapters.

POSSIBLE BIFURCATIONS FOR VARIATIONS OF a AND b

The equilibrium points $(\bar{u}, \bar{w})$ of (2.6) lie on the curve $f(u) = g(u)$:

$$-\frac{\bar{u}^3}{3} + \bar{u}\left(1 - \frac{1}{b}\right) + I - \frac{a}{b} = 0 \tag{2.9}$$

Parameter b changes the slope of the linear w-nullcline, while a translates the w-nullcline vertically in Fig. 2.1. To analyze the basic bifurcation structure of the model we look at the influence of changes in a for different values of b.

When $b < 1$, the slope of the w-nullcline is larger than the slope of the u-nullcline in $u = 0$. As is clear from the left panel in Fig. 2.2 in this case there can only be one equilibrium point for any value of a. When the equilibrium lies on the part of the cubic u-nullcline with negative slope, either on the right of the maximum, or on the left of the minimum, the equilibrium point is always stable. Therefore these parts of the u-nullcline are called the *stable branches*. When the equilibrium point lies on the part of the nullcline with positive slope – the middle branch – the equilibrium is (generally) unstable. Therefore this middle branch is often called the unstable branch.

Below, in a more detailed analysis of the Andronov-Hopf bifurcation that occurs in the transition between the stable and unstable branch we will see that the unstable part
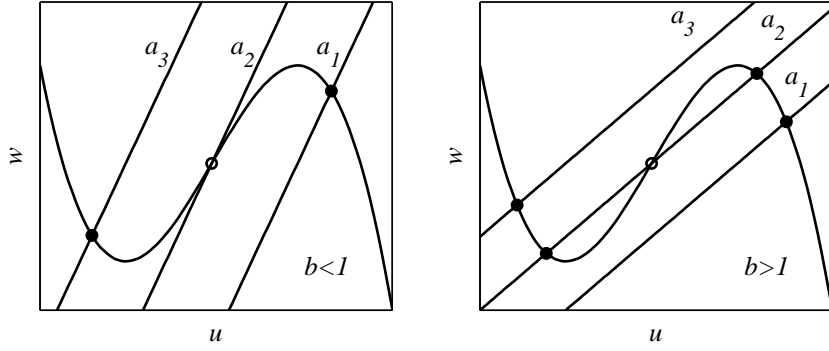
FIGURE 2.2: Bifurcations in the FitzHugh nagumo model. *Left:* Only one equilibrium exists when $b < 1$. *Right:* The number of equilibria depends on a for $b > 1$.

only really comprises the part between the minimum and the maximum in the limit where $b\phi \to 0$. For nonzero values of $b\phi$ the unstable part is slightly smaller, however, we have $b < 1$ and also, we want to have a slow-fast system to ensure spiking-like behavior and thus need $\phi \ll 1$. In practical cases $b\phi$ is therefore nearly always so small that the difference can be neglected. Changes in a translate the linear w-nullcline, thus moving the equilibrium over the cubic. When the equilibrium passes the point where a stable branch changes into an unstable branch, the equilibrium loses stability in a supercritical Andronov-Hopf bifurcation and a limit cycle emerges. This happens twice; once when $a_1 \to a_2$ and once when $a_3 \to a_2$ in the left panel of Fig. 2.2. The supercritical Andronov-Hopf bifurcation is the only bifurcation occurring for $0 < b < 1$ [Kostova *et al.*, 2004; Rocsoreanu *et al.*, 2000].

When $b > 1$ there are two possible situations: the system either has a single equilibrium that has to lie on one of the stable branches of the u-nullcline, or it has three equilibrium points (see the right panel of Fig. 2.2). Of the three points one always lies on the unstable branch and two lie on the respective stable branches. In this case much more complicated bifurcations are possible. Generally, when changing a for fixed ϕ from the situation when three equilibria exist (a_2 in Fig. 2.2, right panel), two of the three equilibria meet when the two nullclines are tangent and the two equilibria then disappear in a saddle-node bifurcation. Also, in some specific cases, degenerate bifurcations exist. When $b = 1$ these points are Bogdanov-Takens bifurcations [Kuznetsov, 1995].

According to some authors, the bistable behavior of the case when $b > 1$ can model bi-stability observed in real neurons [Izhikevich, 2004], but, applying this concretely to data, while preserving the normal functionality of a neuron is probably elaborate. Since this kind of bistable behavior does not occur in our data sets (Chap. 5), we tend to start with $b < 1$.

The presence of a saddle-point is explicitly exploited in some other models, like the Morris-Lecar model [Morris & Lecar, 1981] and the Hindmarsh-Rose model (Sect. 2.4). When $g(u)$ is quadratic, instead of linear, a different mechanism can be used to model the onset of spiking. In the FitzHugh-Nagumo model the onset of spiking is sudden, due to the limit cycle emerging instantly from the Andronov-Hopf bifurcation, and the frequency at the onset is non-zero. This is called type-II behavior. In models with a saddle equilibrium the onset begins at zero frequency, due to the presence of the ghost of the equilibria that disappeared, and the frequency increases smoothly. This is called type-I behavior.
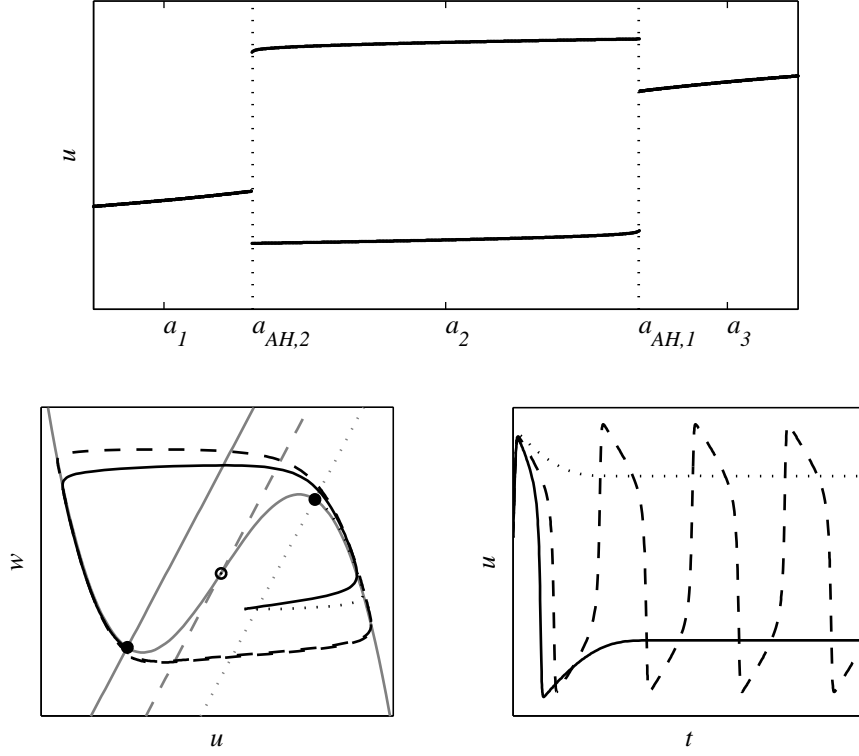
FIGURE 2.3: Asymptotic behavior of the FitzHugh-Nagumo system. *Top:* Bifurcation diagram for $b = 0.8$. The lines represent the extrema of the membrane potential after the transients have died out. The quasi-threshold is so sharp that it is invisible (see text), but in reality the double lines are continuously connected to the single ones on both sides. The points a_1–a_3 refer to Fig. 2.2 *Bottom left:* The phase plane. Solid line: $a = a_3$; dashed line $a = a_2$; dotted line $a = a_1$. *Bottom right:* The membrane potential as a function of time.

A real neuron is nearly always quiescent without external stimulation. Also, when excited, it will emit a spike (or a burst of spikes, but this cannot be modeled by the FitzHugh-Nagumo model, see Sect. 2.4.) This imposes two conditions:

1. The system should have a single equilibrium point.

2. This equilibrium point should be stable.

   Condition 1 means that $0 < b < 1$ (cf. Fig. 2.2). Condition 2 then imposes bounds on a, given b. The bifurcation diagram – the asymptotic behavior of the system as a function of a – for $0 < b < 1$ is shown in the top plot in Fig. 2.3: The part with the double line indicates a stable limit cycle, whereas the parts where there is only a single line indicate a stable equilibrium. The values of $a = a_{AH}$ for which this bifurcation occurs are the Andronov-Hopf bifurcation points. Note that an increase in a moves the linear w-nullcline to the *left* ($a_3 > a_2 > a_1$ in Fig. 2.2), which moves the equilibrium point to the *left*.

ONSET OF SPIKING THROUGH A SUPERCRITICAL ANDRONOV-HOPF BIFURCATION

An Andronov-Hopf bifurcation occurs when the real parts of two complex-conjugate poles of a system linearized in an equilibrium pass the imaginary axes with nonzero speed

[Kuznetsov, 1995]. The Jacobian matrix of the linearization of (2.6) around the equilibrium point $(\bar{u}, \bar{w})$ is given by:

$$\boldsymbol{J}(\bar{u}) = \begin{bmatrix} 1 - \bar{u}^2 & -1 \\ \phi & -b\phi \end{bmatrix} \tag{2.10}$$

Since the trace of the Jacobian matrix is the sum of the eigenvalues and the determinant is the product, the first condition for a Andronov-Hopf bifurcation (eigenvalues on the imaginary axes) can be reformulated as follows [Kuznetsov, 1995, p. 84]:

$$\begin{aligned} \mathrm{Tr}(\boldsymbol{J}) &= 0 \\ \det(\boldsymbol{J}) &> 0 \end{aligned} \tag{2.11}$$

This gives the following conditions for the loci of the Andronov-Hopf bifurcations:

$$\begin{aligned} (1 - \bar{u}^2) - b\phi &= 0 \\ -b\phi(1 - \bar{u}^2) + \phi &> 0 \end{aligned} \tag{2.12}$$

which implies

$$\begin{aligned} \bar{u}^2 &= 1 - b\phi \\ \bar{u}^2 &> 1 - \frac{1}{b} \end{aligned} \tag{2.13}$$

Since $0 < b < 1$ the inequality is always satisfied. The equation gives the locus of the Andronov-Hopf bifurcation as a function of b and ϕ:

$$\bar{u}_{AH,1,2} = \pm\sqrt{1 - b\phi} \tag{2.14}$$

As stated before, in the limit where $b\phi$ vanishes, the loci are at $u = \pm 1$, which corresponds to the maximum and minimum of the cubic nullcline. The condition for existence of the Andronov-Hopf bifurcation that follows from the equation ($b\phi < 1$) is in practice always satisfied.

In the light of the requirement of a stable equilibrium formulated above, the first Andronov-Hopf bifurcation point gives a lower bound on a: the value of the equilibrium $\bar{u}$. This value can be obtained by solving (2.9) for $\bar{u}$. This solution depends on a and b (and I, which we ignore; see above). To have a stable equilibrium, $\bar{u}(a, b) < \bar{u}_{AH}$ should hold. Solving (2.9) for a and equating with (2.14) gives an expression for the lower bound of a. In the limit when $b\phi \ll 1$, this bound simplifies as:

$$a > -\frac{2}{3}b + 1 \tag{2.15}$$

Since in practical situations $b\phi \ll 1$ always holds – even if it does not, if the equilibrium is too close to the bifurcation point, the system will have an unrealistically strong oscillatory behavior – (2.15) can be seen as bound on a valid in all cases.

In principle there is no hard upper bound on a. An important thing to mention is that for $a > 2/3b + 2$ the w value of the equilibrium is higher than that attained during action potentials. It lies so far to the left on the cubic nullcline, that the refractory period disappears: the spike afterpotential shows after-depolarization (ADP; commonly observed in regular spiking excitatory neurons [Connors & Gutnick, 1990]), whereas for $-\frac{2}{3}b + 1 < a < 2/3b + 2$ it shows after-hyperpolarization (AHP; common in fast spiking
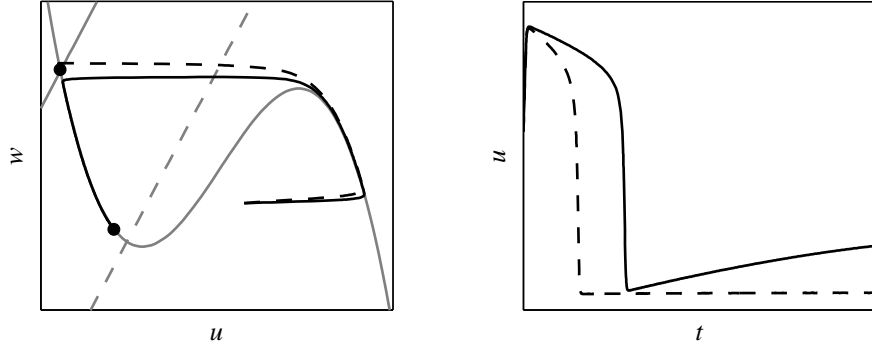
FIGURE 2.4: After-depolarization and after-hyperpolarization. *Left:* Phase plane *Right:* Corresponding time series. Solid line: $a < 2/3b + 2$; dashed line: $a > 2/3b + 2$. Dots indicate equilibrium points.

inhibitory cortical interneurons [Connors & Gutnick, 1990; Toledo-Rodriguez *et al.*, 2002]). See Fig. 2.4 for an illustration.

In summary, the bounds on the parameters we use in this work are:

$$a > -\frac{2}{3}b + 1, \qquad 0 < b < 1, \qquad b < \frac{1}{\phi} \tag{2.16}$$

It should be noted that these are the theoretical bounds. Especially the lower bound on b is never used in practice, since for very small b the model is not excitable any more (see below: in (2.19), the first term $g(u_{AH}) = (u_{AH} + a)/b$ will explode for $b \to 0$).

More exotic bifurcations can also be found in the FitzHugh-Nagumo model, such as homoclinics, saddle-node bifurcations of periodic orbits, although not for the parameter values we use.

INFLUENCE OF STATIC EXTERNAL INPUT

For practical applications it is more useful to know the static value of the current at which the Andronov-Hopf bifurcation occurs. This gives the asymptotic reaction to a step input: if the value of I after the step is larger than the value at the bifurcation point I_{AH}, the model converges to a limit cycle, which means continuous spiking behavior, whereas if the step current is below the bifurcation value, the equilibrium will merely shift. The asymptotic relation between I and u follows from solving $f(u) = g(u)$ in (2.8) for I and is known in neuroscience as the *IV characteristic*. For constant I:

$$\text{for } t \to \infty, \quad I = -u + \frac{u^3}{3} + \frac{u + a}{b} \tag{2.17}$$

For real neurons, this characteristic can only be obtained from voltage clamp experiments – where the membrane potential is fixed and the resulting ionic current measured – since the membrane potential has to be controlled and held steady at values above threshold. For the FitzHugh-Nagumo model, from (2.17), a curve like the one in the left panel of Fig. 2.5 is obtained.

Current clamp experiments, where the current is imposed and the resulting membrane potential measured, are unable to measure steady-state above threshold and therefore can only give the inverse IV characteristic for values below the excitation threshold. Since the
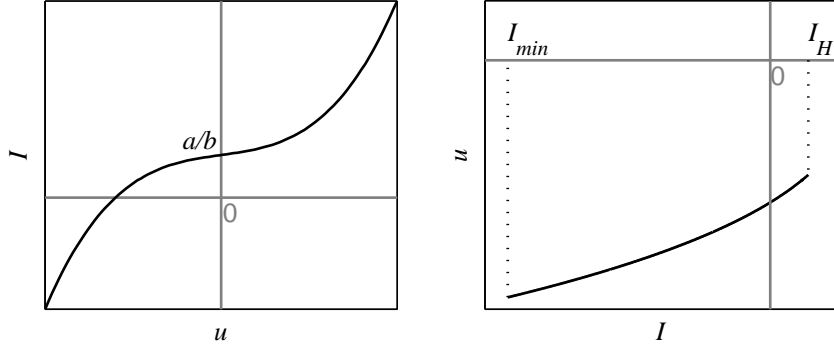
FIGURE 2.5: *Left:* steady state IV characteristic as it can be measured in vitro with current-clamp *Right:* IV curve on the interval below the static threshold as it is observed with patch-clamp techniques.

right hand side of (2.17) is monotonic for $b > 1$, the inverse IV characteristic is uniquely defined for the FitzHugh-Nagumo model. Furthermore, from the right panel in Fig. 2.5, the IV curve is close to linear for sub-threshold values of the current, which corresponds well to the experimental reality (see Chap. 5).

By substituting $u = u_{AH}$ in (2.17), an noting $f' = -u + u^3/3$, we obtain an expression for the value I_{AH} of the current at the Andronov-Hopf bifurcation points:

$$I_{AH}(a, b, \phi) = -f'(u_{AH}) + g(u_{AH}) \tag{2.18}$$

The value of I_{AH} depends on all parameters, though its dependence on ϕ is minimal. Substituting the left bifurcation point ($u_{AH,1}$; negative u) gives the static current above which the neuron will exhibit tonic spiking and substituting the right bifurcation point ($u_{AH,2}$; positive u) will give the current that causes excitation block; the cessation of spiking as the input current increases (dotted line in Fig. 2.3).

   We will call the bifurcation point $I_s \equiv I_{AH,1}$ the *static threshold*, since this is the spiking threshold in the case when the current increases infinitely slowly. The current difference ΔI_s, needed from a certain offset current $I_0 < IAH, 1$ to reach this static threshold is:

$$\Delta I_s = g(u_{AH,1}) - f'(u_{AH,1}) - I_0 \tag{2.19}$$

INFLUENCE OF SLOW-FAST PARAMETER ϕ

The influence of parameter ϕ is complementary to that of the other parameters. It only operates on the dynamical behavior of the system and, unfortunately, it actually fulfills multiple tasks at the same time. To isolate these tasks, we look at the system in the singular perturbed limit. Geometric singular perturbation theory is the analysis of slow-fast systems in the limit of vanishing slow parameter [Rubin & Terman, 2002a]. In the limit $\phi \to 0$, the slow-fast system (2.6) reduces to its *associated system* [Berglund & Gentz, 2003]. Calling the cubic nonlinearity $f(u)$ as before:

$$\begin{cases} \dot{u} &= f(u) - w \\ \dot{w} &= 0, \end{cases} \tag{2.20}$$

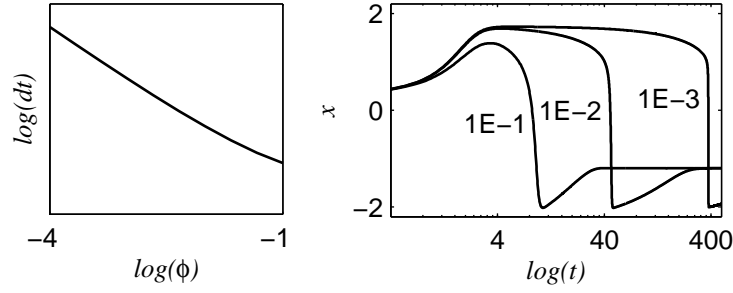in which variable w is now a parameter.

FIGURE 2.6: Influence of slow parameter ϕ on the spike-width dt of the FitzHugh-Nagumo model. *Left:* For ϕ up to $1E-1$ the spike-width is practically inversely proportional to ϕ. *Right:* Examples of three spikes with different orders of ϕ. For $\phi = 0.1$ a deformation of the spike form can be seen.

Another way of looking at the singular perturbed limit is to perform a scaling of time by a factor ϕ. System (2.6) then becomes:

$$\begin{cases} \phi\dot{u} & = f(u) - w \\ \dot{w} & = u + a - bw, \end{cases} \tag{2.21}$$

Setting $\phi = 0$ in (2.21) gives the differential algebraic system

$$\begin{cases} 0 & = f(u) - w, \\ \dot{w} & = u + a - bw. \end{cases} \tag{2.22}$$

The solutions $u^*(w)$ of $f(u) = w$ describe the *slow manifold* of the system and the movement on this manifold is described by the *reduced equation*

$$\dot{w} = u^*(w) - bw. \tag{2.23}$$

The approximation of very small ϕ allows a separation of timescales in the analysis of the oscillatory behavior. The slow movement on the slow manifold can be seen as a perturbation of the equilibrium of (2.20) with slowly drifting parameter w. This drift is governed by (2.23). It is easily verified that this drift of w is only zero in the equilibrium on the left branch of the u-nullcline. On the right branch w always increases. If the state is not on the slow manifold then $\dot{w} \approx 0$ and the movement is horizontal in the (u, w)-plane. Solutions of (2.6) starting in the neighborhood of the slow manifold will approach the manifold in a horizontal way in a time of order $\log(\phi)$ and they behave according to (2.20). These are the "jumps" between the branches of the u-nullcline (cf. Fig. 2.3).

Once in a ϕ-neighborhood of the slow manifold, the approximation done in (2.20) is no longer valid since then $\dot{u} = O(\phi)$ and $\dot{w}$ can no longer be neglected. The solutions then stay in a ϕ neighborhood of the slow manifold and are well approximated by solutions of (2.23), which is of order $O(1/\phi)$, due to the time scaling of (2.21) [Gradstein, 1953; Tihonov, 1952].

This means that the width of a spike in (2.6), which, as long as $\phi \ll 1$ is well approximated by the movement on the slow branch, is of $O(1/\phi)$, which can be seen in Fig. 2.6 where (2.6) is simulated for different values of ϕ. The scaling of the spike-width with ϕ is not a very important issue since the time scale in the FitzHugh-Nagumo model is arbitrary and can be adjusted; it acts as a sort of "hidden parameter".

Unfortunately changes in ϕ not only change the spike width though; also the behavior of the model around threshold – as ϕ becomes smaller the threshold becomes sharper and
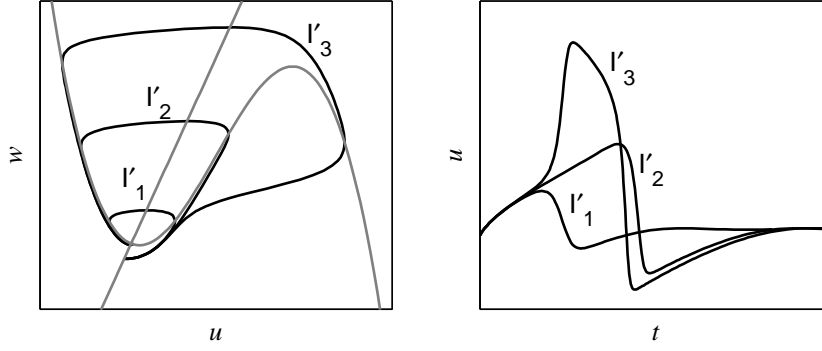
Figure 2.7: The quasi-threshold phenomenon in the FitzHugh-Nagumo model. Simulations are shown of the FitzHugh-Nagumo system under a current step from zero to I'_i, beginning at the onset of the step. $I'_1 = 0.143$, $I'_2 = 1435979$ and $I'_3 = 0.144$ *Left:* The phase plane. *Right:* The membrane potential as a function of time.

in the singular perturbation limit of $\phi \to 0$, the threshold is a hard one – as well as the spike form, especially for not too small ϕ, are influenced. This is the most important use for ϕ, because no other parameter can change the behavior around the threshold, and capturing well the behavior around threshold seems to be very important for spike timing prediction [Brette & Gerstner, 2005]. In the next section it is shown that on top of that ϕ dominates the sub-threshold dynamics.

In summary: decreasing ϕ increases the spike width, which can be countered by changing the time scale, paying with longer simulation times because the system gets stiffer (more slow-fast). Also, decreasing ϕ decreases spike rise and fall times (Fig. 2.6). Finally, the behavior around and below threshold is influenced by ϕ.

2.3.2 Transient phenomena

Until now the analysis limited itself to the static case: what happens to the asymptotic behavior of the system when parameters are changed. This corresponds to the situation with a constant input current I, after the transients have died out. The opposite extreme is when the input current is instantly changed from an equilibrium at $I = I_0$ to a new value $I = I'$, this is called the step response of the system, an experiment often applied to neurons in *in vitro* protocols.

Super-threshold step response

From a geometrical point of view, when a current step is applied the cubic u-nullcline of the system moves vertically – cf. Fig. 2.1 and (2.8) – thus changing instantly the position of the equilibrium. The effect on the membrane potential just after such a change is illustrated in Fig. 2.7: the system has a transient to the new equilibrium. This transient can either follow a small sub-threshold oscillation, or a large trajectory around the right branch of the nullcline, which corresponds to a spike. Strictly speaking the FitzHugh-Nagumo model does not have a real threshold though. If initial conditions are chosen precise enough, intermediate sized spikes can occur (see Fig. 2.7). The precision needed to observe intermediate spikes in simulations is so great that in practical situations the approximation of a real threshold can be made. However this threshold is not a fixed
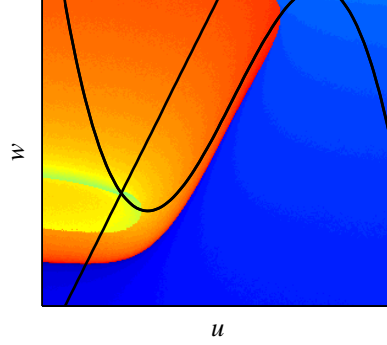
FIGURE 2.8: Simulations of the dynamic threshold in the FitzHugh-Nagumo model. Solutions with initial states in the color range red to yellow follow a subthreshold trajectory to the equilibrium at the crossing of the nullclines, and solutions with initial states in the blue color range follow super threshold trajectories (spikes). The shades of the colors are proportional to the time the solution takes to reach the vicinity of the equilibrium (order ϕ).

one: as opposed to the static spike threshold (2.19), which occurs at fixed values I_s, the *dynamic spike threshold* depends on the parameter values and the state of the system.

The illusion of a threshold is due to the existence of a quasi-threshold [FitzHugh, 1961], which is a canard trajectory; a trajectory that follows the unstable manifold in a slow-fast system [Moehlis, 2006]. Infinitely many of those trajectories exist and nearby trajectories diverge, either to the left, or to the right. The longest canard trajectory follows all the way along the slow manifold, leaving it close to the right branch; the trajectory corresponding to I_2' in Fig. 2.7 is the best approximation of the canard trajectory obtainable with the standard MATLAB ODE solvers [Shampine & Reichelt, 2005], without changing the precision parameters. Figure 2.8 shows a simulation of the quasi-threshold. The slow manifold is located just right of the unstable branch of the nullcline and extends horizontally below the nullcline. For different values of the parameters (we tested combinations of $b \in [0.3, 0.8]$ and $\phi \in [0.08, 0.01]$) this picture does not change visibly.

The dynamic threshold is then the change in current that is necessary to move the cubic nullcline, together with the entire colored picture, up enough for the old equilibrium to fall in the blue area. The state that, just after the change, was still in this equilibrium point will then follow a super-threshold trajectory to the new equilibrium. So, in Fig. 2.7, the current I_3 is above the dynamic current threshold, whereas I_1 is below it.

From figure 2.8 we see that for any value of the stable equilibrium (for the equilibrium $\bar{u}(I_0) < u_{AH}$; left of the minimum of the cubic nullcline), the quasi-threshold is almost a horizontal line. This line is below the level of the w value of the minimum of the cubic nullcline, which, for small enough $b\phi$, is at w_{AH} (cf. (2.13)). Neglecting this difference, one can therefore make a qualitative approximation of the quasi-threshold, allowing for an offset:

$$w = w_0 \approx f(u_{AH,1}) + I_0, \quad \text{for } u < u_{AH,1} \tag{2.24}$$

The corresponding current step should give a value $w_0 > \bar{w} = g(\bar{u}(I_0))$. The value of the equilibrium as a function of I_0 can be obtained analytically as the only real root of the third order polynomial $f(\bar{u}) - g(\bar{u}) + I_0$. The dynamic threshold is then given by:

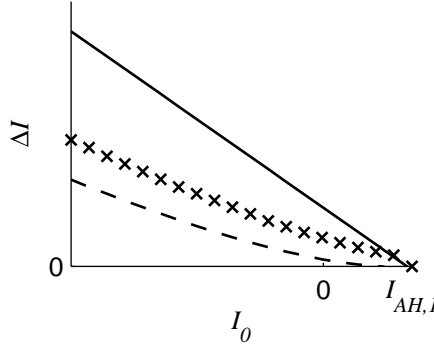$$\Delta I_d = g(\bar{u}(I_0)) - f(u_{AH}) - I_0 \tag{2.25}$$

19

FIGURE 2.9: Static (solid) and dynamic (dashed from (2.25); crosses from simulations) quasi-thresholds in the FitzHugh-Nagumo system as a function of the static offset current I_0

Compare this formula with (2.19) for the static threshold; the difference is the term

$$\Delta I_d - \Delta I_s = g\left(\bar{u}(I_0)\right) - g(u_{AH}) = g\left(\bar{u}(I_0) - u_{AH}\right) \qquad (2.26)$$

The condition for quiescence implies $\bar{u} < u_{AH}$ so we find that $\Delta I_d < \Delta I_s$: the dynamic spike threshold is smaller than the static one, which means that the FitzHugh-Nagumo model can exhibit a *phasic spike* [Izhikevich, 2004]; a neuron fires a spike at the onset of an input and then returns asymptotically to (a different) rest state.

Figure 2.9 shows both static and dynamic current thresholds as a function of the offset current $I_0 < I_{AH}$. Simulation results of the dynamic threshold are indicated by crosses. As expected (2.25) underestimates the threshold, because in (2.24) the estimation of the quasi-threshold is optimistic with respect to the reality observed from Fig. 2.8, where the real quasi-threshold lies below u_{AH}. The important thing is that the slope coincides very well, thus capturing the effect of a growing difference between static and dynamic threshold for more hyperpolarization. If necessary the addition of an additive correction factor, obtained with standard stimuli for threshold estimation, can make (2.25) practically coincide with the real values.

This difference between static and dynamic threshold is a feature that bifurcation models have inherently, whereas threshold-models need to incorporate special terms to account for the variability of the spike-threshold encountered in real neurons. Especially in experiments where in vivo-like situations are being recreated (see Sect. 5.1.3), and highly dynamical currents are injected into the cell (in contrast to standard in vitro protocols, where the input stimuli are most often quite calm), this seems to be an important effect to capture, to be able to predict spike timing [Jolivet *et al.*, 2006a,b].

SUBTHRESHOLD STEP RESPONSE

The behavior of real neurons for *small* excitations is only weakly non-linear, if at all (cf. Sect. 5.3.1). Only near the spike threshold the nonlinear effects become apparent. For currents below the dynamic spike threshold the FitzHugh-Nagumo model is weakly nonlinear, which means that for excitations from the equilibrium that remain below the dynamic threshold, the behavior will be topologically equivalent to the behavior of its linearization around the equilibrium.

The slow-fast properties of the system that are needed for modeling spikes, limit the flexibility of the subthreshold behavior severely. This can be seen from (2.10) as follows:
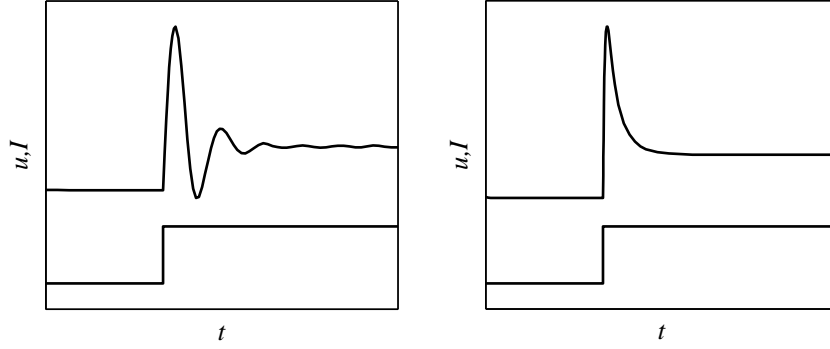
FIGURE 2.10: The two different local subthreshold behaviors of the FitzHugh-Nagumo model. *Left:* For moderate ϕ (here $\phi = 0.1$), the membrane potential (top trace) oscillates around the new equilibrium after a step current (bottom trace) is applied. *Right:* For small ϕ, (here $\phi = 0.01$), the new equilibrium locally behaves as a degenerate node.

the second row of the Jacobian matrix has ϕ as a multiplicative factor. For proper spike modeling as a general rule, ϕ should be at least one order of magnitude smaller than the rest of the model parameters.

For any parameter value in the bounds (2.16), and constant $I = I'$, $\alpha = 1 - \bar{u}^2$ in (2.10) is a positive constant. The eigenvalues of the Jacobian in the equilibrium (2.10) can then be written as:

$$\lambda_{1,2} = \frac{1}{2} \left(\alpha - b\phi \pm \sqrt{(\alpha + b\phi)^2 - 4\phi} \right) \tag{2.27}$$

Now, the equilibrium at $I = I'$, which determines the step response, can have two different forms, separated in parameter space by the curve

$$(\alpha + b\phi)^2 - 4\phi = 0 \tag{2.28}$$

If $(\alpha + b\phi)^2 < 4\phi$, the system has two complex conjugate eigenvalues with real parts $\alpha - b\phi$. The equilibrium is a focus – trajectories in state-space approaching the equilibrium circle it – and the step response is oscillatory. This represents what is known in neuroscience as *subthreshold oscillations*. If on the other hand α is larger, or the system is strongly slow-fast, the linearized system has two real eigenvalues that lie $\sqrt{\alpha^2 - 4\phi}$ apart; in the singular perturbed limit $\phi \to 0$ this means one very small negative eigenvalue and one eigenvalue at 2α. The system then behaves as a degenerate node around the equilibrium. (The latter situation also illustrates the time scaling with ϕ the FitzHugh-Nagumo system exhibits: the dominant time constant, corresponding to the smallest eigenvalue, is proportional to ϕ.)

This analysis reveals the main drawback of the FitzHugh-Nagumo model: Either it models the limited class of neurons with subthreshold oscillations (it behaves like the resonate-and-fire model [Izhikevich, 2001a]), or else it exhibits an unnatural overshoot in the step response, which is rarely observed in vitro in cortical neurons (cf. Chap. 5). This is entirely owing to the slow-fast structure of the model, which is needed to model spiking behavior. So the modeling of fast oscillations takes away the degrees of freedom that are needed to model subthreshold behavior. This theoretical argument is confirmed in Chap. 5 by simulations.

The dynamic threshold phenomenon allows the explanation of one last transient phenomenon modeled by the FitzHugh-Nagumo model: post-inhibitory rebound spikes.
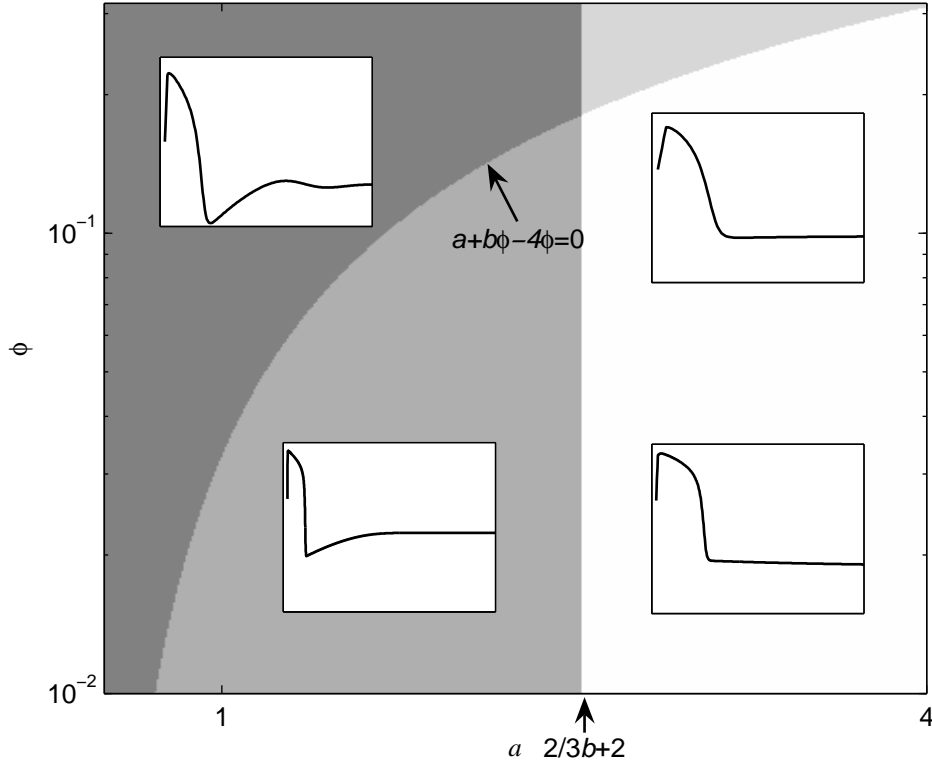
FIGURE 2.11: Regions of qualitatively different behavior in the FitzHugh-Nagumo model operating as quiescent neuron. The small upper right region gives biological not plausible behavior

From a resting state, say at $I = 0$, the membrane is hyperpolarized by injecting a negative current I_1. This moves the static current an amount I_1 to the left in Fig. 2.9. This negative step does not cause a spike, but, it moves the equilibrium to a new value on the solid curve. To depolarize the membrane again, a step of I_1 in the opposite direction has to be taken. If this step is larger than the value of the dynamical threshold (crosses) on the y-axis, the neuron will emit a phasic spike, known as post-inhibitory rebound spike.

2.3.3 OVERVIEW OF THE POSSIBILITIES OF THE FITZHUGH-NAGUMO MODEL

The two parameters of importance in the FitzHugh-Nagumo model are a and ϕ. Parameter b does not have a lot of influence on the qualitative behavior within the range that applies to the use of the model in neuroscience. According to the values of a and ϕ, three different regions of behavior can be distinguished: For $a < 2/3b + 2$, the value of u after a spike shows a refractory period in which it descends below equilibrium value; this corresponds to after-hyperpolarizing cells, whereas for $a > 2/3b + 2$, the membrane potential does not hyperpolarize after a spike. For values of (a, b) above the curve $(\alpha + b\phi)^2 - 4\phi = 0$, the linearized system has two complex conjugated eigenvalues and subthreshold oscillations may occur, which is not the case for parameter values below this curve. The combination between these two possibilities give three plausible situations; the situation with after-depolarization and subthreshold oscillations does not occur for feasible parameter values. The three regions are illustrated in Fig. 2.11.

2.4 THE HINDMARSH-ROSE MODEL

The FitzHugh-Nagumo model only models simple spiking behavior. The Hindmarsh-Rose model goes beyond that; while still belonging to the class of phenomenological generic bifurcation models without direct relation to physiological mechanisms, it is capable of reproducing many of the generic bifurcation scenarios present in more realistic models. In particular it shows bursting behavior and chaos [Abarbanel *et al.*, 1996; De Lange & De Feo, 2006; Rabinovich *et al.*, 2000; Wang, 1993].

The Hindmarsh-Rose model is given by [Hindmarsh & Rose, 1984].

$$
\begin{cases}
\dot{x} & = y - x^3 + bx^2 + I - z, \\
\dot{y} & = 1 - 5x^2 - y, \\
\dot{z} & = \mu \left(s \left(x - x_{rest} \right) - z \right)
\end{cases}
\tag{2.29}
$$

where we conformed to the convention in literature on notation of the state variables as (x, y, z) for this model.

A confusion sometimes encountered in literature is the comparison between the slow-fast properties of the Hindmarsh-Rose model and those of the FitzHugh-Nagumo model, however, although both models fall in the class of slow-fast oscillators, the slow parameter serves a different purpose in both cases. For the FitzHugh-Nagumo model, ϕ is introduced to model spiking behavior, giving the steep flanks of the spikes. In the Hindmarsh-Rose model, the first two equations govern spiking. The slow-fast feature of spiking behavior is modeled by a ghost of a saddle-node bifurcation at the minimum of u. The slow parameter μ in the Hindmarsh-Rose model governs the bursting and adaptation behavior, which is not captured by the FitzHugh-Nagumo model. In this aspect the Hindmarsh-Rose model falls in the same category of type-I models as for instance the Morris-Lecar model [Morris & Lecar, 1981], however the type-I behavior turns into type-II behavior for non-zero μ.

In what follows we suppose that $\mu \ll 1$ (in practice nearly always $\mu < 0.01$). This allows the separation of the system in a fast and slow subsystem; (x, y) and z respectively, which represents the usual adiabatic approach in which the properties of the fast system are studied with the slow variable as a parameter:

$$
\begin{cases}
\dot{x} & = y - x^3 + bx^2 + I - z, \\
\dot{y} & = 1 - 5x^2 - y,
\end{cases}
\tag{2.30}
$$

The behavior of the complete system then changes slowly, qualitatively over time with changes in z.

The equilibria of the complete system are defined by the intersections of the curves

$$
\begin{aligned}
z & = f(x) \equiv 1 - x^3 + (b - 5)x^2 + I \\
z & = g(x) \equiv s(x - x_{rest})
\end{aligned}
\tag{2.31}
$$

The parameters can be interpreted in the following way: I is the input current injected into the cell and b governs the qualitative behavior of the model; over-simplifying things, one might say that it is the switch that changes bursting to spiking behavior and vice versa. However, that would mean neglecting the fact that b also shapes the onset of spiking frequency. Parameter μ controls the speed of the slow variable; in the case of spiking it will alter the frequency of the spikes, whereas in the case of bursting, lowering μ will increase the number of spikes per burst. Parameter s governs adaptation; small s (values around

unity), give fast spiking behavior, without accommodation and subthreshold adaptation, whereas values around $s = 4$ give strong accommodation and subthreshold overshoot, or even oscillations. Finally, x_{rest} sets the resting potential of the system.

2.4.1   BIFURCATION ANALYSIS

The bifurcation structure of the Hindmarsh-Rose model is very complex. A complete bifurcation analysis can give insight in the working of the model on one hand and can be useful in practice for choosing parameter values when applying the model in different situations. Below such an exhaustive bifurcation analysis is presented for parameters b, I and, to a lesser extent μ. We begin by an analytical treatment of the bifurcation and spike/burst mechanisms, first considering the 2-D fast subsystem for clarity and then extending the analysis to the 3-D case. This analysis helps setting the conditions for the numeric bifurcation analysis using exhaustive simulation and continuation techniques, which is presented at the end of this section.

FAST SUBSYSTEM

Putting $I = 0$ and $\alpha = 5 - b$ in (2.31) gives for the equilibria of the fast subsystem (2.30):

$$1 - z = h(x) = x^3 - \alpha x^2 \tag{2.32}$$

The function (2.32) has two critical points where $h' = 0$: $x_{c,1} = -2/3\alpha$ and $x_{c,2} = 0$, such that

$$\begin{aligned} h' > 0, \quad & x_{c,1} < x < x_{c,2} = 0 \\ h' < 0, \quad & x < x_{c,1}, \ x > x_{c,2}. \end{aligned} \tag{2.33}$$

Now, the system can have either one single, or three equilibria, depending on z. Let $z_c = -\frac{4}{27}\alpha^3$, then for z such that

$$\begin{aligned} z_c < z < 0, \quad & \alpha > 0, \\ 0 < z < z_c, \quad & \alpha < 0, \end{aligned} \tag{2.34}$$

the fast subsystem has three equilibria

$$N_1(x_1, y_1), \quad O(x_0, y_0), \quad N_2(x_2, y_2) \tag{2.35}$$

With $x_1 < x_0 < 0 < x_2$ for $\alpha < 0$ and $x_1 < 0 < x_0 < x_2$ for $\alpha > 0$. Then O is a saddle, N_1 is a stable node or a focus, as is N_2. The second point undergoes an Andronov-Hopf bifurcation at $x_{AH1,2} = b \mp \sqrt{b^2 - 3}$. Using the sign of the first Lyapunov quantity from explicit formulas given by [Bautin, 1984] it is possible to show that the bifurcation is supercritical; as z passes the bifurcation point a unique stable cycle appears softly from the equilibrium point N_2 which loses stability in the process [Belykh, 2002].

The preceding analysis shows that the bifurcations of the system are different for $\alpha > 0$ and $\alpha < 0$, or $b < 5$ and $b > 5$, respectively. A further distinction can be made between the cases when $b < \sqrt{3}$ and $b > \sqrt{3}$. The divergence of the vector field $\mathcal{F}$ of the fast system is given by

$$\nabla \mathcal{F} = -3x^2 + 2bx - 1 \tag{2.36}$$

By the Poincaré-Bendixon theorem [Strogatz, 1994, p. 203], for $b < \sqrt{3}$, the divergence is negative everywhere, excluding cycles in the fast system. The state will converge to either

of the stable equilibrium points N_1 and N_2 and their basin of attraction is separated by the stable manifold of O. In summary, the fast subsystem can have three distinct forms, depending on the value of b. For increasing z from a value below:

1. $b < \sqrt{3}$; (no cycles)

2. $\sqrt{3} < b < 5$;

3. $b > 5$

Situation 2 is the one of interest for modeling neuronal behavior: for $b > 5$ the quadratic y-nullcline is convex, which means the slow part of the limit cycle, close to the saddle O, when it exists, lies on the side of large x, which would give an upside down spiking effect, with the refractory period for high membrane potential, and with negative spikes. Also, mathematically it is the most interesting region in parameter space since it comprises the emergence of very complicated dynamics in the full system, in particular in the transition between continuous spiking and bursting and between different bursting states [Terman, 1991, 1992; Wang, 1993]. This scenario also comprises the parameter values usually considered in neurocomputational literature and we will therefore only consider this case. For an extensive classification of types of burst generation in three dimensional slow-fast oscillators, see Hoppenstead & Izhikevich [1997] and Izhikevich [2000a]. For a complete analysis and classification of the three scenarios described above, see Belykh *et al.* [2000].

The generation of bursting in the complete system

Generally speaking, three modes of operation can be distinguished in the full Hindmarsh-Rose model:

1. Quiescent

2. Spiking

3. Bursting

The quiescent mode corresponds to the absence of stable cycles. Spiking means in this context, the continuous generation of action potentials, either regular or irregular, but with no clear formation of packets of spikes. Bursting on the contrary means that action potentials arrive in clear bursts, separated by clear, regular or irregular silent periods [Toledo-Rodriguez *et al.*, 2002]. Figure. 2.12 shows examples of spiking and bursting modes observable in the Hindmarsh-Rose model.

We now study the mechanisms behind the onset of spiking and bursting.

In spiking mode the frequency depends on the value of I and this dependence is shaped by the values of μ and b (Fig. 2.13). For vanishing μ, the spike onset is smooth and happens with zero frequency; the model reduces to the fast subsystem, which is a type-I model for $b < 5$ – the onset of spiking is governed by a saddle-node bifurcation. When μ is increased, the spiking behavior changes towards a type-II behavior, especially for high b. The spike threshold also increases with b.

In spiking mode, the slow z variable remains in a stable equilibrium and the system effectively evolves in two dimensions. The spiking behavior is locally equivalent to that of the fast subsystem (see Fig. 2.14, left).

SPIKING

f=10Hz   *f=30Hz*   *chaotic*

BURSTING

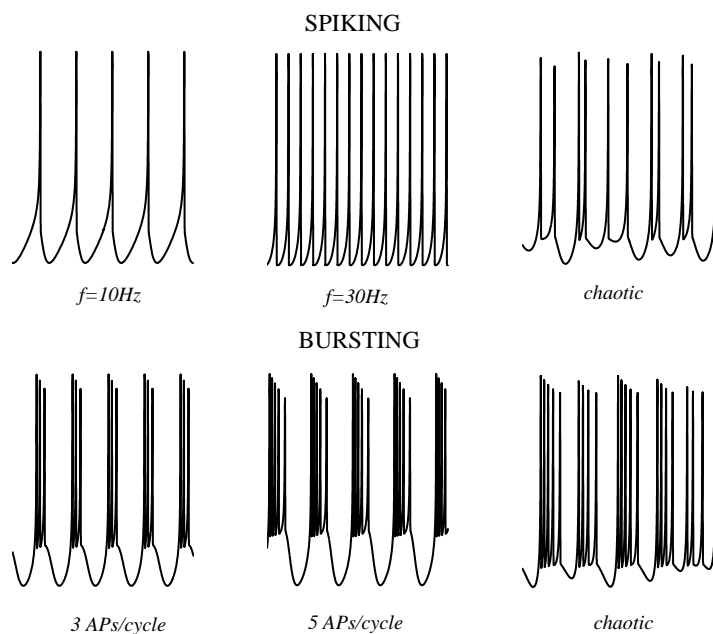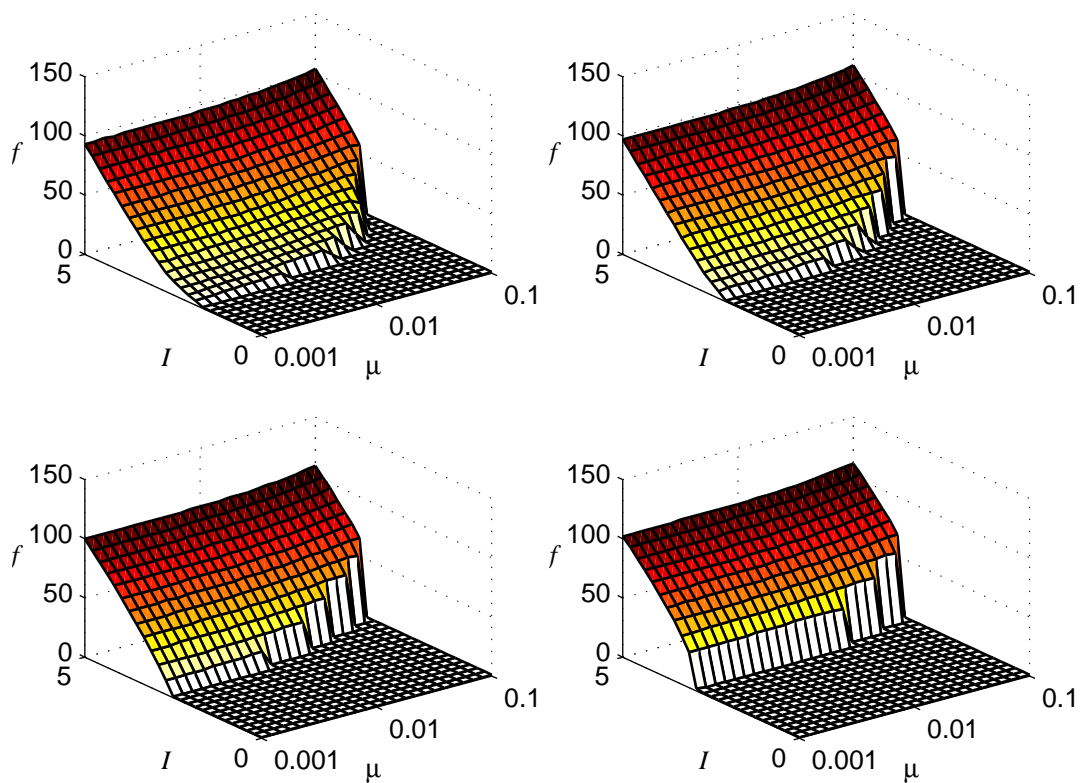*3 APs/cycle*   *5 APs/cycle*   *chaotic*

FIGURE 2.12: Different modes of operation of the Hindmarsh-Rose model

FIGURE 2.13: Spiking frequency of the HR model as a function of input current I and adiabatic parameter r for different values of b: from left to right, top to bottom, $b = 3.4$, $b = 3.6$, $b = 3.8$, $b = 4$, respectively
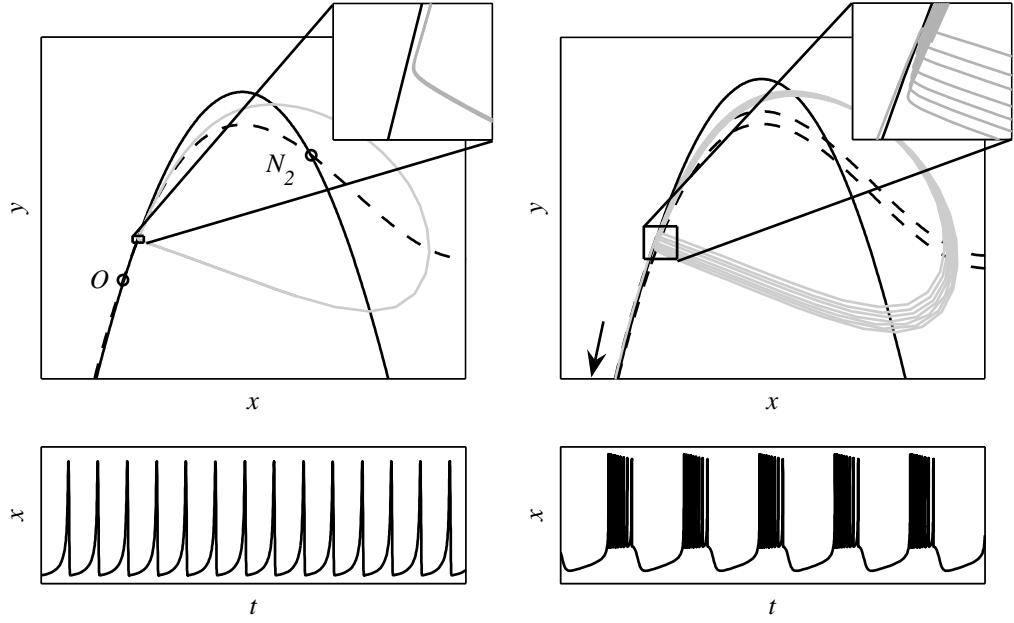
FIGURE 2.14: Spiking and bursting in state space for the Hindmarsh-Rose model. *Left:* Constant z gives spiking in the full system. *Right:* Generation of bursting through a homoclinic loop bifurcation when z fluctuates. The two dotted lines are the x-nullclines for the maximum and minimum values attained by z.

The onset of spiking from quiescent mode can be outlined as follows: For $I = 0$, the equilibrium N_2 is a stable node. When I increases it undergoes a supercritical Andronov-Hopf bifurcation and becomes an unstable focus with a limit cycle encircling it. The limit cycle does not encircle the two other equilibria; the saddle O and the unstable node N_1 (the latter lies below the range of Fig. 2.14 on the left branch). The cycle passes close to the saddle point, slowing the trajectory down, creating the spiking effect with a slow passage for low values of x – the membrane potential – and a fast spiking-like passage for high values of x. When I is increased even further, another Andronov-Hopf bifurcation stabilizes the equilibrium N_1 and spiking ceases (excitation block).

FIGURE 2.15: Sketch of the bursting mechanism in the full Hindmarsh-Rose model.

27

For lower values of b, the slow subsystem comes in action and slow variable z will not converge to an equilibrium, but show periodic (or even chaotic) behavior, which causes the bursting mode in the full system. Beginning the description with the state at the maximum of the period of z; with $z > z_c$, the equilibrium N_1 is globally stable and all solutions of the full system, except the stable manifold of O and the un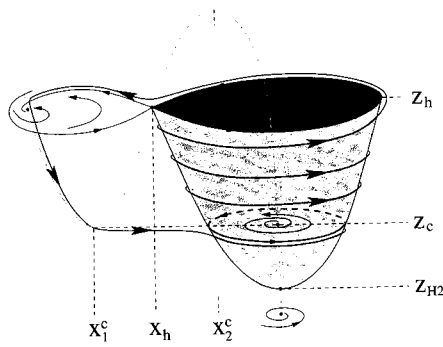stable equilibrium N_2 will converge to N_1. Then, since at N_1, $x < z/s + x_{rest}$, z decreases slowly (cf. (2.29)). For $z_c < z < 0$, the limit cycle exists around N_2, and the unstable manifold of the saddle O separates the stable equilibrium from the limit cycle. Under the adiabatic assumption, the state follows the equilibrium and cannot "accidently" pass the unstable manifold to the limit cycle when perturbed.

When z then passes below zero, N_1 undergoes a saddle-node bifurcation with O and disappears. There are then two possibilities: either the second Andronov-Hopf bifurcation point of N_2, z_{H2} (see Fig. 2.15), is smaller than zero, in which case the stable limit cycle is the only solution when N_1 disappears; or $z_{H2} > 0$, in which case the equilibrium N_2 is globally stable. In both cases the state makes a jump to the other side of what was the unstable manifold of O previously, and $x > z/s + x_{rest}$: z will start increasing. If N_2 was stable before, it will then first undergo an Andronov-Hopf bifurcation for $z = z_{H2}$, otherwise the trajectory will continue immediately on the cycle. For $z = 0$, the stable equilibrium N_1 and the saddle O reappear, but the cycle is separated from N_1 by the stable manifold of O. When z increases, the cycle approaches the stable manifold of O. This is shown in the insets in Fig. 2.14. For $z = z_h$ the cycle collides with the stable manifold of O forming a homoclinic loop, which is immediately followed by a rearrangement of the separatrices of O making N_1 globally stable again and restarting the whole process, after x has approached N_1 enough such that $x < z/s + x_{rest}$.

Two things are clear from this analysis: the qualitative behavior for constant I is governed by b, and the values of μ and s, which influence the speed of the slow subsystem, will influence the period of the solution (frequency for spiking solutions and number of bursts per cycle for bursting solutions). So, depending on the value of b within the range considered here ($\sqrt{3} < b < 5$), three scenarios are possible, which are outlined in table 2.1. The exact values of b that borders these regions depend on the other parameters of the

b	Mode	Bifurcation sequence
Small	Conic bursting	Saddle-node of N_1, $O \rightarrow$ Andronov-Hopf of $N_2 \rightarrow$ Homoclinic
Medium	Square wave bursting	Saddle-node of N_1, $O \rightarrow$ Homoclinic
Large	Spiking	None, for constant I

Table 2.1: Outline of different modes of the Hindmarsh-Rose model for different values of parameter b.

system, especially on I, as will be shown numerically below. The case of conic bursting is not interesting in practice for modeling neuronal behavior and this region of b should be avoided.

The sequence of phase portraits of the fast system, as well as the mechanisms behind the onset of bursting are well known [Belykh *et al.*, 2000; Hoppenstead & Izhikevich, 1997;

Izhikevich, 2000a]. The behavior outlined above is one of the scenarios of burst generation possible in general for bursting slow-fast systems; it corresponds to the fold/homoclinic, circle/homoclinic, Hopf/homoclinic and subHopf/homoclinic bursters in the classification by Hoppenstead & Izhikevich [1997], or to scenario 3 from Belykh *et al.* [2000]. However, especially in the range between (chaotic) bursting and spiking, the precise bifurcation structure is very complex and the complete analytical unraveling has not been reported to date. A numerical bifurcation analysis can not only complement and facilitate this analytical task, but it is also useful for practical applications of the Hindmarsh-Rose model. The Hindmarsh-Rose model is gaining in popularity amongst computational and experimental neuroscientists alike.

Exhaustive simulation analysis

The approach taken to investigate the bifurcation structure of the Hindmarsh-Rose model is a combination between exhaustive simulation, numerical continuation using the software package AUTO 2000 [Champneys *et al.*, 1996; Doedel *et al.*, 2001] and normal form theory [Kuznetsov, 1995]. This approach has been successfully applied to several similar models. The analysis adopted here follows the approach outlined in De Feo *et al.* [2000] and Kuznetsov *et al.* [2001].

As principal bifurcation parameters we consider b and I; the parameter that governs the qualitative behavior, and the input current. Parameters μ and s do not change the bifurcation structure in a fundamental way: decreases in μ cause a shift towards higher frequencies and more spikes per burst, hiding the essence of the bifurcation structure (see below), but not altering it, whereas decreases in s compress the bursting and chaotic regions, with respect to the regular spiking region. The above claim is illustrated for μ, by repeating the simulations for different values.

The first step in the bifurcation analysis is an exhaustive simulation of the parameter space. The parameter space is partitioned and a fine raster is laid out over the (b, I) space. Using an ODE (ordinary differential equation) solver the system is then simulated for every point in the raster and two qualitative features of the asymptotic solution are recorded: the number of spikes per period and the periodicity of the solution (sub-harmonic structure.) This gives a map of the behavior for the parameter space (b, I). The same simulations are repeated for different values of μ. The results of the exhaustive simulation analysis are reported in Fig. 2.16.

As expected, for different μ the picture is very similar. As μ decreases the frequency of spiking increases and the bifurcation structure becomes denser. The results show that the chaotic behavior is inherent to the system and does not depend on the adiabatic condition of small μ. The figure for $\mu = 1E-2$ is the clearest, and since the topology of the classifier is similar for all μ we will continue the bifurcation analysis for $\mu = 1E-2$, nevertheless the general discussion is equally valid for other values of μ.

The road map can be divided in four regions corresponding to quiescence, regular spiking, bursting behavior and chaos, as shown in Fig. 2.17 In the spiking region, changes in I modulate the spiking frequency and b the onset of spiking (threshold, type-I vs. type-II, cf. Fig. 3.7). In the bursting region the behavior is much more complex, especially around the razor blade-shaped dark region, which indicates chaos.
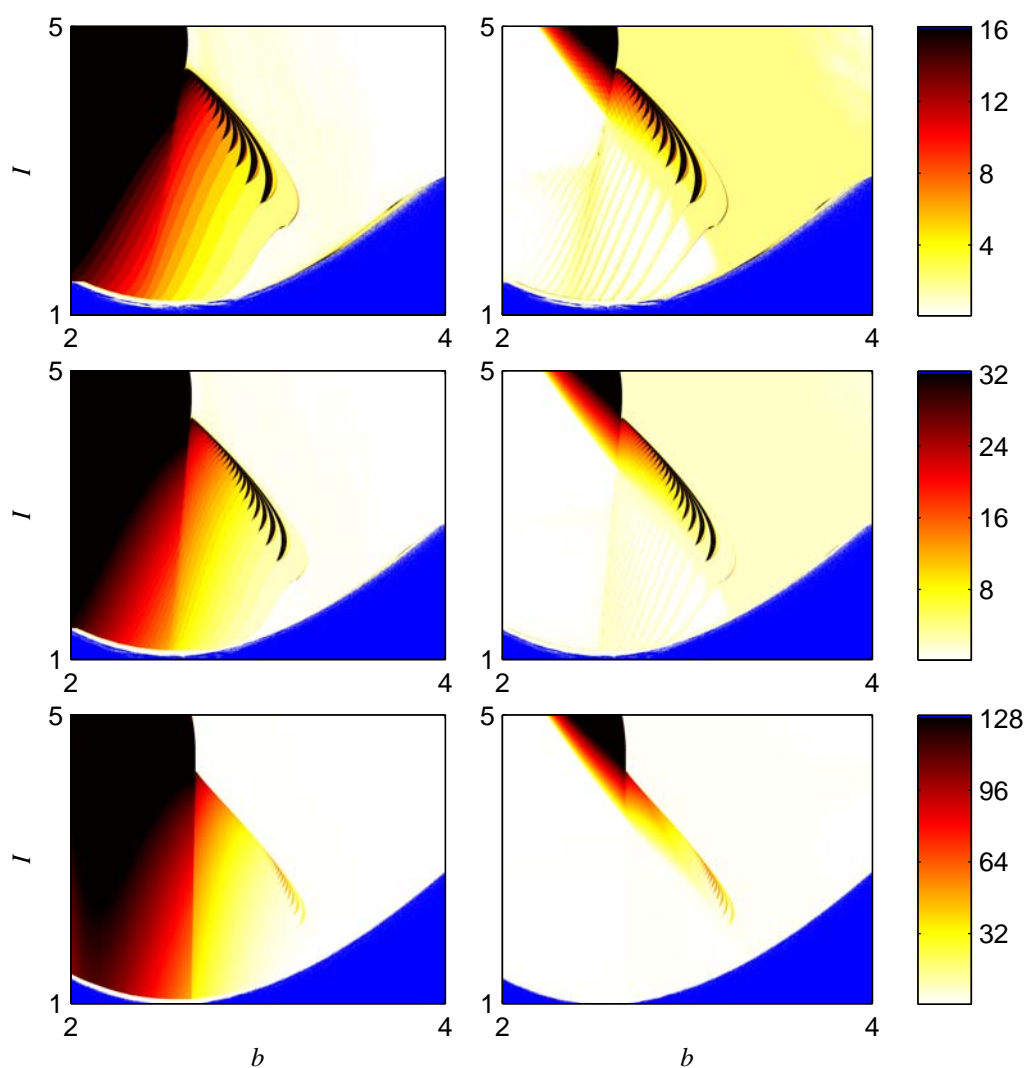
FIGURE 2.16: The classifier road maps of the Hindmarsh-Rose model for different values of μ. *Left column:* Number of spikes per period. Darker colors indicate more spikes. Blue indicates an equilibrium. *Right column:* Sub-harmonic structure of the solution. Darker colors indicate chaos. *Top row:* $\mu = 1E - 2$. *Middle row:* $\mu = 5E - 3$. *Bottom row:* $\mu = 1E - 3$.
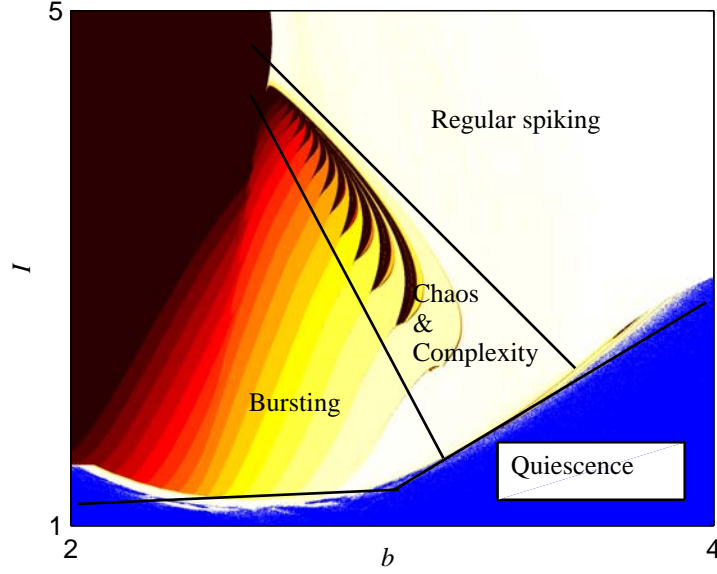
FIGURE 2.17: The classifier road map divided in regions of qualitatively similar behavior.

Continuation analysis

Starting from a point in the road map of Fig. 2.17 the solution of the system can be continued using numerical continuation techniques [Beyn *et al.*, 2002; Doedel *et al.*, 2001]. By following the solutions for the entire parameter space, the organizing principles behind the bifurcation structure can be revealed. A problem is however, that the bifurcation structure is so dense for low b (the darker region), that numerical techniques do not converge anymore.

The results of the continuation analysis are shown in Fig. 2.18. Beginning on the lower left in the quiescent region below the bursting region, when I increases a bursting cycle emerges from a very complex accumulation of folds, flips and Andronov-Hopf bifurcations. When increasing I further and moving through the bursting region, cycles are added to the solution. The different bursting regions are bordered by a fold bifurcation. Next, when I is increased even further, the chaotic region is entered through a homoclinic bifurcation, chaos then emerges on the lower edge of the black tongues from fold bifurcations of cycles. When entering the chaotic region from the spiking side, the chaos emerges from flip bifurcations by the usual Feigenbaum period doubling cascade [Ott, 1993]. Each of the black tongues in the chaotic region is bordered on the right by a flip and on the left by a fold bifurcation. The organizing center seems to be at the point where the flips and folds from these tongues come together and touch the homoclinic at the top of the chaotic region. Another organizing point could be on the bottom left side of the figure, where the folds that organize the regular bursting come together, but we were not able to continue the solutions up to that point. The organizing principles seem to be very similar to those obtained for a tritrophic food chain model by Kuznetsov *et al.* [2001].

Summary

In situations where a real neuron has to be modeled, it is usually assumed that model parameters do not change; this corresponds to moving vertically in the road map. Figure
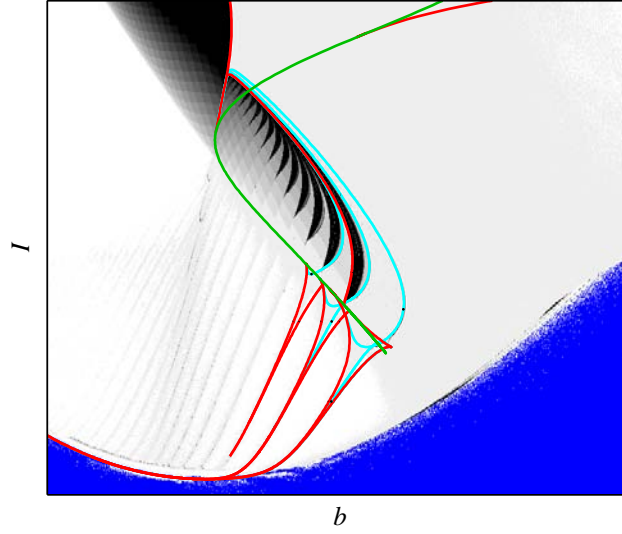
FIGURE 2.18: The continuation diagram of the Hindmarsh-Rose model. Red lines are fold bifurcations, cyan lines flips and the green line is a homoclinic bifurcation.

2.19 shows the qualitatively different types of behavior that may be observed when increasing I for fixed b. For low b, the system begins with bursting with few bursts per cycle. Then, when I is increased, the parameter values move into darker regions, which means that there are more bursts per spike: for these values of b the model is bursting, and I controls the number of spikes per cycle. For intermediate values of b, the solutions for low I are also bursting solutions, but as I is increased we move via the chaotic region – which for low μ might be so small that it is unobservable in practice, cf. Fig.2.16 – into the regular spiking region. This change in firing pattern by changes in the membrane potential has been reported in vivo for neocortical neurons [Steriade, 2004].

2.4.2 TRANSIENT PHENOMENA

In contrast to the limited diversity in transient behavior the FitzHugh-Nagumo model is capable of reproducing, the Hindmarsh-Rose model can show many types of features that are observed in vitro. In vitro protocols usually comprise step and pulse-like currents. Phenomena like after-hyperpolarization and depolarization, accommodation, and the onset part of the classification scheme based on onset-stationary behavior [Gupta *et al.*, 2000] correspond to the transient response of the system [De Lange & De Feo, 2006]. Due to the complex folded bifurcation structure outlined above, many unstable periodic orbits are present at any point in parameter space (infinitely many in chaotic regions [Ott, 1993]) and after a sudden change in current, the system may temporarily follow any of these.

A far from complete selection of discharge responses that can be obtained from the Hindmarsh-Rose model is reported in Fig. 2.20.

2.5 MODELS FOR CONNECTIVITY

Synapses come in two flavors: chemical and electrical, both of which occur in the neocortex, although the chemical ones are much more frequent [Koch, 1999]. Chemical synapses
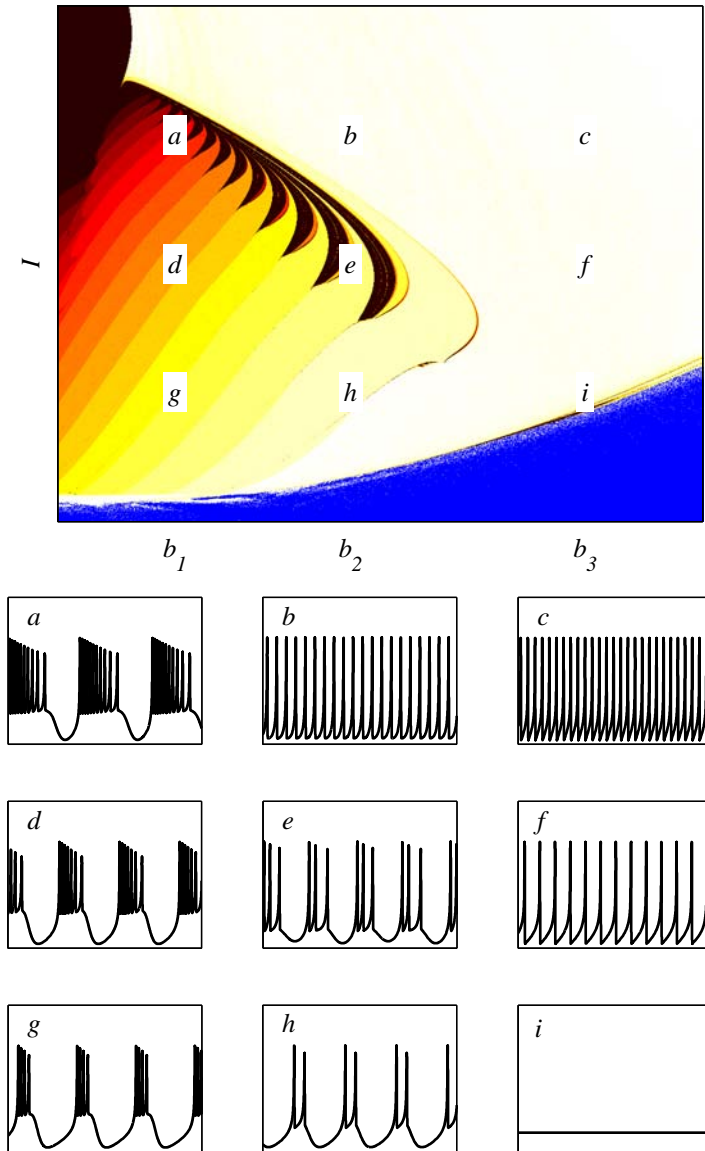
FIGURE 2.19: Examples of time series generated by the Hindmarsh-Rose model when increasing I for different fixed values of b: $b_1 = 2.7$, $b_2 = 3$, $b_3 = 3.4$.
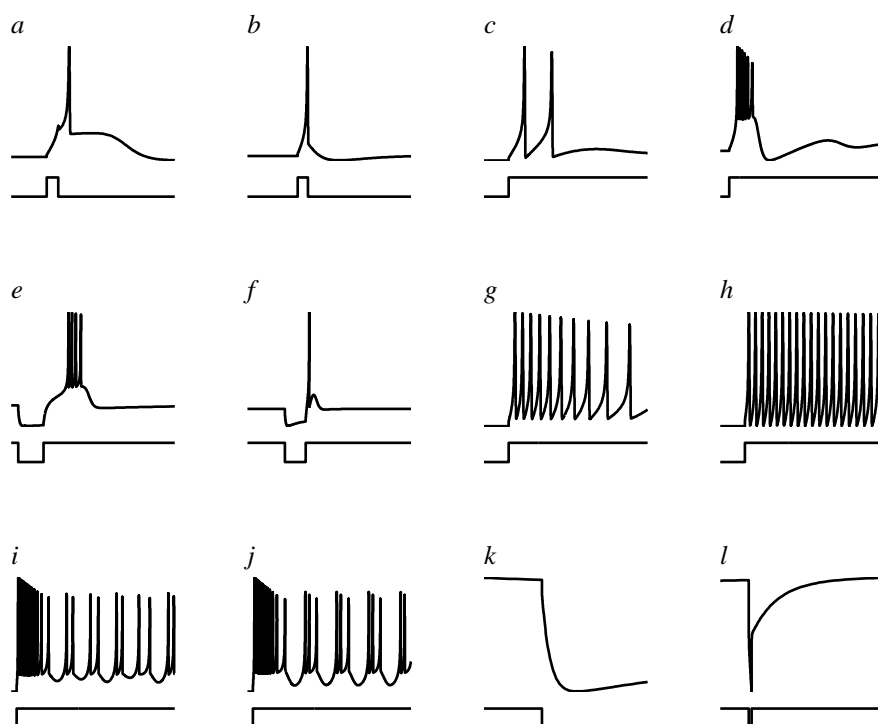
FIGURE 2.20: Different transient phenomena in the Hindmarsh-Rose model. *a*: After-depolarization. *b*: After-hyperpolarization *c*: Double phasic spike. *d*: Phasic burst with subthreshold oscillations. *e*: Inhibitory rebound burst. *f*: Inhibitory rebound spike. *g*: Regular (accommodating) spiking. *h*: Fast (non-accommodating) spiking. *i*: Irregular spiking with initial burst. *j*: Regular bursting with initial burst. *k*: Response to hyperpolarizing current step. *l*: Response to negative delta pulse.

have complex morphology and corresponding complex dynamics, that operates on many different time scales, thus providing memory function. They have a steep activation function and therefore only transmit information about the timing of the spikes (or bursts) in the presynaptic cell. If information is present in the subthreshold membrane potential, it can only be transmitted through electrical synapses. Recent work by Kopell & Ermentrout [2004] indicates that electrical synapses could play an elementary role in synchronization of interneural networks.

In this work the dynamics of the synapses are neglected completely. The purpose is to study the dynamics in networks of neurons on a time-scale that corresponds to that of the dynamics of action potentials in neurons (milliseconds), so short and long term synaptic plasticity can be safely ignored. However the ignoring of the dynamics in the millisecond range, that for instance determine the form of the postsynaptic potential, applied in this work, presents a simplification of reality.

The model used in Chaps. 3 and 4 was proposed by Somers & Kopell [1993]. It is called *Fast Threshold Modulation* (FTM); fast, because no dynamics are incorporated, and threshold modulation, because the model exhibits a threshold-like behavior, either a hard threshold, or a more gradual, continuous threshold. In the FTM model, the current into the postsynaptic cell, I_j, is an instantaneous, but nonlinear function of the membrane potential of the presynaptic cell u_i and the membrane potential, u_j, of the postsynaptic cell:

$$I_j = -g_s \left(u_j - V_s\right) \Theta \left(u_i\right). \tag{2.37}$$

The parameter V_s is the synaptic reversal potential. It determines the type of coupling. If V_s is larger than the membrane potential, the current is positive, directed in to the cell and the membrane potential is de-polarized, thus exciting the cell. If, on the other hand, V_s is smaller than the membrane potential, the current is negative and directed outwards, hyper-polarizes the membrane and inhibits. According to the threshold assumption, activation function $\Theta(u_i)$ is a sigmoidal function, that takes the shape

$$\Theta(u_j) = \frac{1}{1 + \exp\{-\lambda(u_j - \theta_s)\}} \ . \tag{2.38}$$

with θ_s the threshold. In the case of $\lambda \to \infty$, the threshold is a hard one and the sigmoidal function reduces to a Heaviside step function.

Although neurons and synapses are traditionally considered the dominating units in information transmission and processing in the brain, more recently evidence has been found suggesting that astrocytes – star-shaped glial cells that were traditionally considered to be used for physical support, cleaning and nourishing activities – can communicate with other astrocytes and neurons [Bezzi *et al.*, 2004] and play a role in the synchronization of neurons [Fellin *et al.*, 2004]. Also, dendritic spines might play a role in synaptic transmission or influence the shape of the action potential and subthreshold dynamics, although their principal function is most probably in long term memory [Koch & Zador, 1993; Trachtenberg *et al.*, 2002].

2.6 ASSESSING THE QUALITY OF NEURON MODELS

A model is a quantitative description of the input-output relation we observe when we interact with a system [Ljung, 1994, p. 14]. In principle, a model is good when its predictions are sufficient to the purpose it will serve. In neuronal modeling an important

issue is that it is not known yet what the purpose of neurons is; which part of their behavior is essential to their functioning as a computational units, and which is merely a side effect of the means they use to attain their goals.

The focus of this work is on generic bifurcation models, which, depending on the model, are able to display, to greater or lesser extent, behavior beyond simple spiking; thus capturing what is believed the essence of neocortical diversity. The models remain *qualitative* models though, and therefore it is useless, or even meaningless, to express the quality in terms of a distance measure between the membrane potential of the model and that of the real neuron.

The simplest qualitative comparison is the output firing rate. It is often used in literature to assess the quality of predictions of neuron models [Hansel & Mato, 2003]. When treating irregular spike trains, such as the ones occurring from injection of in vivo-like input signals (see Sect. 5.1.3), it is useful to introduce a measure that evaluates the quality of the prediction of the spike timing. We use a measure introduced by Kistler *et al.* [1997] and later slightly altered by Jolivet *et al.* [2006b]. The *coincidence factor* Γ, between two spike trains; the predicted spike train, with N_p spikes, and the reference spike train, with N_r spikes, depends on the number of coincidences N_c between the two spike trains. Coincidences are defined as spikes occurring in both trains within a certain minimum distance Δ of each other. To correct for the fact that any random point process with nonzero frequency would have a probability of getting a certain number of spikes right, a factor $\langle N_c \rangle$ – the mean number of coincidences a random process with the same rate ν_p as the model would get right – is subtracted from the number of coincidences. Finally the expression is normalized between zero and unity by a normalization factor $\mathcal{N}$. Zero meaning that the prediction is not better than that of a random process, and unity meaning that the prediction is perfect: all spikes of the model fall within a distance Δ of all spikes of the real neuron.

$$\Gamma = \frac{N_c - \langle N_c \rangle}{\frac{1}{2}\left(N_p + N_r\right)}\frac{1}{\mathcal{N}}; \quad \langle N_c \rangle = \nu_p \Delta N_r; \quad \mathcal{N} = 1 - \nu_p \Delta \qquad (2.39)$$

Note that although it is not possible for Γ to exceed unity, it is theoretically possible to have values below zero. This indicates a negative correlation between the spikes in both spike trains; a value that could for instance occur when comparing two neurons with inhibitory coupling. In chapter 3 a slightly altered version of this measure is used to assess the quality of a coincidence detector in a noisy environment.

In chapter 5 we will compare the input-output relation of the models to that of real neurons in electrophysiological recordings using a set of measures introduced in [Toledo-Rodriguez *et al.*, 2004]. These measures focus on: the discharge response to step current pulses, the shape of the first two action potentials generated just above threshold, the neuronal response to ramp current injection, the change in spiking behavior with time (adaptation, or accommodation), the hyperpolarization generated after a burst of action potentials, sub-threshold dynamics, and static input-output relationship.

COINCIDENCE DETECTION

Brief — To employ pulse coupling as a model for chemical synapses in networks of generic bifurcation models, a thorough understanding of the specific characteristics of this non-standard coupling is important. This chapter aims to clarify the special features of pulse coupling by studying pairs and triplets of coupled generic bifurcation models. The mathematical arguments are supported by simulations, examples and case studies.

Personal Contribution — Unless specified otherwise, the material in this chapter is original work. The analytical results were obtained in collaboration with Dr. Igor Belykh. Dr. Oscar De Feo advised on the simulations of the qualitative resonance phenomenon in the Hindmarsh-Rose model.

One cannot hope for an understanding of collective behavior in networks of coupled neural oscillators without a thorough understanding of the elements of the networks and of the way they interact. The elements of the networks to be studied in this thesis, as well as the model for the synapses that couple them, were presented in Chap. 2. The work presented in this chapter explores the way pairs of general bifurcation cells interact through synaptic coupling by considering assemblies of two or three neurons (see Figs. 3.1 and 3.2 respectively).

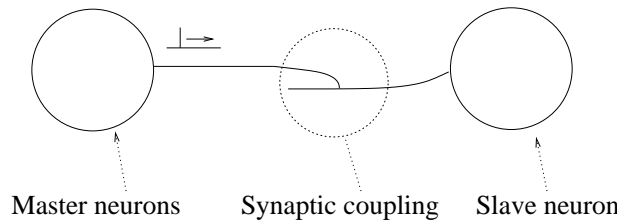
Master neurons   Synaptic coupling   Slave neuron

FIGURE 3.1: The basic master-slave coupled configuration consisting of one presynaptic (master) neuron and one postsynaptic (slave) neuron.

Besides a necessary step on the way to the analysis of larger networks of generic bifurcation type models, the theoretical results presented in this chapter also serve as
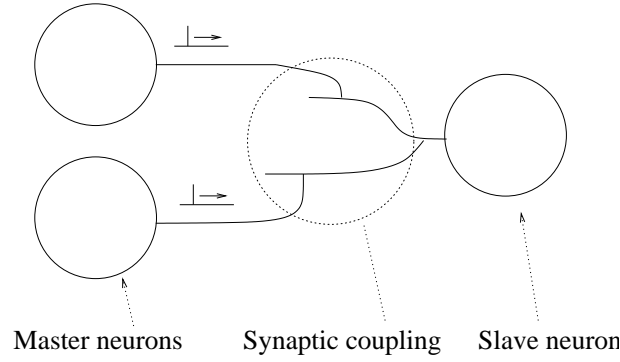
FIGURE 3.2: The basic configuration for coincidence detection: two presynaptic (master) neurons drive a postsynaptic (slave) neuron.

the basis for a study on the realization of a single neuron coincidence detector using these models. Coincidence detection is the ability of individual neurons to detect the coincidence of activity in two different inputs. Neurons with this ability can for instance be found in the auditory systems of birds [Konishi, 1992].

A first step, both in the understanding of the coupling and in preparation for the study of coincidence detection is to look how a single neuron of the generic bifurcation type can detect patterns of activity in another neuron of the same type through FTM coupling. The configurations used in this chapter are the ones shown in Figs. 3.1 and 3.2: one or two presynaptic neurons propagate their signals to a postsynaptic cell through a chemical synapse. In neurocomputational literature this kind of setup is often called *master-slave configuration* because there is no feedback in the system: the postsynaptic (slave) neuron can only follow the signals (obey) from the presynaptic (master) neuron, and not vice-versa. For clarity and brevity we will maintain this, somewhat colonial, terminology throughout this entire chapter.

The chapter is divided in two parts: The first part comprises Sects. 3.1–3.3; there we will focus on two-dimensional behavior using the FitzHugh-Nagumo model as a prototype. Some of the results in this part have been reported at the 2003 workshop on nonlinear dynamics of electronic systems (NDES 2003) [De Lange & Belykh, 2003]. In the second part (Sect. 3.4) we will study some effects that will occur for bursting neurons of the Hindmarsh-Rose type.

In both cases two situations can be distinguished according to the regime of the slave neuron. If the slave neuron is in quiescent mode, the question is whether it can react to incoming spikes from the master neuron and we speak of *spike detection* (Sect. 3.1.2). On the other hand, if the slave neuron is in spiking regime, the question is whether the slave neuron can lock into the activity of the master neuron; we then speak of *master-slave (ms) synchronization*, or, sometimes, *phase locking*, though we will not use this term to avoid confusion with the phase locking as it is usually understood in neuroscience. (We will run in to the latter version in Sect. 3.3).

The principles of the interaction between pairs of neurons coupled by FTM coupling, (2.37), can be applied to design a setup for a model for *coincidence detection* using generic bifurcation neurons. In Sect. 3.2 we present a setup for coincidence detection using the FitzHugh-Nagumo model. We also show how background noise, always present in-vitro, can enhance the threshold detection, a phenomenon often called Stochastic Resonance [Gammaitoni *et al.*, 1998].

38

Section 3.3 shows an application of the FitzHugh-Nagumo coincidence detector in a neurocomputational model of the barn owl's auditory pathway, which was presented originally by Gerstner *et al.* [2000].

Not all cortical neurons are simple spiking neurons, to study possible advantages of the exploitation of the more complex behavior seen in, for example, bursting interneurons, Sect. 3.4 presents a setup for coincidence detection using the Hindmarsh-Rose model.

3.1 INTERACTION BETWEEN NEURON MODELS THROUGH PULSE COUPLING

A logical start to study the properties of chemical coupling when it is applied unidirectionally is to take the most simple setup imaginable: two cells coupled in a unidirectional fashion according to the master-slave configuration shown in Fig. 3.1. We begin by considering only interaction of simple spiking behavior using the FitzHugh-Nagumo model.

The equations of two FitzHugh-Nagumo cells (2.6) coupled in the master-slave configuration are:

$$\begin{cases} \dot{u}_m = u_m - \dfrac{u_m^3}{3} - w_m + I_m \\ \dot{w}_m = \phi_m \left(u + a_m - b_m w_m\right) \\ \dot{u}_s = u_s - \dfrac{u_s^3}{3} - w_s + I_s - g_{s,m}\Theta\left(u_m\right)\left(u_s - V_{syn,m}\right) \\ \dot{w}_s = \phi_s \left(u_s + a_s - b_s w_s\right), \end{cases} \tag{3.1}$$

where the subscripts m and s respectively denote the master and slave neuron.

This setup allows us to study three closely related phenomena: ms-synchronization, resonance and spike detection.

In ms-synchronization we consider two oscillators. That means the two neurons are in spiking regime. The goal is to find out the mechanism and conditions for the slave neuron in to follow the signal of the master neuron. The mathematical phenomenon behind master-slave synchronization is a weak form of synchronization usually called *phase synchronization* [Pikovsky *et al.*, 2001, p. 21].

It is easy to see that in this coupled system full synchronization is not possible since this would require both systems to have identical dynamical behavior in the synchronous regime. Since the very nature of the FTM pulse coupling is that, according to the value of the coupling variable of the master, it adds a term to the coupled variable of the slave, the one-directional coupling scheme from Fig. 3.1 is inherently asymmetric: the equations of both cells in (3.1) can only be identical in the trivial case when no coupling is present.

However it turns out that the slave neuron can *lock* to the signal of the master. This means that, although the signals in both neurons are not identical, the phase difference remains constant on the average. This locking can be $1 : 1$, meaning that the slave neuron reacts on every spike in the forcing signal from the master, or $n : 1$, where the slave only reacts on one out of every n spikes.

Formally, this locking, or *phase synchronization*, is defined as follows [Pikovsky *et al.*, 2001, p. 23]: two systems with phases ϕ_1 and ϕ_2, respectively, are $n : 1$ phase synchronized, if

$$|\phi_1 - n\phi_2| < k, \tag{3.2}$$

where k is some constant. This definition is more general than saying, as is often done in literature (for example by Calitoiu [2006]), that the phase difference remains constant in phase synchronized systems. More correct would be to state that there is a strong resonance between the master and the slave cell; the phase difference must remain bounded and converge to a constant value.

A difficulty in the case of the strongly nonlinear oscillators considered here is that the phase in this case is not well defined. In section 3.1.1, a model example is given to illustrate the mechanism behind phase synchronization in a system where the phase can easily be identified.

Resonance and spike detection are very similar to each other: in both cases the slave cell is silent and can react on incoming spikes from a master cell. In the case of *resonance*, the incoming master signal is periodic, representing continuous spiking. The question to be addressed is whether the slave can react with spiking behavior that follows – "resonates to" – this signal, much like in phase synchronization. Although strictly speaking this resonance is not a form of synchronization, since the slave neuron is not an oscillator [Pikovsky *et al.*, 2001, p. 15], it shows many similarities with ms-synchronization, like $n : 1$ resonance. And indeed, once the resonance is established, the slave can be considered an oscillator, and (3.2) can be applied.

In the case of *spike detection*, there is a single incoming spike. The question is then under which conditions the slave neuron reacts to this spike. Using the setup of Fig. 3.1 we model the simplest case when there is one presynaptic neuron. Besides illustrating the mechanism of neuronal interaction, this allows us to draw some conclusions we can use later when studying coincidence detection (Sect. 3.2).

3.1.1 Master-slave synchronization

In this section we consider parameter values for the cells in (3.1) such that both cells are in periodic spiking regime, though not necessarily with identical frequency. The idea is to study the mechanism that makes two cells, which initially have different phase or frequency, synchronize.

Considerable effort has been devoted to the problem of stability of synchronization and ms-synchronization in chemically coupled neurons. Using geometric singular perturbation methods, Rubin & Terman [2000a,b] proved that the synchronization is locally stable for some class of relaxation oscillators coupled via fast threshold modulation and having a slow parameter μ in the singular perturbation limit ($\mu \to 0$). In a related analysis, Kopell & Somers [1995] show that excitatory coupling through fast threshold modulation leads to local synchronization of the cells when $\mu \to 0$. The central idea was to use the fast-slow structure of the equations and the time to flow between points on the slow manifold as a distance metric. Recently Izhikevich [2000b] has proposed a set of phase models that show some of the properties of relaxation oscillators coupled via fast threshold modulation and having a slow parameter μ. He showed that there is stable synchronization as $\mu \to 0$. However the method he used requires the coupling strength g_s to be much smaller than μ, so the coupling must be extremely weak, which is not the case in most realistic situations.

Mathematical analysis of mutual synchronization of pulse-coupled neurons can be relieved by using the conventional stability methods. In this case the existence of completely synchronized modes is defined by linear invariant manifolds. The stability of the linear invariant manifolds can often be obtained through the construction of a

Lyapunov function for the corresponding difference equations, similar to the approach followed by Belykh *et al.* [2003] (see Chap. 4).

However in the case of the master-slave configuration (3.1) these methods cannot be applied because of the absence of the synchronization manifolds. In fact the synchronization solution defining perfect synchronization does not exist; only in the trivial case when $\Theta \equiv 0$ in (2.37), the two systems can become identical.

To tackle the problem of the stability of master-slave locked trajectories in the general case, where the coupling is not small and the small parameter is not infinitely small, one should introduce the phase of the oscillators and show that the phase difference tends to zero or a constant value, and (3.2) holds. However this only seems to be possible for some special cases and not in the general case.

First we illustrate ms-synchronization in FitzHugh-Nagumo neurons by simulations. Then we present a model example for which the phase can be defined and the existence of ms-synchronization can be shown under some limiting conditions. The example outlines a mechanism of phase locking that justifies the simulation results.

Simulation results

Master-slave synchronization in two pulse coupled Fitzhugh-Nagumo oscillators occurs for values of the coupling strength g_s that are larger than some critical value g_s^*.

It is difficult to show on paper how two dynamical systems evolve in time. An attempt is made in Fig. 3.3, which shows a plot of the master and slave, coupled with coupling strength $g_s > g_s^*$, evolving in the phase plane. Of course, the exact value of g_s^* depends on the parameter values of the FitzHugh-Nagumo oscillators and the value of V_s in the coupling. For the standard values (2.7) and for $V_s = 2$, $\lambda = 10$ and $\theta_s = 0$, ms-synchronization occurs for values of $g_s > g_s^* = 0.04$.

The different markers in Fig. 3.3 indicate a snapshot of the two systems at fixed time intervals. It can be seen from the pictures that the distance between the master and the slave, indicated by a diamond and a circle respectively, does not stay constant. The coupling threshold, $\theta_s = 0$, lies in the middle of the picture. When the master is moving left of the threshold, the coupling is not active, the coupling term in (3.1) vanishes and the master is a little faster than the slave. This effect can best be seen from the difference between pictures 3 and 10. In picture 10, after the right part of the cycle, where the coupling is active, the master has a bigger lead on the slave than in picture 3. The differences in speed on the two parts of the period cancel each other and the systems end up in the same relative position after each cycle thus creating ms-synchronization.

Model example

The model example we study is a simplified model, meant to illustrate the idea behind phase synchronization and to justify the simulation results obtained in this section. Essential for our analysis is the fact that the excited slave system, i.e., the hypothetical system when the coupling is always on, has a stable limit cycle with a smaller radius than that of the non-excited system. This is generally the case for limit cycle neuron models. Although from Fig. 3.4 we see that the radius of the limit cycle is hard to define, it is immediately clear that for the Fitzhugh-Nagumo system, the limit cycle of the excited system is smaller than that of the autonomous system.

The chemical coupling is taken in its limiting form taking a pure on-off coupling and we write $\Theta(\cdot) \equiv H(\cdot)$, with H the Heaviside step function. Furthermore we take $V_{syn,m} = 0$,
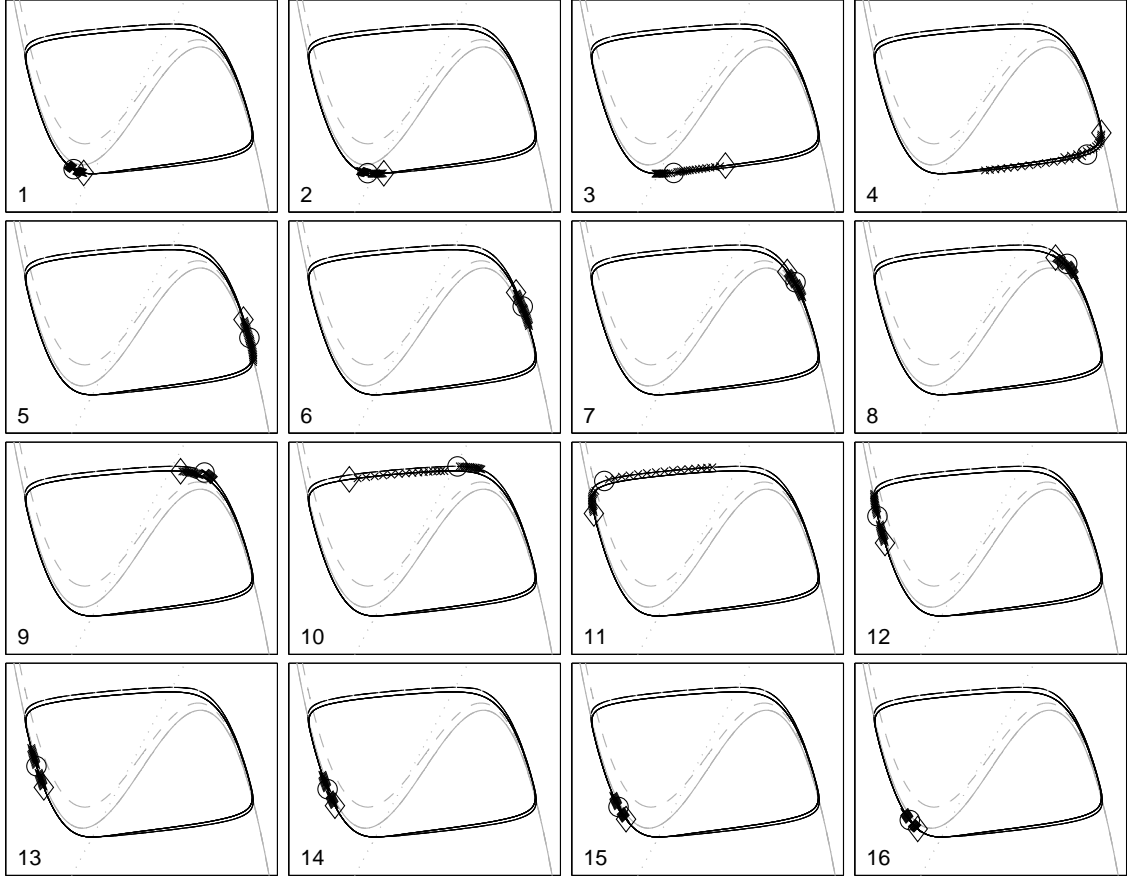
Figure 3.3: Two Fitzhugh-Nagumo neurons evolving in time. In the pictures the nullclines (cf. Fig. 2.1) are indicated in grey. Two cubic nullclines are shown; the solid one is that of the master, which does not change and the dashed one is the one for the slave when the coupling is on. The two trajectories of the neurons in steady state regime (after 800 time steps) are shown in solid lines. The current position of the slave in every plot is indicated by a circle and that of the master by a diamond. Every next picture shows the situation 2 time-steps later. The length of the tail of both markers is proportional to the speed. The coupling in the plot is $g_s = 0.08$

which means the coupling is excitatory. The equation of this model for these two chemically coupled limit cycle oscillators are:

$$
\begin{cases}
\dot{x}_m = & -\lambda(x_m{}^2 + y_m{}^2 - 1)x_m - (1 + \omega(x_m{}^2 + y_m{}^2 - 1))y_m \\
\dot{y}_m = & (1 + \omega(x_m{}^2 + y_m{}^2 - 1))x_m - \lambda(x_m{}^2 + y_m{}^2 - 1)y_m \\
\dot{x}_s = & -\lambda(x_s{}^2 + y_s{}^2 - (1 - \alpha H(x_m)))x_s - \\
& (1 + \omega(1 - \beta H(x_m))(x_s{}^2 + y_s{}^2) - 1))y_s \\
\dot{y}_s = & (1 + \omega(x_s{}^2 + y_s{}^2 - 1))x_s - \lambda(x_s{}^2 + y_s{}^2 - 1)y_s
\end{cases}
\tag{3.3}
$$

We use the subscript indices m and s for master and slave respectively. Indeed the equations for the master system (x_m, y_m) are the normal form for a nonlinear oscillator having a stable limit cycle of unit amplitude; the damping parameters λ and ω are positive. For the slave system (x_s, y_s) the coupling is introduced in such a way that both amplitude and period of the cycle of the excited system are smaller than those of the master system (right plot in Fig. 3.4).
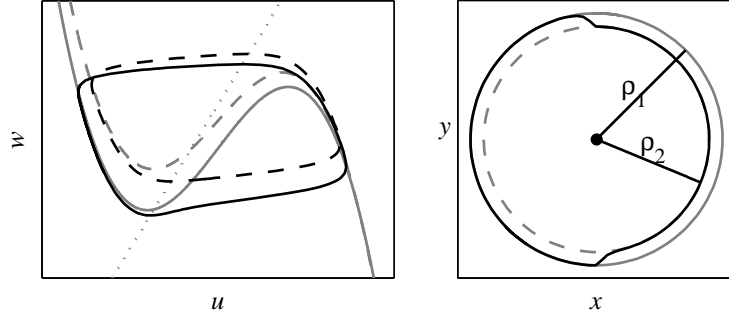
FIGURE 3.4: Limit cycles. *Left:* Solid lines correspond to the limit cycle (in black) and nullclines (in grey) of the autonomous FitzHugh-Nagumo oscillator with $I = 0.4$. Dashed lines correspond to the limit cycle (in black) and nullclines (in grey) of the FitzHugh-Nagumo oscillator when coupling with $g_s = 0.15$ is active (excited system). w-nullcline (grey, dotted) is identical for both situations. *Right:* The stationary trajectories of master and slave system in the model example. The master follows the solid grey circle and the slave follows the solid black trajectory and alternately jumps from limit cycle identical to that of the master to a smaller limit cycle corresponding to that of the excited system shown in dashed grey.

A change of coordinates to polar form with amplitude ρ and phase ϕ, simplifies the state equations:

$$
\begin{cases}
\dot{\rho}_m &= -\lambda(\rho_m{}^2 - 1)\rho_m \\
\dot{\phi}_m &= 1 + \omega(\rho_m{}^2 - 1) \\
\dot{\rho}_s &= -\lambda(\rho_s{}^2 - (1 - \alpha H(\cos\phi_m)))\rho_s \\
\dot{\phi}_s &= 1 + \omega(\rho_s{}^2 - 1)(1 - \beta H(\cos\phi_m))
\end{cases}
\tag{3.4}
$$

where the argument of the Heaviside function $H(\cdot)$ transforms as $x_m = cos(\phi_m)$, which shows clearly how the mode (excited or not) is controlled by the phase of the master system: for $\pi/2 \leq \phi_m < 3\pi/2$ the equations for the slave are equal for those of the master and for $\phi_m < \pi/2$ and $\phi_s > 3\pi/2$, the slave is in excited mode and has an extra term:

$$
\begin{cases}
\dot{\rho}_s = -\lambda(\rho_s{}^2 - 1)\rho_s, & \text{if} \quad \pi/2 \leq \phi_m < 3\pi/2 \\
\dot{\phi}_s = 1 + \omega(\rho_s{}^2 - 1)
\end{cases}
\tag{3.5}
$$

$$
\begin{cases}
\dot{\rho}_s = -\lambda(\rho_s{}^2 - (1 - \alpha))\rho_s, & \text{if} \quad \phi_m < \pi/2, \wedge \phi_m > 3\pi/2 \\
\dot{\phi}_s = 1 + \omega(\rho_s{}^2 - 1)(1 - \beta).
\end{cases}
\tag{3.6}
$$

One can consider the amplitude ρ_s separately from the corresponding phase ϕ_s since ϕ_s does not appear in the $\dot{\rho}_s$ equation in (3.4). Now, looking at (3.5), the influence of the coupling on the amplitude of the oscillations can be seen. When the coupling is off, the slave amplitude equation has two solutions: $\bar{\rho}_{su} = 0$, an unstable equilibrium point and $\bar{\rho}_{ss} = 1$, a stable limit cycle. These are the same as for the slave system. So in steady state, when there is no coupling ($\alpha = \beta = 0$), both systems eventually will move on the unit circle and – provided the parameters of both systems are identical – the phase difference is constant and will depend on the initial conditions. However with nonzero (but small; $\alpha < 1$) coupling, when the coupling is active, due to the extra term in (3.5), the solutions will be: $\bar{\rho}_{su} = 0$ and $\bar{\rho}_{ss} = \sqrt{1 - \alpha}$. So the limit cycle of the excited system will be smaller than that of the master, which confirms the hypothesis (Fig. 3.4).

When the coupling is nonzero, the slave will move on the black trajectory in Fig. 3.4. During most of the period the slave system moves on one of the limit cycles; either the one of the normal system, or the one of the excited system. There is some small transient period where it moves from one cycle to another. If the damping λ is large enough, these transitions will be short and the trajectory can be approximated by two half-circles of different radii. For definiteness we put $\beta = 2$.

To study the stability of ms-synchronization we look at the difference between the phases of the master and the slave system. Calling the phase difference between the two systems $\delta = \phi_s - \phi_m$, $\dot{\delta}$ follows as:

$$\dot{\delta} = \begin{cases} -\omega(\rho_m{}^2 - \rho_s{}^2), & \text{if} \quad \pi/2 \leq \phi_m < 3\pi/2 \\ -\omega(\rho_m{}^2 + \rho_s{}^2) + 2\omega, & \text{if} \quad \phi_m < \pi/2 \,\wedge\, \phi_m > 3\pi/2 \end{cases} \tag{3.7}$$

From the discussion above it follows that always $\rho_s \leq \rho_m = 1$, so during the left half of the master's cycle ($\pi/2 \leq \phi_m < 3\pi/2$), the derivative of the difference equations, $\dot{\delta}$, is negative or zero and the phase difference between the two systems can only *decrease* (i.e. the master will never be slower than the slave). During the other half of the master's cycle, the exact inverse will take place; $\dot{\delta}$ can only be zero or positive, so the slave will never be slower than the master. Furthermore, for a large enough damping λ, the transition phase between the excited and normal state in the slave can be neglected and the mean value of $\dot{\delta}$ is given by:

$$\bar{\dot{\delta}} = 2\omega(1 - \rho_m^2) \tag{3.8}$$

With the master system on a stable limit cycle; $\rho_m = 1$ the averaged value $\bar{\dot{\delta}}$ on the period of the master system equals 0, independently of the value of ρ_s. This illustrates the situation observed in simulations that the average phase difference between the two cells does not change over one period, in synchronized mode. Simulations of the model example shown in Fig. 3.5 illustrate this behavior of constant average phase-lag.

3.1.2   Spike detection and resonance

When the slave neuron from Fig. 3.1 is quiescent, the question of interest is whether it can act as a detector for incoming spikes. Of course, this is the situation that occurs most often in nature. It has to be admitted that in nature the number of presynaptic neurons is more often in the order of thousands than one single, but still the setup with one single neuron can explain most clearly many of the issues for the real situation with many presynaptic neurons. Once a setup for this effect has been established, it can be used to make a model for coincidence detection as outlined in Sect. 3.2.

There is a difference between the detection of a single incoming spike from a static situation, spike detection, and the following of a periodic signal from the master neuron. The latter phenomenon is called *resonance*, and is not considered synchronization, since one of the systems does not have an oscillation of its own [Pikovsky *et al.*, 2001, p. 15]. This resonance effect can be seen as an intermediate situation between spike detection and ms-synchronization.

The mechanism behind both spike detection and resonance can be understood in light of the discussion about the dynamic spike threshold in Sect. 2.3.2. The sudden activation of the coupling term is equivalent to the application of a current step, in which case spiking occurs when the dynamic spike threshold (cf. Fig. 2.9) is passed. The value of the coupling
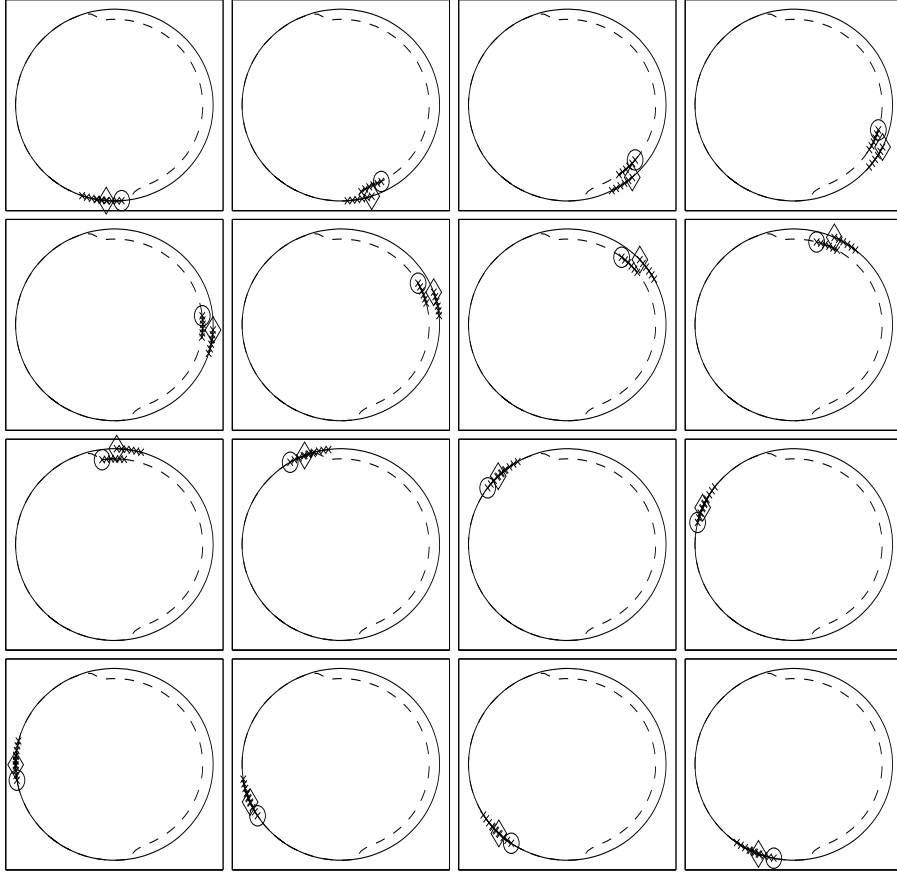
Figure 3.5: An outline of the model example moving in time. The sequence should be read from left to right and from top to bottom. The first plot shows the initial states of the master marked by a diamond and the current state of the slave marked by a circle. The states for the previous five time steps are also plotted as smaller crosses and form the "tail". Every next plot shows the states of the system one sixteenth period later. Parameter values are: $\alpha = 0.2$ and $\beta = 1.1$.

g_s above which an incoming spike induces a crossing of the dynamic threshold defines the critical coupling strength g_s^*. It is clear that due to the dynamic threshold, g_s^* depends not only on the neuron parameter values, but also on a possible offset in the input current.

The left part of Fig. 3.6 shows the spike train of the slave neuron for identical input spike trains for different coupling strengths. Complete resonance occurs for $g_s > 0.08$. The transition to the situation where there is no reaction in the slave neuron ($g_s < 0.06$) is not entirely instantaneous though, as would be the case if a bifurcation were involved in stationary mode. Instead it consists of intermediate states of $1/N$ resonance.

This effect of a non-smooth threshold is clarified when looking at spike detection, shown on the right-hand side in Fig. 3.6. What happens is that when the coupling strength is decreased, a delay in the reaction of the slave occurs. When the delay becomes so long (or the frequency of the master so high) that the slave is still refractory when the new incoming spike occurs, the slave starts missing spikes, causing a $1/N$-type synchrony.

Both effects are quantified in Fig. 3.7. The top graph shows the spiking frequency of the slave when the coupling strength is increased from zero. At a coupling strength of about 0.05 the slave starts to react to the incoming signal. It is not immediately able to follow the spikes from the master though. The reaction is very slow for low coupling
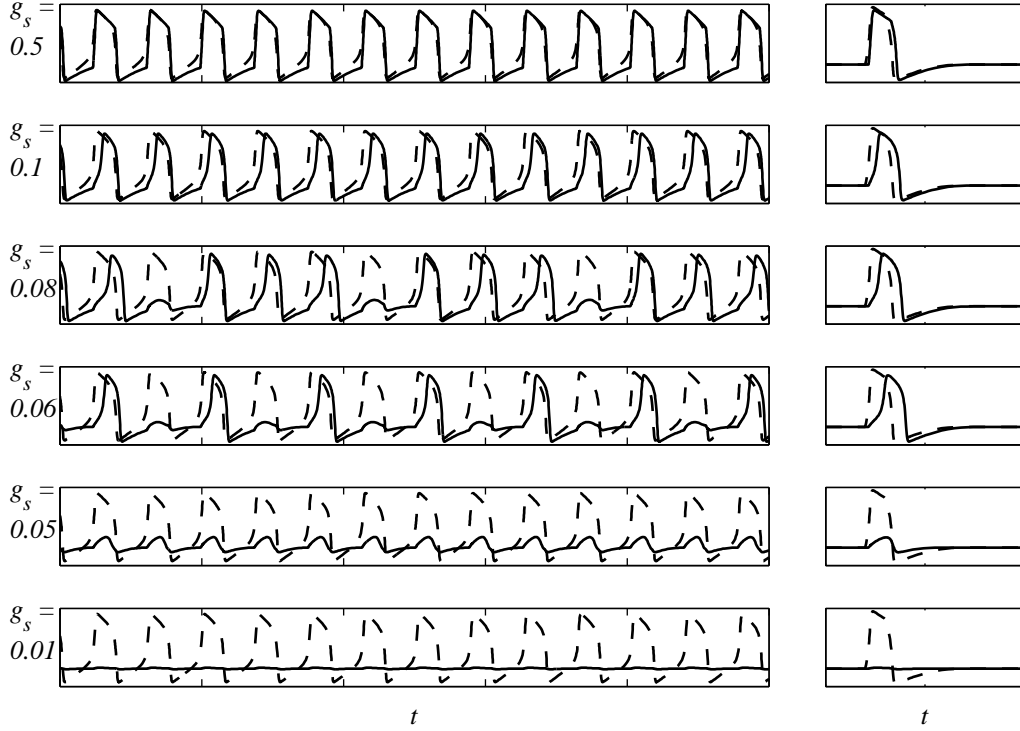
FIGURE 3.6: The influence of coupling strength g_s on spike detection in Fitzhugh-Nagumo neurons. The solid line u_m and the dashed line u_s. *Left:* slave signal when master is continuously spiking. *Right:* slave reaction on single spike from master. Parameter values in addition to standard values: $I_m = 0.6$, $I_s = 0$, $V_s = 2$, $\theta = 0$.

strengths, as can be seen from the bottom plot in Fig. 3.7, where the phase lag of the slave with respect to the master is plotted. For low coupling strengths the slave is unable to react on the next spike and the frequency of the slave will be below that of the master. This can again be seen in the upper plot, which has a small plateau at half the input frequency. Note also that the phase lag in the bottom plot only asymptotically reaches zero: the slave is always a little late in its reaction.

3.2 FITZHUGH-NAGUMO COINCIDENCE DETECTOR

Coincidence detection is the ability of individual neurons to detect the coincidence of spikes from different synapses. Individual coincidence detector neurons play a role in sound localization, especially in birds [Konishi, 1993].

A sound located straight in front of an animal will lead to signals from left and right ear arriving at the exact same time at both ears, whereas a sound coming from the left of the animal will reach the left ear slightly ahead of the right ear, due to the finite speed of sound. Coincidence detector neurons serve to distinguish between these different arrival times. If one now takes an array of such coincidence detector neurons, each connected to both ears with slightly different axon length, one can, through training, have this network detect surprisingly small differences in arrival times and thus locate the prey (or predator) with high precision. These networks have been found in the barn owl's auditory pathway by Carr & Konishi [1990]. Gerstner *et al.* [2000] show how an array of coincidence detectors
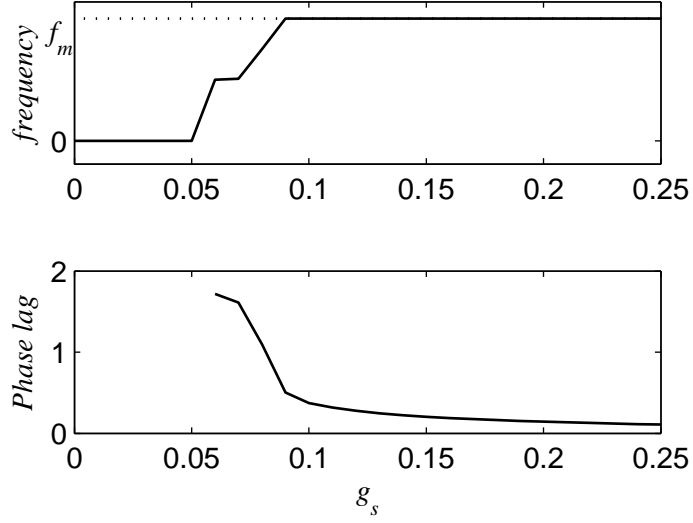
FIGURE 3.7: The effect of changing coupling strength on frequency and phase of slave neuron. *Top:* the spiking frequency of the slave (solid line) and the (constant) frequency f_m of the master (dotted line). *Bottom:* the phase lag of the slave with respect to the master in units of a spike width. Parameter values as in Fig. 3.6

can be trained with Hebbian learning to distinguish between spikes arriving with a high temporal resolution.

In this section a first attempt is made to setup the Fitzhugh-Nagumo model as a (simplified) coincidence detector. The idea is to set up a system of three chemically coupled Fitzhugh-Nagumo oscillators as shown in Fig. 3.2 such that the slave neuron reacts with a spike when the inputs from the two masters is coincident. The two inputs are considered coincident if the time difference between the two peaks of the spikes is within a certain fixed value, much smaller than the period (time between spikes) [Kempter *et al.*, 1998].

3.2.1 SETUP

The approach is to start from the results for spike detection: when two neurons are coupled as in Fig. 3.1 and the slave neuron is quiescent, the slave neuron can react on incoming spikes from the master neuron. For this to happen, the coupling strength g_s has to be larger than some threshold value called g_s^*. The mechanism behind spike detection was shown in Sect. 3.1.2 to be as follows: when the master oscillator crosses the threshold, almost immediately a current of $g_s(v_{post} - v_{syn})$ appears changing the nullclines instantly. The slave neuron therefore is no longer in equilibrium and either follows a subthreshold trajectory to the new equilibrium, or, if the difference is larger than g_s^*, emits a spike.

The idea behind a setup for coincidence detection with two master neurons (c.f. Fig. 3.2) is that now the slave oscillator should not react when only one of the masters is active, however if both couplings are active the slave oscillator should react with a spike.

The state equations for the three FitzHugh-Nagumo neurons coupled as in Fig. 3.2 are

$$
\begin{cases}
\dot{u}_{m1} &= u_{m1} - \dfrac{u_{m1}^3}{3} - w_{m1} + I_{m1} \\
\dot{w}_{m1} &= \phi\left(u + a - bw_{m1}\right) \\[2mm]
\dot{u}_{m2} &= u_{m2} - \dfrac{u_{m2}^3}{3} - w_{m2} + I_{m2} \\
\dot{w}_{m2} &= \phi\left(u + a - bw_{m2}\right) \\[2mm]
\dot{u}_{s} &= u_{s} - \dfrac{u_{s}^3}{3} - w_{s} + I_{s} - g_{s,m1}S\left(u_{m1}\right)\left(u_{s} - V_{syn,m1}\right) \\
& \quad - g_{s,m2}S\left(u_{m2}\right)\left(u_{s} - V_{syn,m2}\right) \\
\dot{w}_{s} &= \phi\left(u + a - bw_{s}\right),
\end{cases}
\tag{3.9}
$$

where, as before, the indices m and s denote the master and slave neuron, and the masters have an extra index that enumerates the two.

If the coupling strengths $g_{s,m1}$ and $g_{s,m2}$ are put a little below the value of g_s^* for spike detection, a single input will not yield any reaction in the slave system. However, two simultaneous inputs *will* do so since the coupling term $(u_s - V_{syn,mi})$ will occur twice in the slave equations in (3.9) and have double impact. If the spikes are exactly coincident and the parameters of the coupling are identical for both synapses, this combined coupling can be seen as a single one with strength $g_{s,tot} = g_{s,m1} + g_{s,m2}$. So coincidence detection will work if we take the coupling such that $g_{s,tot} > g_s^* > g_{s,m1}, g_{s,m2}$. This same reasoning applies if the coupling parameters are not equal, but similar (i.e., same type of coupling; excitatory or inhibitory and approximately same threshold in S).

3.2.2 SIMULATION RESULTS

We simulated system (3.9) with the standard parameter values for the FitzHugh-Nagumo cells and the standard values for the FTM coupling (cf. Sects. 2.3 and 2.5). Also, both synapses are identical: $V_{s,m2} = V_{s,m2} = V_s$. As will be clear from the results and the discussion on spike detection, what matters is the total coupling felt by the slave at the moment of the coincidence, which is

$$
-g_{s,m1}(u_s - V_s) - g_{s,m2}(u_s - V_s) = -(g_{s,m1} + g_{s,m2})(u_s - V_s) \tag{3.10}
$$

so the value of the individual coupling strengths do not matter, as long as $g_{s,mi} < g_s^*$ for both synapses. Without loss of generality, we therefore take $g_{s,m1} = g_{s,m2} = g_s$.

Simulation results for a value of $g_s = 0.03$ are shown in Fig. 3.8. This value of the coupling strength results in a total coupling of 0.06 – a value for which spike detection works with our standard model parameter values (see Fig. 3.6). As can be seen from Fig. 3.8, the coincidence detection works well. Single spikes are ignored almost completely by the slave neuron, whereas coincident spikes are reacted upon with a spike.

In this case we chose a coupling value of 0.03, this value is robust to noise though. The range of coupling values for which this setup works is quite large; from about $g_s = 0.026$ up to $g_s = 0.05$. This confirms the earlier claim (Sect. 3.1.2) that with FTM coupling the exact coupling value is not important, which is a plausible situation in the context of neuroscience, where factors as noise and variation in parameters, both in the system and in the outside world, are often very strong. The (possibly even positive) influence of noise is the subject of the next section (3.2.3)
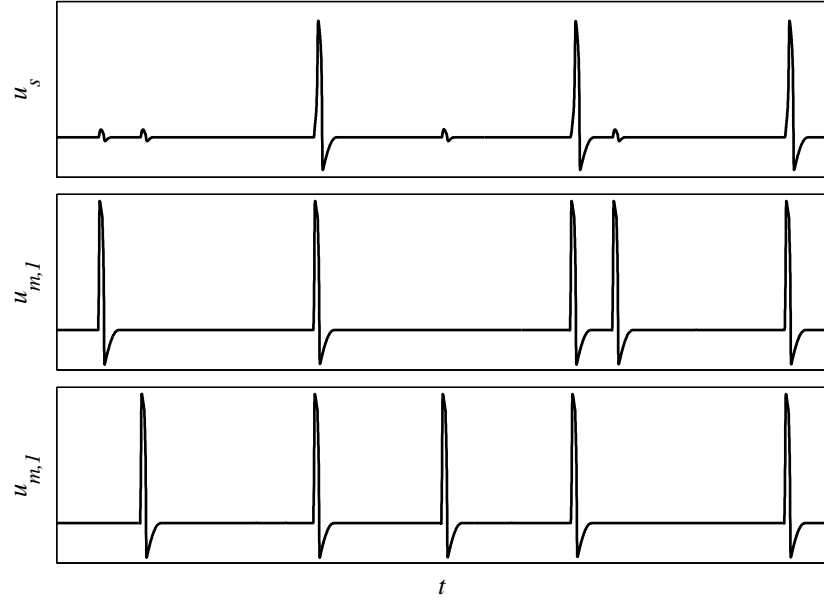
FIGURE 3.8: Simulations of a FitzHugh-Nagumo coincidence detector (cf. Fig. 3.2). $g_s = 0.03$, other parameter values standard values (2.7).

This flexibility in the value of the coupling strength makes the coincidence detection as such very robust, however it also allows a fine-tuning of the *sensitivity* of the coincidence detection. It turns out that within the range of coupling strengths for which the coincidence detection works, changing it slightly will make the detection more or less sensitive to the exactness of the coincidence. Increasing the coupling strength causes spikes that overlap less precisely to be detected as well and decreasing the coupling strength makes the coincidence detection more sensitive up to the point where it collapses altogether and the slave remains silent.

This effect can be clearly seen from simulations when the two master neurons are put in periodic spiking regime with slightly different frequencies. This causes a *beat phenomenon*; the two cells will periodically spike in and out of phase with each other, much like the church bells of two different churches on Sunday morning. In figure 3.9 simulations of the slave neuron for different coupling strengths are shown in the top four figures. For low coupling strength the slave neurons does not react. Then, when the coupling is increased, the slave neuron begins by emitting a spike only for exact coincidences. When the coupling is increased even further, also less exact coincidences are detected.

Figure 3.10 shows the time window within which two spikes are detected as coincident as a function of g_s. For coupling strengths larger than $g_s = 0.045$ the coincidence detection will stop working and $\Delta t_{max} = \infty$. This effect shows that the coupling strength, i.e., the synaptic weight, directly tunes the sensitivity of the coupling. Therefore, a scheme like that outlined in Gerstner *et al.* [2000], where the difference in axon length is used to tune the array of coincidence detectors, could perhaps be made even simpler, by using a differential scheme and tuning the coupling strength directly.
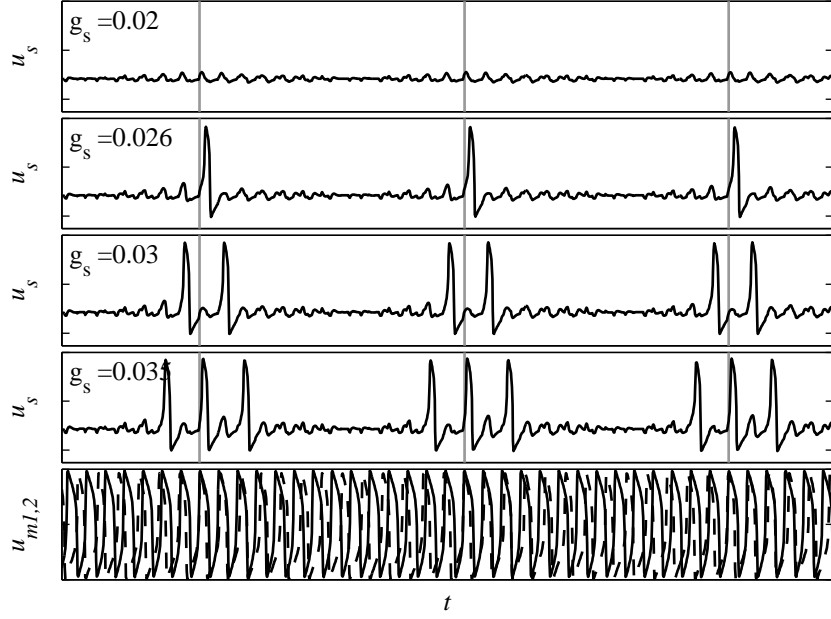
FIGURE 3.9: The influence of coupling strength g_s on coincidence detection in Fitzhugh-Nagumo neurons. Top four figures: slave output. Bottom: master signals.

3.2.3 THE INFLUENCE OF NOISE – FROM DESTRUCTIVE TO PERFORMANCE-IMPROVING

All real-world systems are subject to noise and neurons are certainly no exception to this rule. Usually in science and engineering noise is a nuisance; something that deteriorates or prevents altogether the proper functioning of the system, since it contains no information itself and will get in the way of the information transmitted by the system.

In neuronal measurements – *in vitro* and *in vivo* alike – noise always seems to be present. However, as long as we have not cracked the neural code and we do not know how neurons transmit information, we cannot decide if what we consider noise actually contains information. Furthermore, even if we can decide that this noise contains no information, it is often not clear if it is proper to the brain or if it comes from the measurements themselves. There is evidence that a noisy environment increases the reliability of spike

FIGURE 3.10: Time window for coincidence detection as a function of g_s. The vertical axes is the maximum difference in arrival time between spikes in the two masters for which the slave neuron emits a spike

50

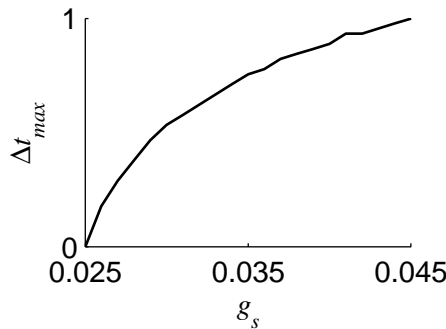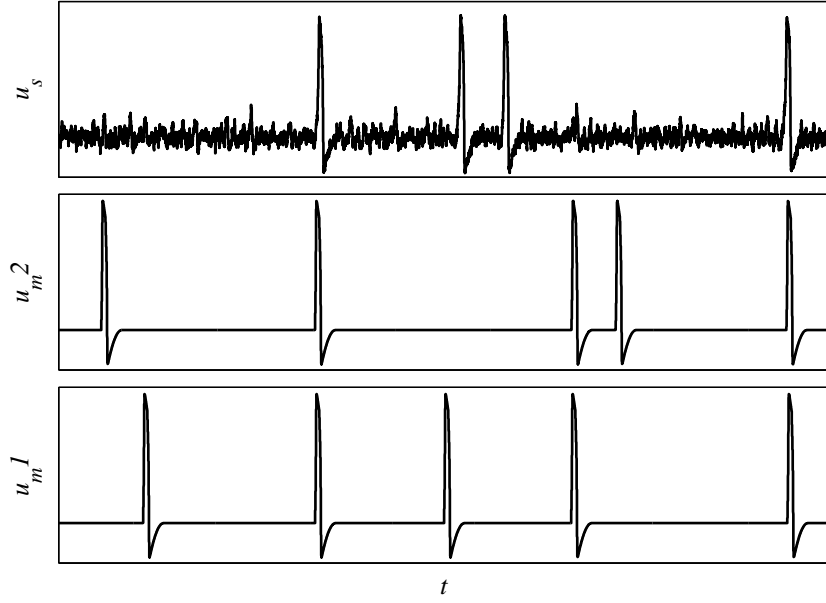FIGURE 3.11: Coincidence detection for sub-threshold coupling value in the presence of Gaussian noise. Coupling $g_s = 0.021$, noise variance $\sigma = 0.35$ rest of the parameters as in Fig. 3.8

transmission [Mainen & Sejnowski, 1995]. On the other hand in-vivo neurons often produce irregular spiking behavior in the absence of any structured input [Softky & Koch, 1993].

The aim of this short section is not to contribute to the question whether noise is or is not used by the brain in a constructive way, or even to take a stand point on this matter, but rather to both illustrate that the performance of the coincidence detection presented before is not considerably worsened by the possible presence of noise, and to show that it can even, in some cases, profit from its presence through a phenomenon known as *stochastic resonance.*

Stochastic resonance, or, more exactly, noise-enhanced threshold detection, is the phenomenon in bistable or threshold systems that the addition of noise can increase the sensitivity of the system [Gammaitoni *et al.*, 1998]. Subthreshold signals that in the noise free case would never exceed the threshold and thus yield no reaction whatsoever can, in the presence of noise, lead to a response.

We show stochastic resonance in the coincidence detector (3.9) by lowering the coupling strength below the critical value (see Fig. 3.9). To simulate the presence of noise, a noise current is added to the input of the slave neuron. The noise is zero mean Gaussian noise. All other parameters are identical to the ones used before.

As an example Fig. 3.11 shows the same plots as for the noise free case (Fig. 3.8) when a white Gaussian noise current with a standard deviation of $\sigma = 0.35$ is injected into the slave (added to the $\dot{u}_s$ equation in (3.9)) and the threshold is lowered to the subcritical value $g_s = 0.021$. As can be seen from Fig. 3.8, for this value of the coupling strength the coincidence detection does not at all work without noise. The threshold for the working of the coincidence detection is therefore lowered by the noise, hence the term enhanced threshold detection.

Obviously the addition of noise improves the performance of the system, since now two of the three coincidences are detected. A difference with the noise free case is that

now the detection, if it works, is no longer perfect: the second coincidence in Fig. 3.11, is missed. Before, for supra-critical coupling values the coincidence detection was perfect, but now, as a price to pay for the enhanced threshold detection, some of the coincidences are missed as well. Even for super-threshold coupling values.

Additionally the presence of noise might cause spontaneous spikes, like the third spike of the slave in Fig. 3.11. In this case this is really a spontaneous spike, and can be easily filtered out, however the occurrence of spontaneous spikes is often caused by one of the master neurons spiking, thus creating a more grave error in the coincidence detection.

A MEASURE FOR THE PERFORMANCE OF THE COINCIDENCE DETECTOR

Since in the noisy case the performance of the system is no longer either perfect or zero, we need a measure to quantify the performance of the coincidence detector and compare it to the noise-free case. Our measure should count the number of coincidences and at the same time penalize spurious spikes – otherwise the perfect coincidence detector would be one that continuously emits spikes.

We introduce the *reliability factor* Γ, inspired on the Coincidence Factor introduced by Kistler *et al.* [1997] – which is not, as the name would suggest designed for coincidence detection, but as a measure for reliability of spike trains – but adapted for coincidence detection. It is calculated as follows:

$$\Gamma = \frac{1}{\mathcal{N}} \frac{S_{det} - \langle P_{det} \rangle}{\frac{1}{2}(M_{coinc} + S_{tot})}. \tag{3.11}$$

In (3.11), S_{det} is the number of coincidences correctly detected by the slave neuron, S_{tot} the total number of output spikes in the slave neuron, i.e., the detected spikes plus the spurious output spikes due to noise. M_{coinc} is the number of actual coincidences between the spikes of the masters – the number of coincidences to be detected.

The factor $\langle P_{det} \rangle$ is designed to compensate for the fact that even a purely random spike generator could get some of the coincidences right. It is the number of coincidences that would be correctly detected by a Poisson process which has a rate equal to the rate of the slave neuron. This number is not necessarily integer and can be calculated directly as $\langle P_{det} \rangle = \nu \Delta M_{coinc}$ with ν the rate of the process and Δ the time window for which a spike is considered correctly detected. Here we use a value of 10 time steps for Δ, which, in the case of a FitzHugh-Nagumo neuron, corresponds roughly to the width of one spike. Although results do depend on the value of Δ, this dependence is not strong as long as Δ is chosen within a range of 1–2 times the width of a spike [Jolivet, 2005; Kistler *et al.*, 1997]. Finally a normalization factor $\mathcal{N} = 1 - 2\nu \Delta$ is added to set the maximum of Γ at unity.

Note that the value of Γ can become negative in theory. This happens when there is some negative correlation between the coincidences and the detection, i.e., when the detector performs worse than a random Poisson process would do. Inhibitory coupling would accomplish this for example.

Example 1. *As an example we calculate the reliability factor for the coincidence detection shown in Fig. 3.11. Note however that this is only for illustration purposes. To account for the randomness in the system we would need a much longer recording to get a realistic estimate of Γ.*

The number of coincidences correctly detected by the slave neuron is $S_{det} = 2$. The total number of coincidences in the recording is $M_{coinc} = 3$. The total number of output spikes

in the slave neuron is $S_{tot} = 3$. Finally, we take $\Delta = 10$, so the number of spikes that would have been detected by a Poisson process of rate $\nu = 3/1800 = 0.0017$ is $\langle P_{det} \rangle = 0.1$, so for this case the coincidence factor $\Gamma = 0.6552$.

This nonzero value of Γ confirms that the addition of noise improves the performance of the system, since without noise, for the same value of g_s, the slave neuron will remain without output spikes and thus $S_{det} = 0$ and $\Gamma = 0$.

SIMULATION RESULTS

We already showed that the addition of noise makes the coincidence detector respond to input signals, even if the coupling is too weak to yield any reaction in the noise-free case. It can even be concluded from Fig. 3.11 that this reaction is not completely random and that, when the measurement is longer to introduce redundance, a fairly good decision can be made about, for instance, the coincidence rate in the master signals.
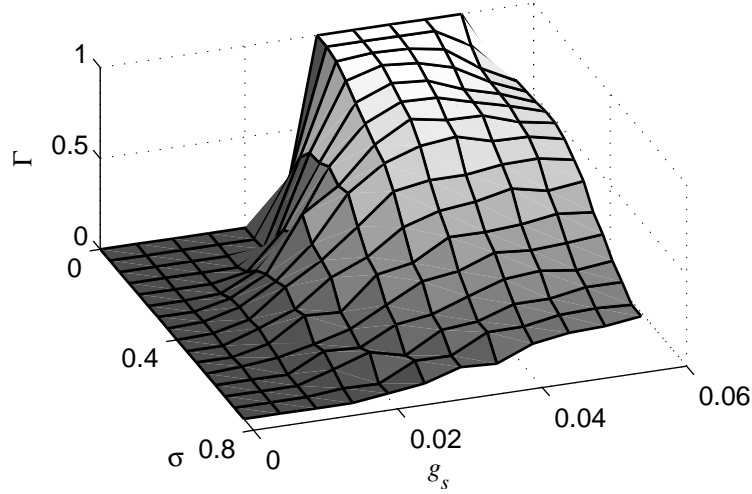

FIGURE 3.12: Reliability of coincidence detection in a noisy environment; $g_s^* = 0.025$.

To quantify this feeling Fig. 3.12 shows the reliability factor Γ (3.11) as a function of both the coupling strength and the noise level. For every point in the graph we did 10 simulations of $10'000$ time steps of (3.9) with the additional noise current described above. Each of the masters would fire randomly with a rate of once every 150 time steps on the average, which, in the unscaled FitzHugh-Nagumo system (3.9) corresponds to roughly 15 spike-widths.

On the high g_s side of the Fig. 3.12 the spike threshold for a single spike is exceeded, which degrades the performance. For a reasonably large range of g_s below that value, the system performs best (perfect) when no noise is present; any noise will decrease the performance, but for lower values of the coupling strength the performance suddenly falls to zero when arriving below the critical coupling. When noise is added, Γ is still positive, and even quite acceptable, for values below the critical coupling, but never reaches unity, even for $g_s > g_s^*$.

This effect of noise-enhanced threshold detection can clearly be seen from Fig. 3.13, where left and right plot show projections on the (g_s, Γ) plane and the (σ, Γ) plane of Fig.3.12 respectively. Whereas for values below $g_s = 0.025$, the reliability is zero in the noise-free case, it can attain values as large as 0.65 when noise is added. The solid line

in the right-hand plot shows the typical curve associated to Stochastic Resonance: for sub-critical coupling values, the performance is a concave function of the noise level and attains an optimum for a non-zero noise level. The right-hand plot also shows that for super-critical coupling values noise always worsens the performance.
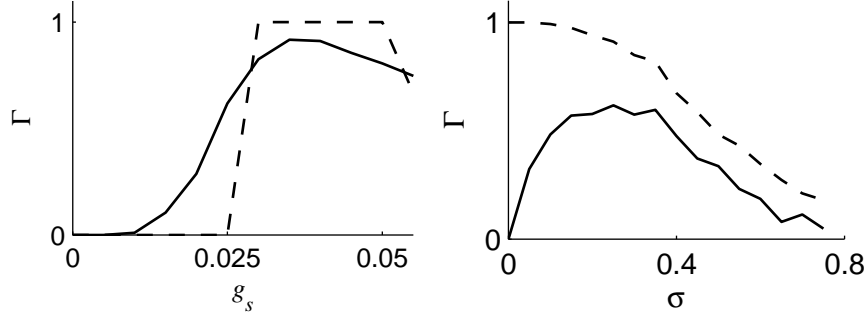

FIGURE 3.13: Stochastic Resonance and performance deterioration due to noise. *Left:* Noise enhanced-threshold for sub-critical coupling values (Stochastic Resonance), dashed line: no noise, solid line: $\sigma = 0.25$. *Right:* Stochastic resonance (solid line, $g_s = 0.025$) and degradation of reliability due to noise (dashed line, $g_s = 0.04$) for super-critical coupling value.

3.3   THE FITZHUGH-NAGUMO COINCIDENCE DETECTOR IN A REALISTIC CASE STUDY

As the previous sections show, the Fitzhugh-Nagumo model can be used successfully in situations where precise timing of spikes is to be detected. The question whether spike timing does in fact represent information in the brain is still an open one and if it does not, indeed, even simpler models than the ones treated in this work might suffice to describe the essential behavior of neurons.

As said before, we will not go into the question whether spike-timing in general plays a role in the neural code. In any case, even today most scientists agree on a few specific cases known where spike timing has been proven to play an important role and in this section we will use one of these neural systems – the auditory pathway in birds – to study the performance of the FitzHugh-Nagumo system in a more realistic setting.

It is known from biology that some birds, especially hunters, are able to locate other animals – prey in the case of hunting birds – with an astonishing precision, purely from the sound they make. The barn owl for instance, which is the subject of our case study, can locate a sound source in the horizontal plane with a precision of about 1–2 degrees [Knudsen *et al.*, 1979]. Since the bird uses the interaural time difference (ITD) – the phase difference between the sound arriving at the left ear and the sound arriving at the right ear due to the finiteness of the speed of sound in air – the system that processes the information must be capable of handling speeds in the microsecond range. Knowing that an excitatory postsynaptic potential (EPSP), even though neurons in these birds' brains are especially rapid, still lasts around a millisecond, and that the inter spike interval is at least a couple of milliseconds, this is quite an astonishing performance [Carr & Konishi, 1990; Reyes *et al.*, 1994] and one may wonder how it can be attained with relatively slow neurons.

We begin this section with a very brief overview of the neuronal system that is able to treat this microsecond information. For a more detailed review, see the article with the

original idea by Jeffress [1948], and the article by Carr & Konishi [1990]. The work in this section is inspired by the study done by Gerstner *et al.* [1996a, 2000] for integrate-and-fire neurons. See these references and the chapter on plasticity and coding in Gerstner & Kistler [2002] for a more detailed explanation of the setup.

In Sect. 3.3.3 we present a simulation of a coincidence detector in the barn owl's auditory system using Fitzhugh-Nagumo neurons. The basic framework for building the model is the one presented in Sect. 3.2. We analyze the performance of the coincidence detector in terms of temporal precision and robustness to noise influences and compare the results to those of Gerstner *et al.* [1996a, 2000] where appropriate.

3.3.1 Overview of the system to be modeled

The neurons in the auditory pathway of birds are specialized for sound localization and are very fast. Due to a special outward rectifying current, their effective membrane time constant can be as low as 0.1 ms, which is at least a factor 100 lower than that of mammalian cortical neurons [Destexhe *et al.*, 1996]. However this is still an order of magnitude *larger* than the temporal precision necessary for sound localization. A possible solution to this enigma is the model proposed by Jeffress [1948].

Jeffress's model for sound localization

For sound localization an animal needs the difference in phase between a signal coming from a single sound source arriving at the left and the right ear. The way Jeffress proposes to transmit and process this information is through an array of delay lines with phase-locked spikes that are connected to coincidence detectors. Figure 3.14 shows the model schematically.

Each coincidence detector is sensitive to zero phase difference between incoming signals. This will be the case if the interaural phase difference is compensated by an equal and opposite difference in transmission delay in the path from each ear to the coincidence detector. Each coincidence detector has its own specific difference in path length between signals from left and right ear and is thus sensitive to a specific phase lag in the incoming signal. For instance neuron 1 will react when sound arrives at the right ear first since the wavelength from the left ear is much shorter.
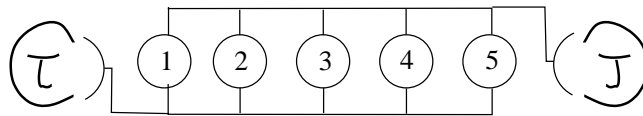
FIGURE 3.14: Jeffress's model for sound localization. In this schematic representation sounds arriving from left and right ears are led to an array of five coincidence detector neurons labeled 1–5.

When a sound arrives at the ear of the animal it will have a certain phase with respect to the sound source. When the sound source is not exactly in front, the phase difference between both ears is nonzero, due to the ITD. Neurons connected to the ear of the animal are able to preserve this phase information and to transmit it to an array of coincidence detectors.

The neurons that connect the ears to this array transmit the information through their axons, which have a certain transmission speed. Each of the coincidence detectors in the array gets its information from a neuron with an axon with slightly different length. In
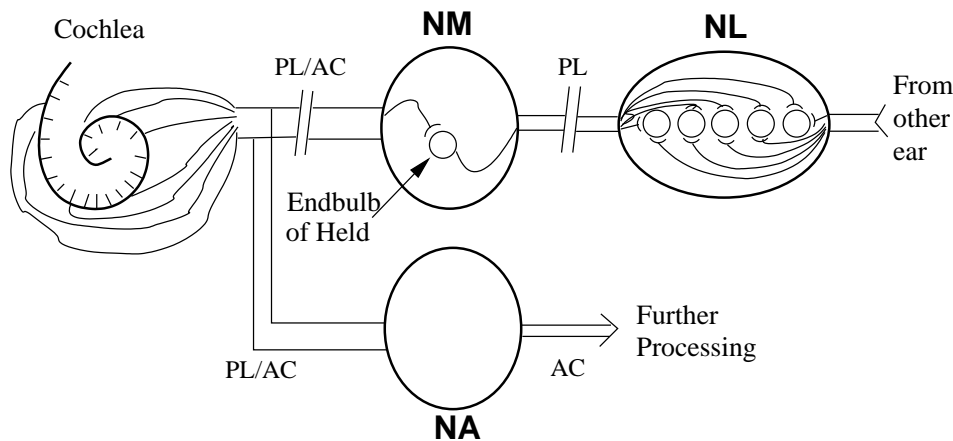
FIGURE 3.15: Schematic overview of one side of the barn owl's auditory pathway. Sounds are coded into phase locked (PL), amplitude coded (AC) spikes by the auditory nerve afferents from the cochlea. They are transmitted to the nucleus magnocellularis (NM), where the phase locking is reinforced in the specialized endbulb of Held synapses. The phase locked spikes are further transmitted to the nucleus laminaris (NL), where coincidence detection is performed. A symmetrical pathway arrives from the other ear in the NL. In a parallel fashion the phase locked and amplitude coded spikes are transmitted from the cochlea to the nucleus angularis (NA), which codes for changes in amplitude.

this way, each of the coincidence detectors, which in itself is only capable of detecting synchrony, i.e., zero phase difference, is sensitive to a different ITD.

In the *tabula rasa* situation, in the animal's brain each element in the array gets input from many neurons with slightly different axon lengths. Through training, the synapses of the neurons with the right axon length can then be reinforced, whereas those of the neurons with the wrong axon length can be made zero. In this way we have a system for coincidence detection that can be tuned by experience [Gerstner *et al.*, 2000].

THE AUDITORY PATHWAY OF THE BARN OWL

The architecture of the auditory pathway of the barn owl corresponds surprisingly well to Jeffress's model (or rather vice-versa). We give a very brief overview of this system. For more information see Carr & Konishi [1990] and references therein.

Figure 3.15 shows a schematic overview of the barn owl's auditory pathway. When a sound arrives at the ear of the animal it is first separated into discrete frequency bands in the cochlea. Hereafter we focus on the pathway of a sound of one single frequency. For every frequency band a parallel system exists.

Once separated into frequency bands in the cochlea, the information about the phase of the signal is preserved by hundreds of neurons connected to the hair cells tuned for that specific frequency. These neurons phase lock onto the signal: the firing times of a neuron tend to occur with higher probability around a certain phase of a modulating signal. Because this is a statistical effect, it is hard to determine from a single recording, but the sum of the activity of many neurons will show a clear pattern; this can be seen in Fig. 3.16, which illustrates the principle of phase locking.

The chemical synapses at the hair cell receptors also code for amplitude by increases in spike rate. The phase locked and amplitude coded spikes are transmitted along the auditory nerve to the nucleus angularis, which, unlike the name suggests, only codes for amplitude, and to the nucleus magnocellularis, which reinforces the phase locking, in
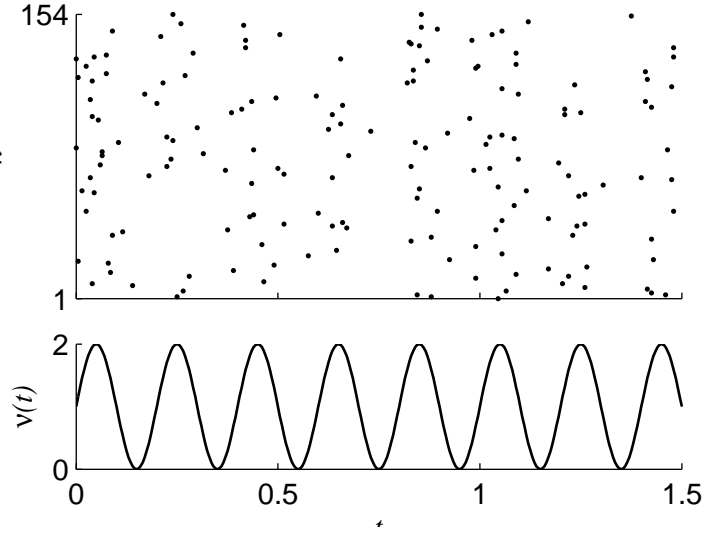
FIGURE 3.16: Phase locking. The spike times of 154 presynaptic neurons (top) and the amplitude of the input tone (bottom) for 1.5 ms of simulation of the system presented in Sect. 3.3.2.

parallel. In the nucleus magnocellularis the spikes are relayed in the endbulb of Helm, which is a highly specialized synapse that is able to preserve the phase locking.

The spikes are then transmitted further to the nucleus laminaris. The nucleus laminaris has an anatomy equivalent to the array described in Jeffress's model. There are regular changes in delay in axons with the depth into the nucleus laminaris. This whole pathway exists twice in the barn owl's brain: once for each ear and both pathways come together in the nucleus laminaris. The nucleus laminaris serves as the coincidence detector array in Jeffress's model. It will give a precise estimate of the ITD in the way Jeffress describes.

Finally the information for that specific frequency band is combined with that of other frequencies to obtain a more robust system and to resolve ambiguities.

3.3.2 METHODS

Our goal is to simulate one coincidence detector from the array in the nucleus laminaris in Fig. 3.15. The idea is to use the master-slave setup presented in Sect. 3.2, but to take many masters instead of just two. We take 154 master cells, of which half has phase preference zero and the other half, representing the input coming from the other ear, phase preference $\phi \in (0, \pi)$. Each of the masters will spike with highest probability around its preferred phase as outlined in Fig. 3.16.

The FitzHugh-Nagumo model does not have an absolute time scale, so an estimate has to be made of the scaling of the time axis. From investigations by Carr & Konishi [1990] we know that the fast neurons of the nucleus magnocellularis that transmit the signal to the coincidence detector have a spike width of less than 0.3 ms. In the simulations we fixed the timescale to 50ms^{-1}. This value corresponds to a membrane time constant of roughly 0.1 ms (see Sect. 2.3), which is the same value as the one taken in [Gerstner *et al.*, 2000]. Note that these values are a fairly arbitrary choice, that suffices for the purpose of illustrating the principle.

The spike times of the masters are obtained from a nonhomogeneous Poisson processes with a sinusoidal rate function with a frequency corresponding to the frequency of the channel we consider (5 kHz and 1 kHz). The nonhomogeneous Poisson process is simulated

57

by Lewis's method of thinning [Lewis & Shedler, 1978]. We then generate a vector $\mathbf{w}$ of the 154 values for the coupling strength of the synapses with a Gaussian distribution around the mean $\langle w \rangle$ and a standard deviation of 10% of the mean.

To simplify the computations we do not simulate all 154 masters, but make use of the threshold nature of the FTM coupling, which, especially when the sigmoidal function is taken to be the Heaviside function, only transmits information about the timing of the spike and discards any information about spike-form and sub-threshold membrane potential. This means that a spike in the master will always cause the same reaction (EPSP) in the slave and that we can compute a template for synaptic current that elicits the EPSP, which we will call $P(\cdot)$. We then simply have to sum over all spike times for all masters multiplied by the vector of the synaptic strength $\mathbf{w}$, to obtain the total coupling signal into the slave neuron:

$$z_s(t) = \sum_i w_i \sum_f P(t - t_i^{(f)}), \tag{3.12}$$

where $t_i^{(f)}$ is the fth firing time of the ith neuron.

When we take the limit of $k \to \infty$ in the coupling function (2.38), it reduces to the Heaviside step-function and the template P for the EPSP caused by a spike can easily be calculated. It is depends on the coupling function S in the following way:

$$P(t) = S(t) - S(t - t_s), \tag{3.13}$$

where $S(t)$ is defined as:

$$\begin{cases} S(t) = 0, & \text{for } t < 0, \\ S(t) = 1, & \text{for } t > 0. \end{cases} \tag{3.14}$$

The resulting synaptic current is a unity amplitude block wave of length equal to the time the coupling variable of the master is larger than coupling threshold θ. Since we take $\theta = 0$, which is considerably larger than the spike threshold of the model, the coupling is only on during a spike and, since the spike form is to a large extent independent of other parameters, we can take it constant. From test simulations we measure it to be $t_s = 0.2\,\text{ms}$; equal to the spike-width, which we (purposely) evaluated at this threshold.

The width of the elicited EPSP turns out to be about the same as the one taken in Gerstner *et al.* [2000]. However in our case it follows directly from the spike width of the presynaptic neuron, whereas for the Spike Response Model – that models neither phenomenon implicitly – taken in Gerstner *et al.* [2000] both values have to be fixed separately.

Once the spike times of the masters have been simulated and total synaptic current has been calculated, the slave can be simulated with the synaptic current as external current.

3.3.3 Simulation results

The time constant of the each of the 154 single masters, although much higher than that of a typical cortical neuron, is still in the order of milliseconds. Furthermore the phase locking of these individual neurons has a temporal jitter due to the fact that the locking is governed by a modulated Poisson process (cf. Fig. 3.16). Still, the sum of the synaptic currents of the 154 neurons shows a clear phase locking to the 5 kHz driving signal as can be noted from the short piece of a simulation run shown in Fig. 3.17.

This phase modulation of the coupling signal causes the coincidence detector to fire, with high probability, close to the maximum of the driving signal. Due to the speed
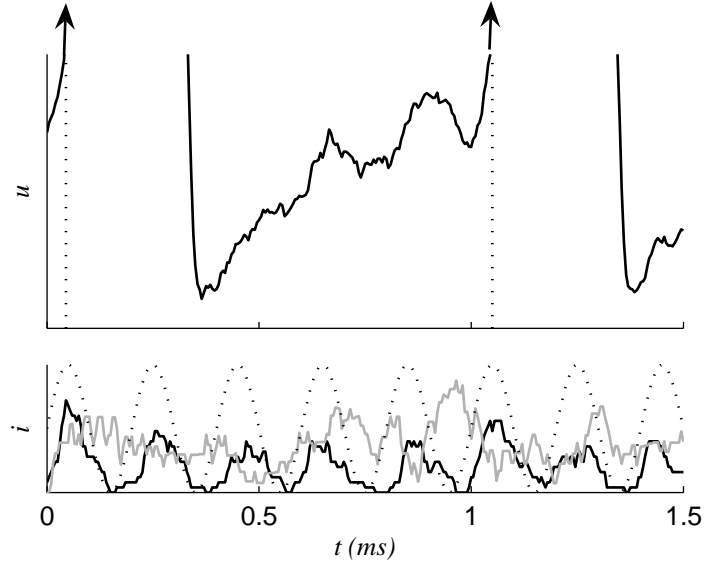
FIGURE 3.17: Integration of the summed synaptic currents. *Top:* The membrane potential of the FitzHugh-Nagumo slave neuron for 1.5 ms of simulation with two spikes (indicated by arrows and a dotted line to allow a zoom on the sub-threshold voltage). *Bottom:* The total coupling signal, as experienced by the slave cell, which is the sum of the synaptic currents of the individual masters. The solid black line is for $\delta\phi = 0$ and the grey line for $\delta\phi = \pi$. The dotted line indicates the 5 kHz driving signal.

limitations of the neuron this does not happen each period of the driving signal, but it does happen with an amazing accuracy. Figure 3.18 shows phase histograms of the spiking in the coincidence detector. The phase histograms are drawn with respect to the phase ϕ of the driving signal, with maximum at $\phi = 0$, the driving signal being $\cos(2\pi f t)$ with $(f = 1/T)$.

From Fig. 3.18 it can be seen that there is a delay in the reaction time of the coincidence detector, which becomes apparent for the 5 kHz tone. This delay gives a limit on the temporal precision that can be attained.

It was already shown that the reaction time of a FitzHugh-Nagumo spike detector depends on the total experienced coupling strength (see Figs. 3.6 and 3.7). This effect can also be observed for the coincidence detector in this case study. Figure 3.19 shows the relation of the delay and the precision in the coincidence detection to the average coupling value $\langle w \rangle$. For the response delay the same behavior is observed as in the spike detection case: for weak (average) coupling, the delay is higher and then it settles to an asymptotic value. In this case the minimum delay is about 0.11 ms.

Figure 3.19 reports the width of the peak as a function of the delay for two different choices of $\langle w \rangle$. A change in the width of the peak could possibly be detected. For low $\langle w \rangle$ the optimal precision is actually attained at nonzero phase difference. This effect is persistent for both frequencies, though much more apparent for the low tone.

The difference in peak width shown for the 1 kHz tone permits a good location of the phase difference. For the 5 kHz tone the detection will fail since the width of the peak in the spike histogram is constant for a large range of phase differences. Part of this failure to arrive at the same speed as the real neurons and integrate-and-fire models do can be explained in the light of the discussion in Chap. 5 about the degrees of freedom in the
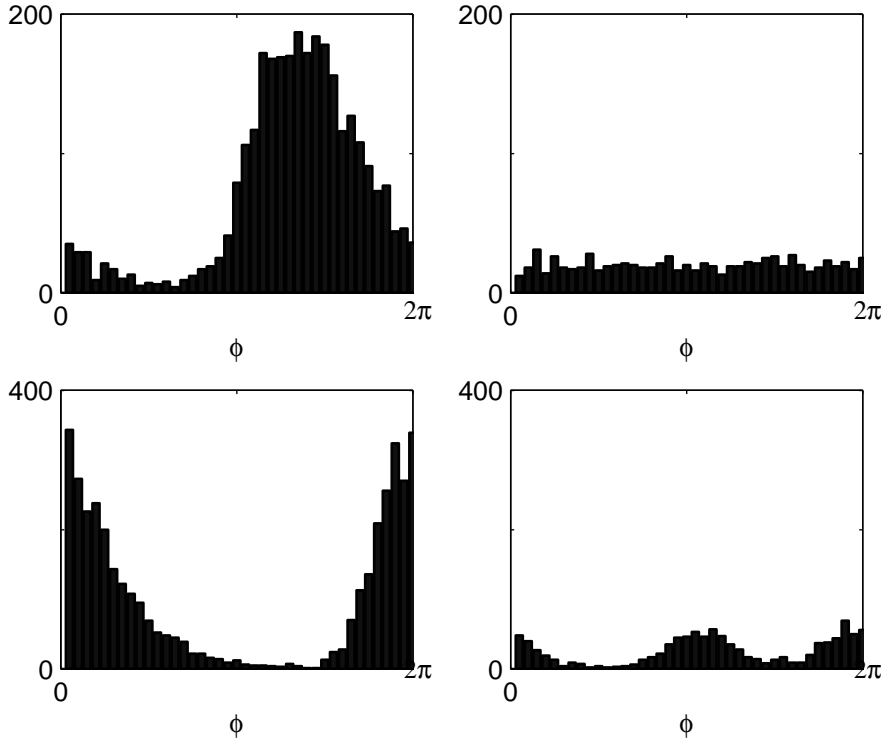
59

FIGURE 3.18: Phase histograms of output spikes. *Top left:* No interaural phase difference, 5 kHz tone *Top right:* Maximum interaural phase difference (π rad; 5 kHz tone). *Bottom left:* No phase difference, 1 kHz tone *Bottom right:* Maximum phase difference, 1 kHz tone. Average coupling strength of the 154 masters $\langle w \rangle = 0.010$.

FitzHugh-Nagumo model. We fixed the spike width, thus fixing entirely the dynamics of the model. Parameter ϕ then determines the speed of the model. Decreasing, while maintaining the spike width constant by adapting the time scale should improve the results. This shows that the standard choice in literature of parameter values for the FitzHugh-Nagumo can be criticized. More on this in Chap. 5.

3.3.4   DISCUSSION

The FitzHugh-Nagumo model can successfully be employed to model a coincidence detector in the barn owl's auditory system. Although the speed limitations of an individual neuron prevents it to follow a 5 kHz signal, the use of many neurons in parallel, followed by a coincidence detector gives the desired temporal precision necessary for successful sound localization.

This case study shows a situation where the FitzHugh-Nagumo model basically works like an Integrate-and-Fire neuron. This integrate-and-fire-like behavior of the FitzHugh-Nagumo model in noisy situations will be discussed in more detail in Chap. 5.

3.4   HINDMARSH-ROSE BURST AND COINCIDENCE DETECTION

There are basically two ways in which bursting neurons can synchronize: burst synchronization and full synchronization. Burst synchronization means that the envelopes of the bursts of the two neurons coincide, but the individual spikes within the bursts do
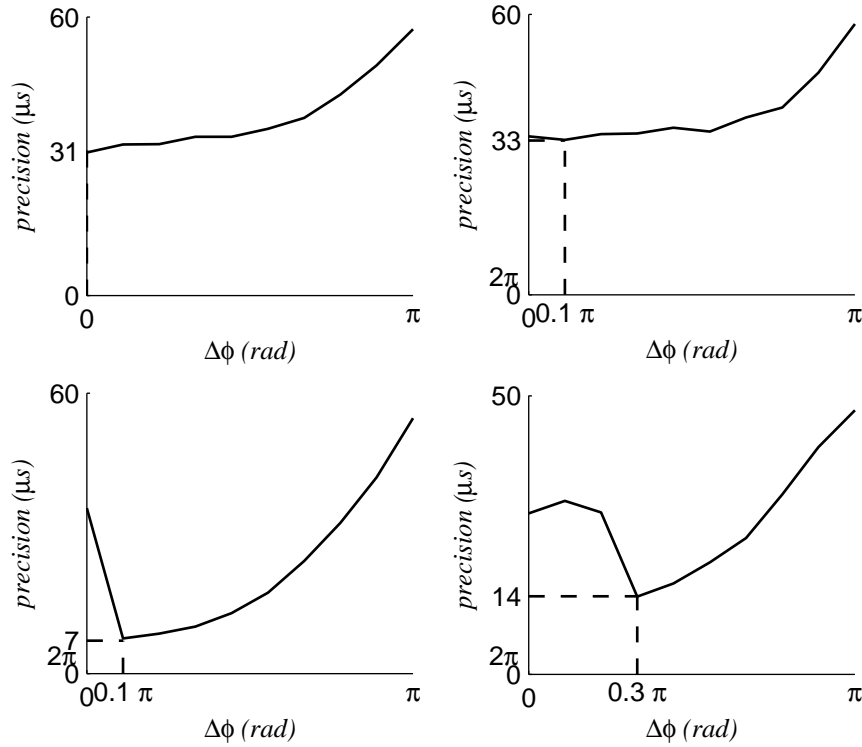
FIGURE 3.19: Width of the peak in the spike histogram as a function of the phase difference. *Top left*: Detection is optimal at zero phase for $\langle w \rangle = 0.015$, 5 kHz tone *Top right*: Detection is optimal at nonzero phase for $\langle w \rangle = 0.01$, t kHz tone *Bottom left*: Detection shows strong optimum at slight phase difference for $\langle w \rangle = 0.015$, 1 kHz tone. *Bottom right*: Detection shows strong optimum at large phase difference for $\langle w \rangle = 0.01$, 1 kHz tone

not. This weak form of synchronization appears in many situations and for all types of coupling. Full synchronization means that all synchronized systems are identical and move on an invariant synchronization manifold. Full synchronization is much more difficult to accomplish. Not only the coupling has to be stronger in general, also the systems have to be able to become identical and therefore have to have identical parameters [van Vreeswijk & Hansel, 2001].

As for the two-dimensional, spiking, case, the features and mechanism of synchronization of bursting neurons have been studied extensively for linear (electrical) coupling [Dhamala *et al.*, 2004; Sherman, 1994]. For pulse coupling, the type of coupling chemical synapses provide, the question of synchronization appears to be a more complex one. In linear coupled systems, the coupling terms, which contains the difference between a state variable in both systems, disappears when the systems synchronize, thus automatically creating the invariant manifold, provided that both systems are identical. In pulse coupling this is not the case. Therefore the synchronized solution only exists in some specific situation when coupling terms in both systems cancel each other; in mutual coupling for instance. In this chapter we consider unidirectional coupling of two or three neurons (Figs. fig:Master-slave coupling scheme and 3.2). For this type of coupling the complete synchronization solution does not exist, since the slave neuron will always have the coupling term that makes it different from the masters, which will prevent complete synchronization. Chapter 4 considers configurations which do have a complete synchronized solution.
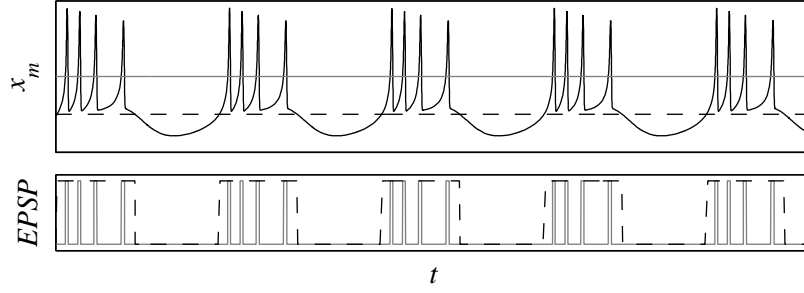
FIGURE 3.20: The EPSP resulting from FTM coupling on a HR neuron for two values of θ. Solid grey line $\theta = 0$, dashed black line $\theta = -1$.

The mathematical argument outlined above shows that full synchronization is very unlikely to occur in real biological neural networks since the cells show an intrinsic diversity in morphology and electrophysiological behavior and, even if we are able to capture this diversity in a single model (see Chap. 5), the parameters for different neurons in the network would vary strongly. On top of that the topology of the network would only very rarely be regular enough to permit full synchrony.

However the question we should ask ourselves might be whether full synchronization is important in information transmission. If we admit that information is indeed encoded in spike timing, then that timing information is transmitted by the chemical synapse in the form of the timing of the transition of the synaptic threshold. Using models for chemical synapses, there is no information about the state of the presynaptic cell other than this transition timing that is transmitted to the postsynaptic neuron (cf. Sect. 2.5).

Then the question of importance concerning the temporal resolution of the encoded information is whether the synaptic threshold is below the minimum potential during a burst or not (see Fig. 3.20 for the case of the FTM model for chemical synapses). When the synaptic threshold is below typical values within the burst, only timing information about the burst envelope is transmitted by the EPSP. When the threshold is within the burst much faster timing information about individual spikes within the burst is transmitted. In this section we assume this is not the case and therefore the only information transmitted to the postsynaptic cell is the timing of the onset of the burst, the neurons will not be able to fully synchronize and we will focus on burst synchronization, postponing a discussion about full synchronization to the next chapter (4). There we will see that indeed to allow full synchronization we have to increase the synaptic threshold to the range of membrane potentials attained within the bursts and thus transmit much more detailed timing information.

In this section we will explore the interaction of pairs and triplets of pulse coupled bursting neurons. The parts of neuron and coupling are played by the Hindmarsh-Rose model (Sect. 2.4) and the FTM coupling (2.37) respectively. We first look at the interaction between pairs of neurons in Sect. 3.4.1). We show how pulse-coupled bursting cells can synchronize and also how the synchronization is more robust to parameter mismatch if the chaotic properties are exploited with *Qualitative Resonance* [De Feo, 2001, 2004a,b]. Next we build two types of coincidence detectors: a regular one and one using inhibitory coupling (Sect. 3.4.2).

3.4.1 Interaction of two Hindmarsh-Rose neurons

The equations for two FTM coupled HR neurons connected in the master-slave configuration from Fig. 3.1 as considered in this section are (see Sects. 2.4 and 2.5):

$$
\begin{cases}
\dot{x}_m &= y_m - x_m^3 + b_m x_m^2 - z_m + I_m, \\
\dot{y}_m &= 1 - 5x_m^2 - y_m, \\
\dot{z}_m &= \mu\left(s_m\left(x_m - x_0\right) - z_m\right), \\
\dot{x}_s &= y_s - x_s^3 + b_s x_s^2 - z_s + I_s - g_{s,m} S\left(x_m\right)\left(x_s - V_{syn,m}\right), \\
\dot{y}_s &= 1 - 5x_s^2 - y, \\
\dot{z}_s &= \mu\left(s_s\left(x_s - x_0\right) - z_s\right),
\end{cases}
\tag{3.15}
$$

where, as before, the indices m and s indicate the master and slave cell respectively. Note however that in this section the parameters are not always identical for both cells. This will be mentioned specifically.

Master-slave synchronization in identical bursters

When the parameters in (3.15) are taken such that both neurons are identical and in regular bursting mode (see Sect. 2.4), they are able to synchronize for $g_{s,m} > g_s^*$, where g_s^* is the critical coupling strength, as it was defined before for master-slave synchronization in FitzHugh-Nagumo neurons (Sect. 3.1.1).

Figure 3.21 shows simulations of two master-slave coupled HR cells. We take identical cells that are started at opposite phase. With the coupling off, obviously they will remain non-synchronized, but when the coupling is turned on, the slave quickly converges to the rhythm of the master. By transmission of the timing of the threshold transition only, the slave cell received enough information to start bursting in sync with the master.

The left plots, which plot the membrane potential (variable x in the HR model) of the master versus that of the slave, show that, although the bursts clearly coincide when the coupling is on, both neurons are not completely synchronized, in which case the plot would be a perfect diagonal.

We took cells with identical parameters, however the burst synchronization is robust to a mismatch in parameters between both cells. The allowed variability is too weak though to resist the variability that would be common in nature. A possible solution to this problem is to use the chaotic properties of neuron models.

Robustness through chaos

"A system with chaotic behavior organized by a homoclinic bifurcation to a saddle-focus (Shil'nikov-like attractor) can synchronize to a periodic forcing signal that is similar to its corresponding generating cycle. This approximate chaos synchronization is called *Qualitative Resonance* (QR)" [De Feo, 2004b].

The theory of QR has been developed for the case of linear coupling in De Feo [2004a,b]. Small investigations into the effects of nonlinear coupling have shown that it applies, in a modified form, in that case too, but no reports have been made about QR in pulse coupled systems.

Without going into the details of the necessary modifications and additions to the theory of QR, we would like to present a first study of a possible application of QR in pulse-coupled systems.
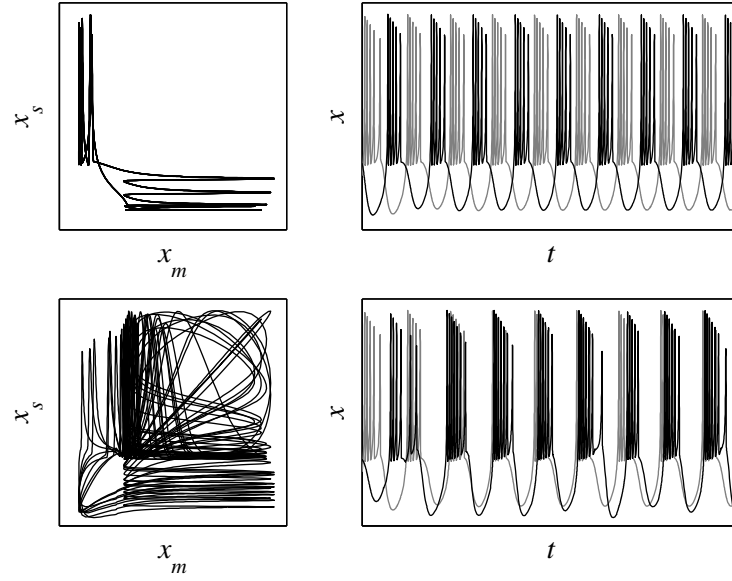
FIGURE 3.21: Synchronization in two identical FTM coupled HR neurons in master-slave configuration. Master neuron in grey and slave neuron in black. Top plots shows that when we start the individual neurons at opposite phase, without coupling they remain de-synchronized. Bottom plots show the same system with the same initial conditions when the coupling is activated ($g_s = 0.06$), the neurons quickly converge to identical phase and remain burst-synchronized. The left plot shows that the synchronization is not perfect since in that case the x_m vs. x_s plot would be the line $x_m = x_s$. Parameter values: $I_m = I_s = 3.00$, $b_m = b_s = 2.80$

The fact that in QR the forcing signal only has to be *similar* to the generating cycle of the chaos, and not (nearly) identical, introduces a flexibility that makes it particulary suitable for feature extraction and pattern recognition [Baier, 2005; De Feo, 2005a,b].

The HR model is organized by chaotic regions which serve somehow as prototypes for regions of bursting solutions with identical number of cycles per burst (cf. Fig. 2.17). So if we take a chaotic solution its generating cycle will correspond to an entire region in the periodic part of the parameter space. This means it can synchronize, and hence transmit timing information, from cells with a large variability in their parameters.

In an unreported communication, De Feo did explore the possible application of QR to master-slave coupled HR cells. However the coupling was done on the third, slow, state variable and the model for the coupling was a modulated linear coupling – below threshold the coupling was set to zero, and above threshold it was identical to linear coupling. De Feo's experiments showed that QR did indeed occur and that it made the synchronization more robust.

Here we propose to go one step further and apply these ideas to the pure FTM pulse coupling, which transmits no information whatsoever about the state of the master. Figure 3.22 illustrates QR in this situation. Both neurons start approximately synchronized and we see that in the case when coupling is off they quickly diverge, whereas when a coupling is applied they stay approximately synchronized. The attractor of the chaotic system changes as well, reflecting the identification of the forcing signal (the scales in both plots are identical). What is interesting is that, contrary to what could be induced from QR theory, the attractor becomes completely periodic with an additional spike with respect to the driving signal. This feature cannot be explained with current theory and requires additional study.
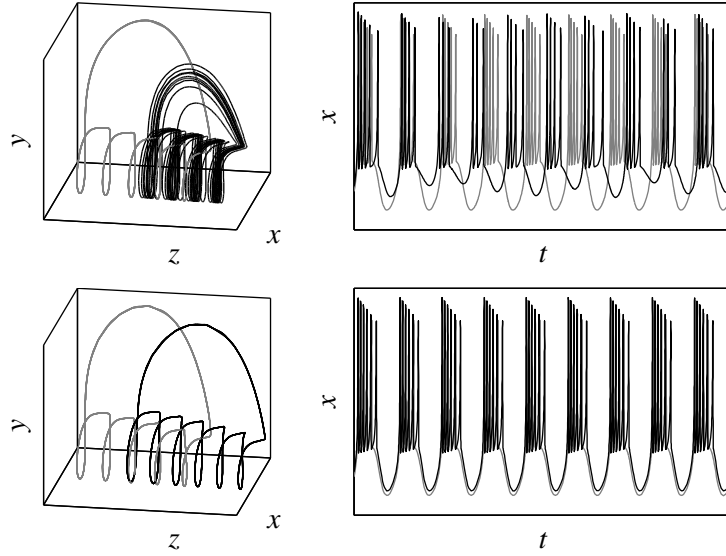
FIGURE 3.22: Qualitative resonance in synchronizing two different FTM coupled HR neurons in master-slave configuration. Master neuron in grey and slave neuron in black. Master is periodically bursting and slave chaotically bursting. Top plots shows that without coupling they remain de-synchronized and the slave follows its irregular, chaotic, trajectory of which the attractor is shown in the left plot together with the regular one of the slave. Bottom plots show that when the coupling is activated ($g_s = 0.02$), the slave remains burst-synchronized to the forcing signal and assumes a new attractor which has features of the attractor of the master. Parameter values: $I_m = 3.00$, $b_m = 2.80$, $I_s = 3.22$, $b_s = 2.92$

To investigate the robustness of the QR we did two simulations of the system (3.15) first taking the slave in the periodic region and then within the chaotic region and varying the master's parameters over the (I_m,b_m) parameter space such as to obtain a map to be superimposed on the ones presented in Fig. 2.17.

For every point on the map we simulated the system and assessed the quality of the transmission of the timing information as follows: From the transitions of the coupling threshold $x = V_s$ in both directions for both neurons, two coupling signals are composed:

$$I_{syn} = H(x_i - V_s) \tag{3.16}$$

where i is the index, either for the master, or the slave. The signal of the slave, of course, is artificial. We then compute the difference between these signals and take the mean of the energy in the difference signal for some simulation period T as the total timing error:

$$\epsilon = \frac{1}{T} \int_T (S(x_m) - S(x_s))^2 dt, \tag{3.17}$$

where $S(\cdot)$ is as usual the coupling function of the FTM coupling. Here we take the standard values for FTM and fix the threshold $\theta = -1$ (see Sect. 2.5 and the discussion above).

Taking the average energy in the difference between the coupling signals automatically normalizes the error between zero and unity, where unity only occurs if the slave is either in perfect anti-phase, or never crosses the coupling threshold, and thus cannot pass on information. Vice versa, the case $\epsilon = 0$ represents perfect synchrony. The error measure therefore indicates well the level of burst synchronization between the two neurons.

In Fig. 3.23 histograms of the simulations are shown. On the basis of these histograms and of visual study of trial simulations we decide that $\epsilon < 0.1$ is a good indication for synchronization and the reliable transmission of information.
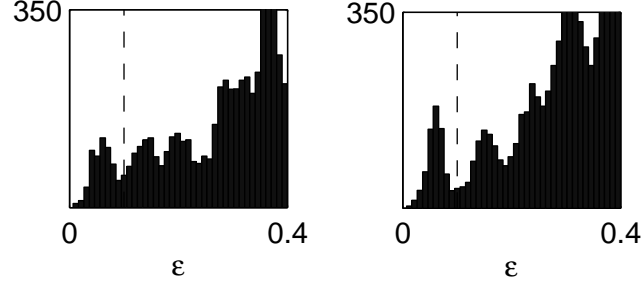

FIGURE 3.23: Histograms of synchronization measure ϵ for simulations of a partition of parameter space (b, I). *Left:* Regular slave *Right:* Chaotic slave. The range simulated was $b = [2, 3]$, $I = [2, 4]$ and the resolution 200x200, which gives a total number of points of 40'000 of which most have $\epsilon > 0.4$. Dashed line indicates the threshold of $\epsilon = 0.1$ that was chosen.

Figure 3.24 reports the results of the simulations. Although the absolute size of the synchronization regions does depend on ϵ, the relative sizes do not. We can see that in the case of a periodic slave the region for which the error is reasonable is quite small, whereas in the case of a chaotic slave neuron the information is transmitted correctly for a larger region of the parameter space. It is interesting to note furthermore that the two regions hardly overlap. They seem to complement each other. This is an additional effect that could be used in neural coding. Also interesting to note is that the periodically bursting neuron does not synchronize with itself. The reason is probably that in identical bursters the on-off nature of the coupling disturbs the slave system and "knocks" it on a different transient trajectory. This did not happen for the FitzHugh-Nagumo model that has a simpler structure and does not contain complex transients. This is also the reason we had to take g_s larger in Fig. 3.21 to show synchronization between two periodic bursters. We could also have taken the slave in the blue region in the left plot of Fig. 3.24.
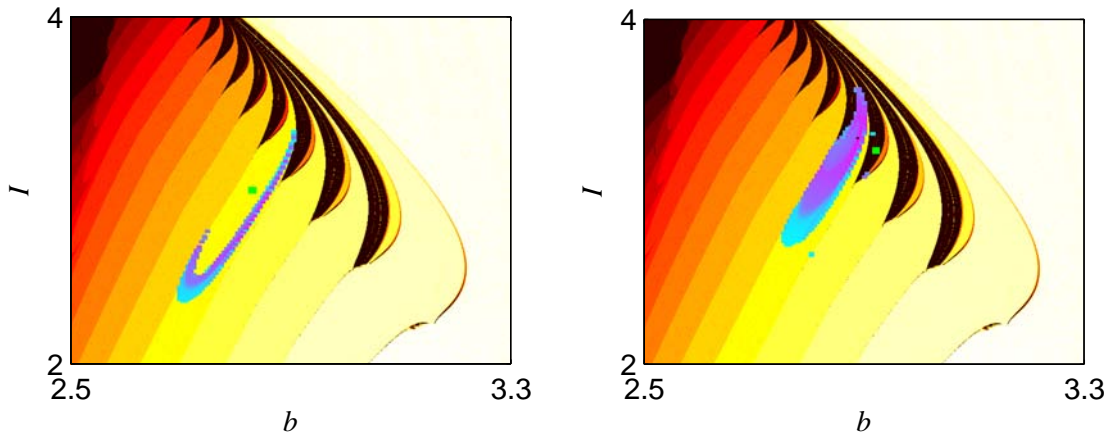

FIGURE 3.24: Robustness of master-slave synchronization. *Left*: Periodic bursting slave *Right*: Slave in the chaotic region. Green markers indicate slave parameters. Blue graded region indicates where the slave synchronized. The color range is from light blue for $\epsilon = 0.1$ to violet for $\epsilon = \min(\epsilon) \approx 0.01$. Other parameters as before; $g_s = 0.02$

3.4.2 Coincidence detection

The ways to build a coincidence detector from HR neurons are not entirely analogous to those for the FitzHugh-Nagumo neurons presented in Sect. 3.2. This is mainly due to the much more complex bifurcation structure of the HR model. The influence the coupling has on the slave is that of an input current. As we can see from the bifurcation diagrams in Fig. 2.16, for a specific value of parameter b, changes in the current can have many different effects and can even change the qualitative behavior of the slave cell. Also the system contains many unstable trajectories it could follow in transients, especially in the chaotic region. This creates many possibilities for different types of coincidence detectors. Here all cells considered are of the bursting type.

The equations describing the HR coincidence detector of Fig. 3.2, are:

$$
\begin{cases}
\dot{x}_{m,1} & = & y_{m,1} - x_{m,1}^3 + b_{m,1}x_{m,1}^2 - z_{m,1} + I_{m,1}, \\
\dot{y}_{m,1} & = & 1 - 5x_{m,1}^2 - y_{m,1}, \\
\dot{z}_{m,1} & = & \mu_{m,1}\left(s_{m,1}\left(x_{m,1} - x_0\right) - z_{m,1}\right), \\
\dot{x}_{m,2} & = & y_{m,2} - ax_{m,2}^3 + b_{m,2}x_{m,2}^2 - z_{m,2} + I_{m,2}, \\
\dot{y}_{m,2} & = & 1 - 5x_{m,2}^2 - y_{m,2}, \\
\dot{z}_{m,2} & = & \mu_{m,2}\left(s_{m,2}\left(x_{m,2} - x_0\right) - z_{m,2}\right), \\
\dot{x}_s & = & y_s - x_s^3 + b_sx_s^2 - z_s + I_s - g_{s,m,1}S\left(x_{m,1}\right)\left(x_s - V_{syn,m,1}\right) \\
& & -g_{s,m,2}S\left(x_{m,2}\right)\left(x_s - V_{syn,m,2}\right), \\
\dot{y}_s & = & 1 - 5x_s^2 - y_s, \\
\dot{z}_s & = & \mu_s\left(s_s\left(x_s - x_0\right) - z_s\right).
\end{cases}
\tag{3.18}
$$

An extra subscript index has been added to the masters' variables to distinguish between the two. Otherwise (3.18) is identical to (3.15) with the addition of the second master. Again, for brevity, subscripts to most parameters are omitted, but they can differ.

Regular coincidence detection

Proceeding in the same way as for spiking neurons in Sect. 3.2, we take the parameters b and I of the masters identical, and act on μ such as to create a slight difference in frequency. This creates a situation where the phase difference between the systems increases steadily, causing the beat phenomenon that makes them burst alternatingly in and out of synchrony. The slave is made quiescent by keeping b_s fixed and lowering I_s below the bifurcation that stabilizes the equilibrium (blue area in Fig. 2.17).

Figure 3.25 reports the simulations of this system. It can be seen that the slave neuron reacts reliably with a short burst when bursts in the masters coincide.

Coincidence detector with inhibitory coupling

Varying the different parameters of the coupling and of the neurons in (3.18) we can obtain many different types of functionalities. One idea is to use a coincidence detector to detect synchrony, or the absence of synchrony, between two neurons.

The total coupling current caused by coupling from the two master neurons from Fig. 3.26 has two possible forms. If the slaves burst in synchrony the current is a block wave with large amplitude $(g_{s,m,1} + g_{s,m,2})$. On the other hand if the neurons are out of
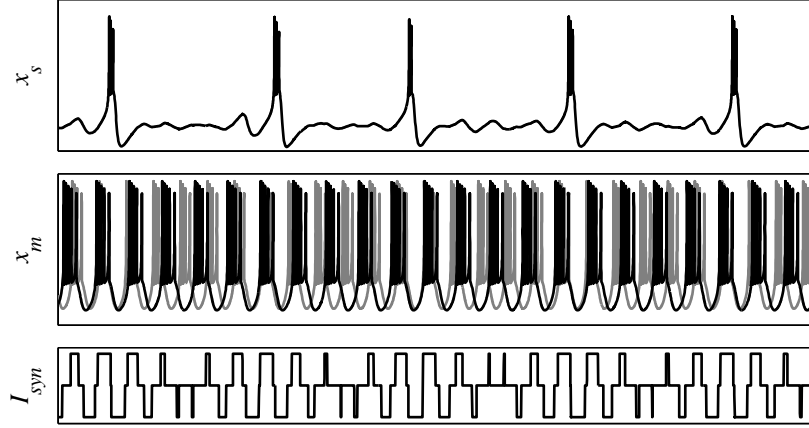
FIGURE 3.25: Coincidence detection with HR neurons. Top picture slows slave membrane potential. Middle picture shows membrane potentials of masters. Bottom picture the synaptic coupling current. Parameters other than standard values: $\mu_{m,2} = 0.08$, $I_m = 2.85$, $b_m = 2.9$, $I_s = 1$ and $b_s = 2.6$

sync the resulting current has a more regular form. It alternates between 0, $g_{s,m,1}$ and $g_{s,m,2}$. Especially if both are in anti-phase and the coupling values are not too different, the synaptic current is practically constant.

When the coupling is inhibitory – such that $V_s < x_s(t), \forall t$ – the synaptic current will produce a hyperpolarizing current proportional to its amplitude, instead of the depolarizing current produced in the excitatory case considered up to now. The constant synaptic current when neurons are out of sync would then suppress bursting in the slave cell through the inhibitory action, whereas the irregular synaptic current that occurs when the slave cells are synchronized will make the slave fire in anti-synchrony.

Simulations for a setup with inhibitory coupling are shown in Fig. 3.26. The slave bursts when the masters are synchronized and is quiescent when they are out of sync. This setup works even better with more than two master neurons – for example in a setup like the one in Sect. 3.3 – since then the difference between the amplitudes of the synaptic currents in synchronized and unsynchronized situations will be even larger.

Note that with the parameter values used here the slave is bursting even when there is no activity in the master, which is in contrast to the coincidence detector presented in Fig. 3.25, where the slave was normally off. This means that this setup is not simply a less sensitive coincidence detector, but really only reacts on anti-synchrony. Note that unclear if this situation is neurophysiologically plausible, nevertheless it serves as an indication of the wide range of applications the Hindmarsh-Rose has to transmit information when used in coupled networks.

3.5 DISCUSSION

This chapter explores the application of a model of a chemical synapse to spiking and bursting models of the generic bifurcation type. More specifically, the use of the fast threshold modulation model for chemical synapses is applied to pairs and triplets of Fitzhugh-Nagumo and Hindmarsh-Rose neuron models.

When connecting models of the generic bifurcation type through fast threshold
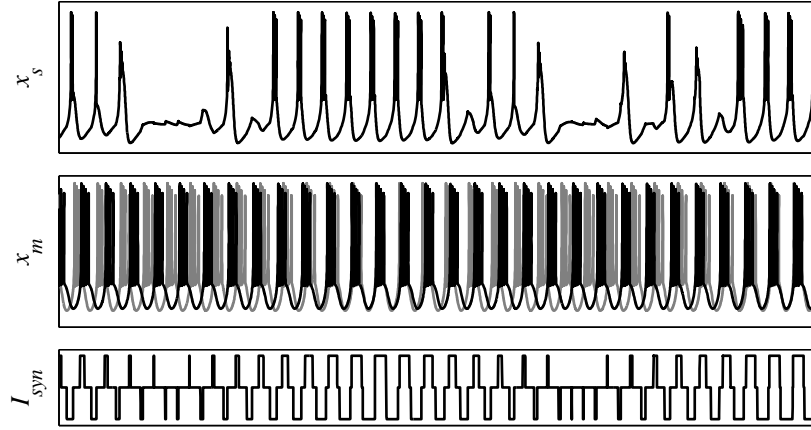
FIGURE 3.26: Coincidence detector with inhibitory coupling. The slave neuron is turned off when masters are completely de-synchronized. Parameters other than ones from Fig. 3.25: $V_s = -2$, $I_s = 1.6$, $b_s = 2.686$

modulation, the information transmitted is only information about timing in the crossing of some synaptic threshold. The coupling is of the on–off type and no information about membrane potential arrives at the postsynaptic cell other than the time it crosses this threshold. Hence the name threshold modulation. In spite of this, a two-dimensional neuron model can synchronize with the presynaptic cell through this timing signal. We revealed the mechanism behind this master-slave synchronization through simulations and a model example.

Another question of interest is whether the postsynaptic spike can accurately react on incoming spikes and transmit timing information coming from one or more presynaptic neurons. We showed first for one presynaptic neuron how this is the case and studied the properties of this reaction – response delay and accuracy. Then we presented a setup for a coincidence detector using this spike detector as building block. The coincidence detector is robust to changes in the synaptic coupling strength and the presence of noise on the input. Noise can even improve the performance of the coincidence detector for low values of the coupling strength; a phenomenon known as noise-enhanced threshold detection, or stochastic resonance.

Coincidence detectors appear in nature when animals have to localize a sound precisely. If a sound source is not straight in front of the animal the sound arrives with a slight delay at the ear that is further away. Hunting birds, such as the barn owl, are especially good at this task considering the small size of their heads and the resulting smaller delay between the signals.

We presented the application of Fitzhugh-Nagumo neurons coupled with fast threshold modulation to model the barn owl's auditory pathway. The model is capable of reproducing qualitatively the features of the physiological system, but a quantitative comparison does not have any signification because of the liberty in choice of the time scale.

The interaction between three-dimensional neuron models through chemical coupling is more complex because these models have a much richer variety of behavior. We illustrated

that master-slave synchronization is through burst synchronization in these models. This preserves information about the envelopes of the burst, such as the burst duration and timing, but not about the contents of the bursts. To transmit this information a stronger synchronization is needed (full synchronization; [Belykh *et al.*, 2005b])

When using periodically bursting neurons, the parameter values of both cells have to match exactly for the cells to be able to synchronize and thus transmit information about the rate and timing. We show that this constraint can be gotten rid of employing the phenomenon of qualitative resonance. When the postsynaptic neuron is in chaotic bursting regime it is able to synchronize to presynaptic cells with a wide range of parameter values. Whether real neurons can exhibit chaotic behavior is still not clear although some (mostly circumstantial) evidence exists [Faure & Korn, 1997].

Because of the much larger variety of different types of behavior bursting neuron models display, a panoply of possibilities exist to connect them. We chose two out of the many ways to construct a coincidence detector using Hindmarsh-Rose cells. The first one reacts with a burst when bursts of the two presynaptic cells coincide exactly. This is a coincidence detector in the proper sense. All properties that apply to spiking coincidence detectors apply here as well: it is robust to noise and fluctuations in the coupling strength and the sensitivity can be tuned.

The second coincidence detector we presented uses inhibitory coupling and detects the absence of synchrony. It is periodically bursting as long as the two presynaptic bursters are burst-synchronized or quiet. When they drift away and end up in anti-synchrony however, the postsynaptic neuron becomes quiescent. It is therefore not a coincidence detector in the proper sense, but an anti-synchrony detector.

The study of interaction through FTM in this chapter revealed some details about the working of interaction between two units of generic bifurcation neuron models when coupled by a model for chemical synapses. Another very interesting distinguishing feature of this type of coupling, is discovered when studying larger networks of neurons. This is discussed in the next chapter.

SYNCHRONIZATION IN NETWORKS OF HINDMARSH-ROSE NEURONS

Brief — This chapter presents an analytical study of the influence of coupling strength and network topology on synchronization behavior in pulse-coupled networks of bursting Hindmarsh-Rose neurons. Surprisingly, we find that the stability of the completely synchronous state only depends on the number of signals each neuron receives, independent from all other details of the network topology. This is in contrast with linearly coupled bursting neurons where complete synchrony strongly depends on the network structure and number of cells. The analytical results are obtained under very restrictive and biologically implausible hypotheses, but simulations show that the theoretical predictions hold in more realistic cases as well.

Personal Contribution — This chapter is a reproduction of and article co-authored with Dr. Igor Belykh and Prof. Dr. Martin Hasler. The analytical part was mostly performed by Dr. Belykh and Prof. Hasler, whereas I was responsible for the simulations. Some extra simulation results are added at the end that do not appear in the original article.

Synchronized neuronal firing has been suggested as particularly relevant for neuronal signal transmission and coding. While its involvement in cortical processing remains somewhat controversial, the presence of synchronization has been shown in special areas such as the olfactory system and the hippocampal region. Model studies of neuronal synchronization can be separated in those where threshold models of the integrate-and-fire type are used and those where conductance-based spiking and bursting models are employed. Bursting occurs when neuron activity alternates, on a slow time scale, between a quiescent state and fast repetitive spiking. There has been much work on mechanisms that produce such bursting. In contrast to coupled spiking neurons, whose synchronous dynamics is relatively simple, interacting bursting neurons may exhibit different forms of synchrony; including synchronization of individual spikes, burst synchronization when only the envelopes of the spikes synchronize, and complete synchrony. Typically, burst synchronization arises at a low coupling strength whereas complete synchrony, which

involves both burst and spike synchronization regimes, requires a stronger coupling. Models of interacting bursting neurons often use one of two different forms of coupling depending on whether the synapse is electrical or chemical. In the first case, the coupling through gap junctions is linear and directly dependent on the difference of the membrane potentials. In the second case, the coupling is pulsatile and often modeled as a static sigmoidal nonlinear input-output function with a threshold and saturation. One important question about interacting bursting neurons with such linear and pulsatile couplings is that of complete synchronization: What are the conditions for the stability of the completely synchronous state, especially with respect to coupling strengths and coupling configurations of the network? This problem was intensively studied for linearly coupled networks of bursting neurons, and more generally, of limit-cycle and chaotic oscillators. In particular, it has been shown that synchrony in such networks strongly depends on the structure and size of the network.

Studying a network of pulse-coupled Hindmarsh-Rose neurons we show that all that matters for the onset of complete synchrony is the number of signals, k, received by each neuron. This is independent of all other details of the network structure. More precisely, the synchronization threshold is inversely proportional to the number of incoming signals k. This criterion applies to a neuronal network with *any* coupling topology admitting complete synchrony. For this property to be true, each neuron must receive signals from k others, where k is identical for all neurons.

The synchronization condition we derive below is not restricted to the HR neuron, but is directly applicable to many other bursting Hodgkin-Huxley-type neurons as well; including the 3D Morris-Lecar [Izhikevich, 2000a], Sherman [Sherman, 1994], and Wilson [Wilson, 1999] models. In this work, we shall concentrate on networks of HR neurons exhibiting square-wave bursting, which is very resistant to synchronization.

The contents of this chapter are an adapted version of the article that appeared in Physical Review Letters [Belykh *et al.*, 2005b] and at the 2005 International Symposium on Nonlinear Theory and its Applications [Belykh *et al.*, 2005a]. Some previously unreported simulation results have been added.

4.1 TRANSFORMATION OF THE MODEL

The single HR neuron model is presented in Sec. 2.4. Here we use a slight generalization of (2.29), with some additional parameters:

$$
\begin{cases}
\dot{x} = y - x^3 + bx^2 + I - z, \\
\dot{y} = 1 - dx^2 - y, \\
\dot{z} = \mu \left(s \left(x - x_{rest} \right) - z \right)
\end{cases}
\tag{4.1}
$$

For the analytical treatment in this chapter, a slightly different version of the model will be used that can be obtained by the substitution

$$
\begin{bmatrix} x \\ y \\ z \end{bmatrix} \rightarrow \begin{bmatrix} x \\ 1 - y \\ 1 + I + z \end{bmatrix},
\tag{4.2}
$$

by introducing the following new parameters

$$a = b$$
$$\alpha = d - b$$
$$b = s$$
$$c = -1 - I - sx_{rest}$$

This gives the following model, which has a minimal set of parameters – the original model has one non-independent parameter due to the free choice of x_{rest} the model allows.

$$\begin{cases} \dot{x} = ax^2 - x^3 - y - z, \\ \dot{y} = (a + \alpha)x^2 - y, \\ \dot{z} = \mu(bx + c - z). \end{cases} \tag{4.3}$$

Furthermore, in the simulation results presented here the following parameter values have been used: $a = 2.8$, $\alpha = 1.6$, $c = 5$, $b = 9$, $\mu = 0.001$.

4.2 NETWORK STRUCTURE

We consider fast instantaneous coupling of the FTM type, as discussed in Sect. 2.5. When n identical Hindmarsh-Rose models 4.3are coupled using FTM, the equations of motion read:

$$\begin{cases} \dot{x}_i = ax_i^2 - x_i^3 - y_i - z_i - g_{\mathrm{s}}(x_i - V_{\mathrm{s}}) \sum_{j=1}^{n} c_{ij}\Theta(x_j), \\ \dot{y}_i = (a + \alpha)x_i^2 - y_i, \\ \dot{z}_i = \mu(bx_i + c - z_i), \ i, j = \overline{1, n}. \end{cases} \tag{4.4}$$

The reversal potential V_{s} is assumed to be greater than $x_i(t)$ for all x_i and all times t, i.e. the synapse is excitatory. The synaptic coupling function is modeled by the sigmoidal function (2.38):

$$\Theta(x_j) = \frac{1}{1 + \exp\{-\lambda(x_j - \theta_{\mathrm{s}})\}} . \tag{4.5}$$

The threshold θ_{s} is chosen such that every spike in the single neuron burst can reach the threshold (see Fig. 4.1). Hereafter, θ_{s} and V_s are chosen and fixed as follows: $\theta_{\mathrm{s}} = -0.25$, $V_s = 2$. $\mathbf{C} = (c_{ij})$ is the $n \times n$ connectivity matrix: $c_{ij} = 1$ if neuron i is connected to neuron j, $c_{ij} = 0$ otherwise, and $c_{ii} = 0$.

Matrix $\mathbf{C}$ can be asymmetric such that both mutual and unidirectional couplings are allowed, however, we require equal row-sums $k = \sum_{j=1}^{n} c_{ij}$, $i = 1, ..., n$. This requirement is necessary since without it the existence of the synchronous solution, namely the invariance of hyperplane $D = \{\xi_1(t) = \xi_2(t) = ... = \xi_n(t)\}$, $\xi_i = (x_i, y_i, z_i)$, $1 \leq i \leq n$, is not guaranteed. The equal row-sum property implies a network where each cell has the same number k of inputs from other neurons.
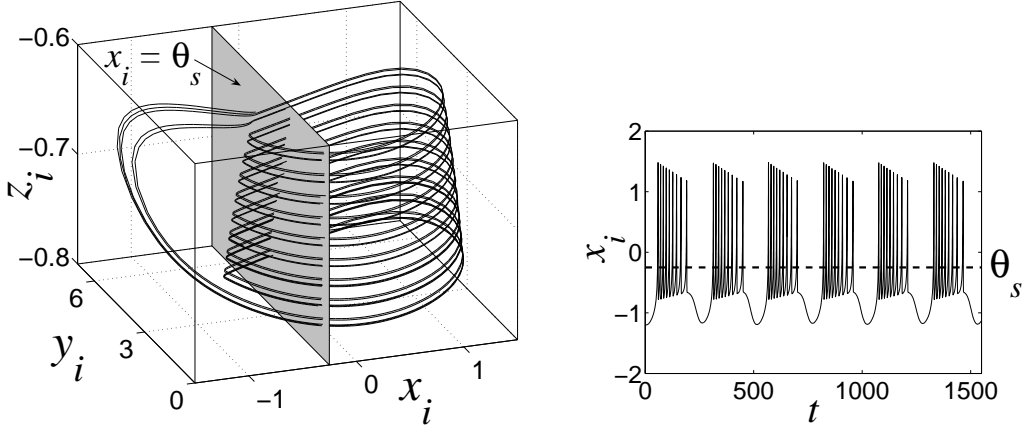
FIGURE 4.1: Square-wave burster of the HR model and the corresponding time series.

4.3 DERIVATION OF THE STABILITY CONDITION FOR SYNCHRONY

Synchronous behavior on the manifold D is generated by the system:

$$\begin{cases} \dot{x} = ax^2 - x^3 - y - z - kg_{\mathrm{s}}(x - V_{\mathrm{s}})\Theta(x) \, , \\ \dot{y} = (a + \alpha)x^2 - y \, , \\ \dot{z} = \mu(bx + c - z). \end{cases} \tag{4.6}$$

Next we add and subtract an additional term $g_{\mathrm{s}}(x_i - V_{\mathrm{s}}) \sum\limits_{h=1}^{n} c_{ih}\Theta(x_i) = kg_{\mathrm{s}}(x_i - V_{\mathrm{s}})\Theta(x_i)$ from the x-equation of system 4.4, and introduce the differences between the neural oscillator coordinates:

$$\begin{aligned} \xi_{ij} &= x_j - x_i \, , \\ \eta_{ij} &= y_j - y_i \, , \\ \zeta_{ij} &= z_j - z_i \, , \quad i, j = 1, ..., n \, . \end{aligned} \tag{4.7}$$

In the limit when these differences are infinitesimal, we derive the stability equations for the transverse perturbations to the synchronization manifold D:

$$\begin{cases} \dot{\xi}_{ij} = & (2ax - 3x^2)\xi_{ij} - \eta_{ij} - \zeta_{ij} - kg_{\mathrm{s}}\Theta(x)\xi_{ij}+ \\ & + g_{\mathrm{s}}(V_{\mathrm{s}} - x)\Theta'_x(x)\left(k\xi_{ij} + \sum\limits_{h=1}^{n}\{c_{jh}\xi_{jh} - c_{ih}\xi_{ih}\} \right) , \\ \dot{\eta}_{ij} = & 2(a + \alpha)x\xi_{ij} - \eta_{ij}, \\ \dot{\zeta}_{ij} = & \mu(b\xi_{ij} - \zeta_{ij}) \, . \end{cases}$$

The derivatives calculated in the point $\xi = 0, \eta = 0, \zeta = 0$, and $\{x(t), \ y(t), \ z(t)\}$ corresponds to the synchronous bursting solution defined via (4.6). The first coupling term $S_1 = -kg_{\mathrm{s}}\Theta(x)\xi_{ij}$ accounts for the number of inputs k. The contribution of the second coupling term $S_2 = g_{\mathrm{s}}(V_{\mathrm{s}} - x)\Theta'_x(x)(\cdot)$ depends on the coupling configuration. Note that the term $\sum\limits_{h=1}^{n}\{c_{jh}\xi_{jh} - c_{ih}\xi_{ih}\}$ is the same as for linear coupling [Pecora, 1998; Pecora & Carroll, 1998].

74

In terms of the original variables x_i, the corresponding coupling matrix $\mathbf{G} = \mathbf{C} - k\mathbf{I}$ is the Laplacian of the connected graph, except for a sign change. It is well known that $\mathbf{G}$ has one zero eigenvalue γ_1 and all other eigenvalues have non-positive real parts[1].

The eigenvalue γ_2 with the largest real part is crucial for the stability analysis of the synchronized solution. If the coupling is mutual, as is assumed in this analytical treatment, $\mathbf{G}$ is symmetric and all eigenvalues are real. For simplicity, suppose that γ_2 is simple. Then, applying the linear transformation that diagonalizes $\mathbf{G}$ to (4.8), we obtain the stability equation for the most unstable transverse mode:

$$
\begin{aligned}
\dot{\xi} &= (2ax - 3x^2)\xi - \eta - \zeta - \Omega(x)\xi \,, \\
\dot{\eta} &= 2(a + \alpha)x\xi - \eta \,, \\
\dot{\zeta} &= \mu(b\xi - \zeta) \,,
\end{aligned}
\tag{4.8}
$$

where $\Omega(x) = kg_{\mathrm{s}}\Theta(x) - g_{\mathrm{s}}(V_{\mathrm{s}} - x)\Theta'_x(x)(k + \gamma_2)$.

System (4.8) is an analog of the Master Stability function [Pecora & Carroll, 1998] for pulse-coupled networks.

If γ_2 is not simple we can write similar equations to (4.8) for the vectors spanning the corresponding blocks in the Jordan normal form of $\mathbf{G}$. The stability discussion, however, is essentially the same. In the next section we apply the stability condition to basic network configurations.

4.4 Application to basic network configuration

The networks considered in this analytical treatment are all regular mutually coupled. As we will see, the stability condition does not depend on the number of cells n in the network and, as argued before, the only other free parameter that determines the structure of these networks is the number of inputs per neuron k.

We distinguish four cases:

Global coupling: Every neuron is connected to all others and $k = n - 1$.

Dense coupling: Every neuron is connected to many, but not all, other neurons. An example is a ring of $2K$-nearest neighbor coupled neurons, where K is close to $n/2$.

Intermediate coupling: Every neuron is connected to about half of the other neurons.

Sparse coupling: Every neuron only receives a few inputs from other neurons. The typical example is local coupling, where, in a ring of neurons, every neuron only receives an input from it's neighbors ($2 - K$-nearest neighbor coupling with K=1).

For each of these four cases the eigenvalue γ_2 with the largest real part has a different value. For each case the value of γ_2 gives a stability condition, which, in the end, is conjectured to be identical for all cases.

---

[1]If any two distinct nodes of the graph can be connected respecting the orientation of the graph edges, the zero eigenvalue γ_1 of $\mathbf{G}$ is simple

4.4.1 GLOBALLY COUPLED NETWORKS

In this case, $k = n - 1$ and $\gamma_2 = -n$. Consequently,

$$\Omega(x) = kg_{\text{s}}\Theta(x) + g_{\text{s}}(V_{\text{s}} - x)\Theta'_x(x). \tag{4.9}$$

The function $\Theta(x)$ together with its derivative $\Theta'_x(x)$ is non-negative, and $(V_{\text{s}} - x)$ is always positive (the synapses are excitatory). Therefore $\Omega(x)$ is always non-negative and the coupling term $-\Omega(x)\xi_{ij}$ stabilizes the zero equilibrium of (4.8); corresponding to the synchronous solution.

The function $\Omega(x)$ strongly depends on whether the membrane potential $x(t)$ exceeds the threshold θ_{s} or not. In fact, kg_{s} is a lower bound of $\Omega(x)$ in the region $x(t) > \theta_{\text{s}}$ and strongly contributes to the stability.

At the same time, when $x(t)$ is below θ_{s}, the first term in $\Omega(x)$ rapidly decreases to zero, and the second coupling term becomes decisive in a small region close to $x = \theta_{\text{s}}$. This region is defined by the parameter λ (see the left panel of Fig. 4.2). Applying the Lyapunov function method to the stability of system (4.8), similar to the approach outlined by Belykh *et al.* [1998], we prove that the synchronous state can be made stable, provided the coupling g_{s} is sufficiently strong. The analysis shows that the major part of the quiescent (slow) mode of the synchronous solution, where the contribution of $\Omega(x)$ is negligible, lies in a stable zone where, the derivative of the Lyapunov function is always negative, i.e., where the solutions of the individual systems converge to each other. On the other hand, the part of the bursting solution that is the most difficult to synchronize lies in the region $x(t) \geq \theta_{\text{s}}$, where the contribution of $\Omega(x) = kg_{\text{s}}$ is strong and depends on k.
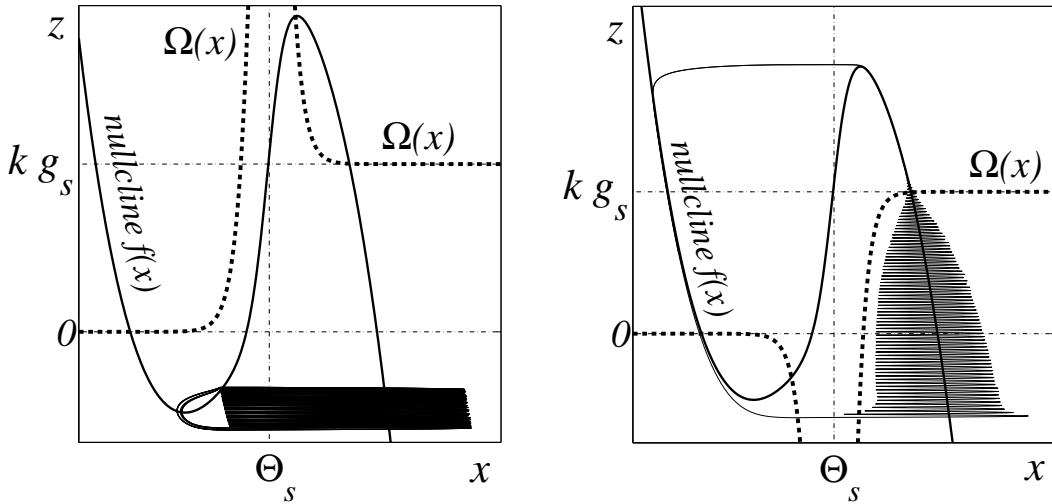
FIGURE 4.2: The function $\Omega(x)$ and the corresponding synchronous bursting. *Left:* Globally coupled HR neurons ($k = n - 1$, $\lambda = 10$). *Right:* Ring of locally coupled HR neurons ($k = 2$, $\lambda = 10$).

Similarly, we prove that the remaining spiking part of the synchronous solution for $x(t) \leq \theta_{\text{s}}$ can be stabilized by increasing g_{s} under the constraint that $\Theta(x)$ is not the Heaviside function (λ is not too large). Hereafter, we postpone the detailed proof and

give only the main result. Our stability conditions give the following estimate for the synchronization threshold:

$$g_s^* = g_s^{(n=2)}/k \ , \tag{4.10}$$

where $k = n-1$, and $g_s^{(n=2)}$ is a constant corresponding to the synchronization coupling threshold between two mutually coupled HR neurons ($k = 1$). The constant $g_s^{(n=2)}$ comes from sufficient conditions and therefore gives an overestimate for the real coupling strength that leads to complete synchronization of two HR neurons: 2.94 predicted versus 1.285 actual for the above mentioned parameters and $\lambda = 10$. However, using the numerically obtained $g_s^{(n=2)}$, we can predict the threshold g_s^*, for any k, from (4.10), as shown in the numerical examples in Sec. 4.5.

4.4.2 Densely coupled networks

The eigenvalue γ_2 of $\mathbf{G}$ for such networks is very close to $-k$. For example, for a ring of $2K$-nearest neighbor mutually coupled neurons, $\gamma_2 = -4\sum_{l=1}^{K} \sin^2 \frac{l\pi}{n}$ with $n = 10$, $K = 4$, and $k = 2K = 8$, we obtain $\gamma_2 \approx -7.976$. Consequently, the function $\Omega(x)$ becomes close to $kg_s\Theta(x)$. Therefore, if k is sufficiently large, the bound for the synchronization threshold will be nearly identical to that for globally coupled networks.

4.4.3 Intermediately and sparsely coupled networks

When the number of links between the neurons in a network is small, the eigenvalue γ_2 is also small such that the second term in $\Omega(x)$, $-g_s(V_s - x)\Theta'_x(x)(k + \gamma_2)$ no longer favors the stability. Consequently, the function $\Omega(x)$ takes negative values in the region close to the threshold θ_s and defines the instability zone, where the coupling de-synchronizes the neurons.

At the same time, the stability zone is defined by the first term in Ω, $kg_s\Theta(x)$, which is bounded from below by kg_s in the region $x(t) \geq \theta_s$ (cf. right panel of Fig. 4.2). Strictly speaking, while we are no longer able to prove that the systems synchronize within the framework of the Lyapunov function method, the slow-fast structure of (4.3) yields the following.

The excitatory coupling raises the x-nullcline $f(x) = -\alpha x^2 - x^3 - kg_s(x - V_s)\Theta(x)$ of (4.8) such that the right-branch attractor corresponding to spiking gradually moves to the right from the threshold $x = \theta_s$. Finally, it leaves the zone Z_{ngt} where $\Omega(x)$ is negative, provided g_s is large enough. Note that the raising of the nullcline and the shift of the attractor are also governed by kg_s (cf. (4.8)).

In the singular perturbation limit ($\mu \to 0$), the synchronous trajectory traverses the instability region Z_{ngt} via fast jumps from the quiescent mode to repetitive spiking, and spends almost all its time in the stability regions. Consequently, the negative contribution of Z_{ngt} to the stability is unimportant. The first stability zone corresponding to the slow motion along the left branch of the nullcline is always stable (similar to the case of global coupling). At the same time, the second zone corresponding to spiking must be made stable by increasing g_s. As in the case of the global coupling, the stability in this region is defined by kg_s.

Hence, once again we see that (4.10) is a good estimate for the synchronization threshold. Consequently, the synchronization threshold in locally FTM-coupled networks

is constant – $g_{\mathrm{s}}^* = g_{\mathrm{s}}^{(n=2)}/2$ for mutually nearest-neighbor coupled neurons – and does not depend on the number of neurons n. This is in sharp contrast with linearly coupled networks where the coupling required for stable synchronization has a quadratic dependence on n [Belykh *et al.*, 1998].

Collecting all the considered coupling topologies, we come to the following assertion:

Conjecture 4.4.1: The synchronization threshold estimate (4.10) $g_{\mathrm{s}}^* = g_{\mathrm{s}}^{(n=2)}/k$ is valid for the networks (4.4) with *any* coupling configuration (whether global or local, regular or random, mutual or unidirectional) under the constraint that each neuron has the same number of inputs k.

4.5 Simulation results

The power of (4.10) is illustrated by a series of simulations on different types of networks. We not only verify conjecture 4.4.1, but go beyond the hypotheses taken in the proof in Sec.4.3.

First we show results for regular networks of different size for the three coupling configurations discussed in Sec. 4.4. The relation between the number of neurons in the network and the threshold for synchrony is illustrated for the different coupling configurations and a comparison with linear coupling is made.

Next the hypothesis of regularity is loosened and randomly generated networks with *unidirectionally* coupled neurons are studied. Of course, to guarantee the existence of the synchronous solution, the number of incoming connections per neuron still has to be constant, but these results show that this really is also a sufficient condition for application of (4.10).

Finally the condition of uniformity of the coupling strength is relieved and we study networks of neurons with a Gaussian distribution on the coupling strength. In this case, although full synchronization is no longer possible, the stability condition (4.10) can still be applied substituting the mean of the coupling strength for g_{s}^* and defining a measure for the synchronous state.

In addition to the case assumed in the analytical treatment, where the step is moderately steep ($\lambda = 10$), to guarantee a transitional region, we also do simulations for a situation where the step function is very steep, close to the Heaviside step function ($\lambda = 50$). In all simulations the value of $g_{\mathrm{s}}^{(n=2)}$ used in (4.10) was determined from a simulation of two mutually coupled HR neurons. This value is $g_{\mathrm{s}}^{(n=2)} = 1.285$ for $\lambda = 10$ and $g_{\mathrm{s}}^{(n=2)} = 1.139$ for $\lambda = 50$. Simulations were done for two values of steepness λ of the step function in the coupling.

4.5.1 Regular networks

Regular networks of varying size for three coupling configurations (local, intermediate and global), were simulated. The synchronization threshold measured was compared to the value predicted by (4.10).

From the results shown in Fig. 4.3 it can be seen that the prediction is nearly perfect. The results even extend to large λ, when the synaptic function $\Theta(x_i)$ approaches the Heaviside function.
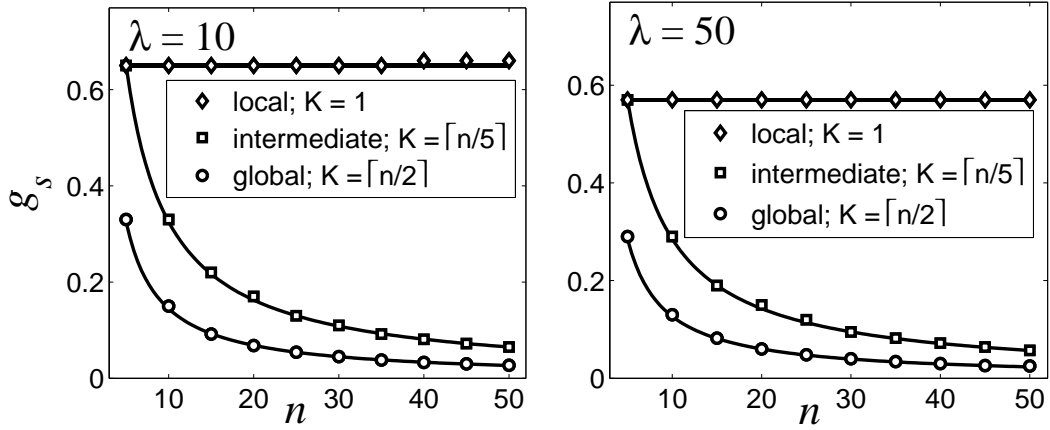
FIGURE 4.3: Synchronization thresholds g_s^* in a ring of $2K$-nearest neighbor coupled HR neurons as functions of n for various coupling configurations (different K). Markers: Simulation results. Solid line: (4.10).

4.5.2 RANDOM, UNIDIRECTIONAL NETWORKS

The hypotheses used to obtain (4.10) were quite severe and admittedly not very realistic. To do a step in the direction of the reality of networks of neurons with more irregular coupling structure, we study the application of condition (4.10) to networks with random coupling structure.

We no longer use regular networks, but randomly generate coupling matrices for a given number of neurons n. Of course, the one restriction we have to maintain is the constant number of inputs per neuron k, since it is a necessary condition for the existence of global synchrony.

We generated four different types of networks as illustrated in Fig. 4.4. Of each type, ten realizations were generated and simulated to obtain the coupling threshold. All calculated thresholds still coincide perfectly with (4.10) for both values of λ.

4.5.3 NONUNIFORM COUPLING STRENGTH

Finally, we tested robustness of the synchronization with respect to a mismatch in the synaptic strength. We simulated networks of 20 neurons for the local, global and intermediate case, introducing a mismatch in the synaptic strengths around the average g_s. Full synchronization is no longer possible in these cases, due to the absence of the synchronization manifold. What happens is that there is always an error in the synchronization. However, for a given value of g_s this error falls rapidly and then remains constant when g_s is further increased. This point can be seen as the synchronization threshold, for approximate synchrony occurs. Its value coincides perfectly in all simulated cases with the value of the synchronization threshold without mismatch as shown in Fig. 4.3. The synchronization has been verified to be robust for mismatches in g_s of up to 5%.
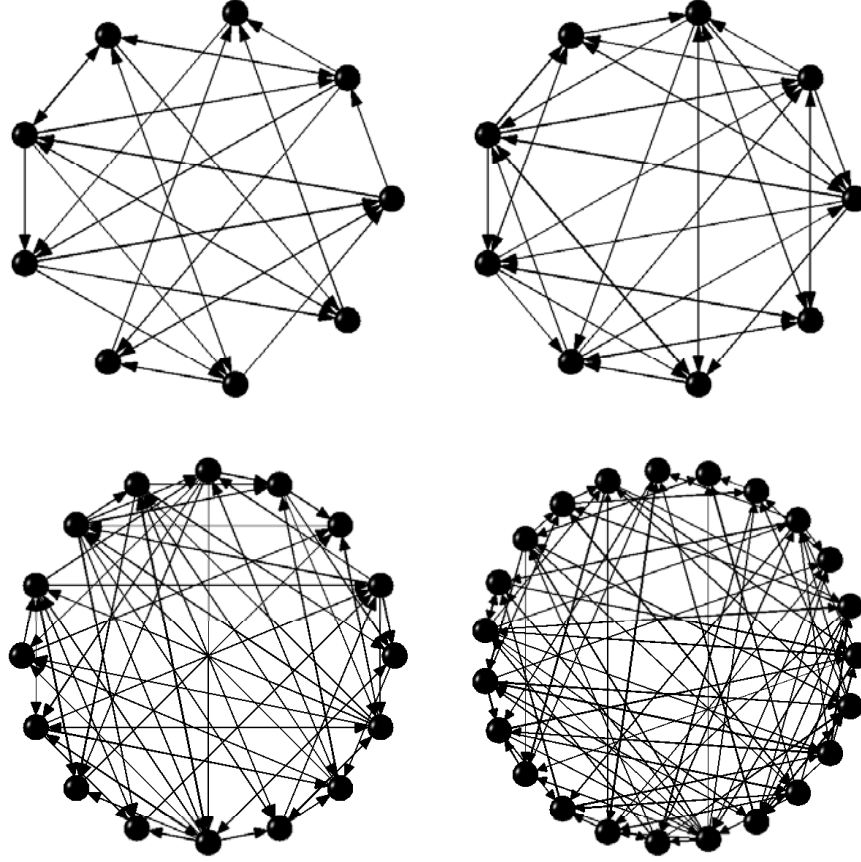
FIGURE 4.4: Examples of the unidirectional networks simulated. *Top left* $n = 9$, $k = 3$; *Top right* $n = 9$, $k = 4$; *Bottom left* $n = 16$, $k = 4$, *Bottom right* $n = 26$, $k = 4$.

4.6 DISCUSSION

The single condition (4.10) ensures the onset of complete synchronization in networks of FTM coupled bursting neurons (4.4) with any coupling topology in which each neuron receives signals from k others. The synchronization condition depends on the number of inputs k and *not* on the connectivity matrix, such that only the number of signals k matters for the onset of complete synchrony. This is in sharp contrast with linearly coupled networks where the coupling required for stable synchronization has a quadratic dependence on the number of neurons n in the network.

The equal k constraint is often invalid for biologically relevant networks with a complex structure where the number of inputs is not necessarily constant, but if k is constant for a group of neurons, synchronization within this group of neurons can occur.

The synaptic strengths can also change as a result of pre- and postsynaptic cell activity such that the inputs to the neurons become equal only for a specific interval of time. The consequence is transient synchronization that is believed to be a collective mechanism for spatiotemporal neuronal integration [Hopfield & Brody, 2001]. This work promises to allow an analytical treatment of even transient synchrony in bursting cells.

Modeling neocortical diversity

Brief — The realism of the generic bifurcation models is put to a test in this chapter by identification of their parameters from in vitro measurements. The identification problem is addressed by resorting to standard techniques combined with heuristics based on the results of the reported mathematical analysis and on a priori knowledge from neuroscience. Two types of experimental data are considered: the first is a standard in vitro protocol applied to many different neocortical interneurons and the second is a conductance based noisy signal repetitively applied to neocortical pyramidal neurons.

Personal Contribution — The contents of this chapter are all original work, unless specifically mentioned otherwise. The study of spike time prediction of in vivo-like signals is based on a similar study by Dr. Renaud Jolivet and Prof. Dr. Wulfram Gerstner

The neocortex is organized in vertical columns composed of a large variety of morphologically different neurons [DeFelipe, 1993; Gupta *et al.*, 2000; Peters & Jones, 1984]. In vitro electrical recordings of neocortical neurons display corresponding wide range of different intrinsic firing patterns. In the last two decades many of these firing patterns have been identified and different classification schemes were proposed. Important contributions are early ones of McCormick *et al.* [1985] and Connors & Gutnick [1990] and the more recent classification schemes by Kawaguchi & Kubota [1997], Gupta *et al.* [2000], Toledo-Rodriguez *et al.* [2002] and Markram *et al.* [2004]. To date, the exact number of neocortical cell types, and the criteria for distinguishing them are not universally agreed upon, especially in the case of inhibitory interneurons.

The diversity in firing patterns results from a variability in types and density of ion channels [Bargas & Galarraga, 2002; Hille, 2001; Johnston & Wu, 1995; Toledo-Rodriguez *et al.*, 2002]. Ion channels are state dependent, stochastic units and their properties may change according to different conditions [Steriade, 2004]. Under standardized stimulation conditions in vitro, neuronal responses are stable for long periods of time [Rauch *et al.*, 2003, Fig. 1C], which makes in vitro experiments the tool by excellence to study the different types of electrical behavior neurons may exhibit in vivo.

Generic bifurcation models contain neither details about dendritic structure, nor about individual ion currents and is unrealistic to expect that they can perform as well as high-dimensional multi-compartment models that include dendritic structure and many ion channels. The power of generic bifurcation models lies in their aptitude to analytical treatment.

The goal of the work presented in this chapter is to investigate the possibilities of capturing the essence of the dynamics of the diversity in neuronal discharge properties in models of the generic bifurcation type. Therefore we are interested in obtaining simple methods and heuristics that give estimates of parameter values, or ranges of parameter values, that make a certain model produce some specific type of behavior.

Our sample of neocortical diversity consists of a set of patch clamp recordings from over 200 neurons from the rat neocortex. The data set was provided by Maria Toledo from the Brain and Mind Institute at the Ecole Polytechnique Fédérale de Lausanne [Toledo-Rodriguez *et al.*, 2004].

In a first approach, techniques from nonlinear system identification are used to investigate the aptitude of the FitzHugh-Nagumo and Hindmarsh-Rose model to describe the electrical responses of the different models in the data set. Section 5.1 introduces the basic notions and techniques from system identification, employed for this investigation as well as the data set used for the identifications.

The traditional stimulation protocol for in vitro studies consists of step, pulse and ramp currents of different height and duration. A technique that has become increasingly popular in the recent years is the use of conductance injection in vitro, to recreate an in vivo-like environment. [Destexhe & Paré, 1999; Destexhe *et al.*, 2001; Harsch & Robinson, 2000; Prinz *et al.*, 2004; Robinson & Kawai, 1993] This technique allows the study of properties observed in vivo in a more controlled environment. An additional advantage of this method is the higher frequency content and temporal variation of these kind of signals; it is important to excite as much modes of the system as possible, to identify the dynamics from the input output relation [Nelles, 2001, pp. 569–574], [Ljung, 1987, Chap. 14], [Mehra, 1974].

Section 5.4 presents a study on the fitting of the FitzHugh-Nagumo and Hindmarsh-Rose model to responses to conductance injection of neocortical pyramidal cells from a different data set provided by Dr. Alexander Rauch from the University of Bern [Rauch *et al.*, 2003]. This data set was collected exclusively on excitatory pyramidal cells, by far the most common cells in the neocortex and considered very consistent in their discharge responses, in contrast to inhibitory interneurons. It has been shown that the spike timing in this specific data can be represented faithfully by simple threshold models [Jolivet *et al.*, 2006b]. In section 5.5, the results of this chapter are summarized in guidelines for the choice of parameters in the Hindmarsh-Rose model.

5.1 Theoretical background

This section introduces the notions that will be needed in the rest of the chapter. First we give a brief overview of different types of neocortical neurons and how they are classified before presenting the two data sets that were used in Sects. 5.3 and 5.4. Finally some basic notions from system identification theory will be introduced to motivate the choices of the methods used for the fitting of the models.

5.1.1 Classes of neocortical neurons

The most fundamental classification made in neocortical neurons is that between excitatory and inhibitory cells. Excitatory neurons make up 70–80% of the neocortex and two morphological types are distinguished: Pyramidal cells (PC) and Spiny stellate cells (SSC) [Peters & Jones, 1984]. The inhibitory cells that make up the remaining 20–30% show a much larger variety in different morphologies. See the left side of Fig.5.1 for an overview of different cell classes.

The classification we are interested in is the one made on electrical discharge patterns. Although the relation between the discharge patterns measured in vitro are not universally accepted as direct indications of the function of the cells in live animals [Steriade, 2004], studies indicate that the diversity increases the computational powers of neuronal circuits [van Vreeswijk & Hansel, 2001].

Neuroscientists classify neocortical neurons based on discharge patterns that the cells exhibit after injection of a current step (step response) [Markram *et al.*, 2004]. The classification scheme we consider distinguishes between four types of steady state behaviors for inhibitory cells (Fig. 5.1, right panel), combined with three types of onset behavior. Excitatory cells are generally believed to have only one type of spiking behavior; regular spiking (RS), which is subclassified in strong accommodation; (the interval between subsequent spikes changes strongly after onset of spiking) and weak accommodation [Toledo-Rodriguez *et al.*, 2002].

The steady state behaviors distinguished for inhibitory cells are accommodating (AC) and non-accommodating (NAC) spiking, stuttering (STUT; periods of spiking are alternated with prolonged, irregular, periods of inactivity), irregular spiking (IS; single spikes follow each other in an irregular pattern) and bursting (BST; clear groups of spikes of regular with separated by periods of silence). The onset can be a burst, a single spike or quiescence (a distinct delay).

The classification is purely qualitative, and therefore it is most instructive to look at the examples given in Fig. 5.1. References that give an overview of this classification schemes are those by Connors & Gutnick [1990], Gupta *et al.* [2000], Toledo-Rodriguez *et al.* [2002] and Markram *et al.* [2004] for instance.

5.1.2 In vitro stimulation protocol

The first set of in vitro recordings considered in this work consists of somatic whole-cell recordings from over 200 cells taken from layers 2-6 from the rat somatosensory cortex. For a complete description of the technical details of the slice preparations, electrical recordings etc. see the methods sections in Toledo-Rodriguez *et al.* [2004], Gupta *et al.* [2000] and Markram *et al.* [1997]. The stimulation protocol used in these experiments has recently been standardized and baptized "eCode" [Markram *et al.*, 2005].

The eCode protocol now consists of over 20 different stimulus protocols, but the data set used in this work contained not all of those and not all stimuli were applied to all cells. The ensemble of stimulus protocols we consider – the ones that were applied to all cells – can be divided in nine distinct types, that fall in three groups. The nine main types of stimulus protocols are shown in Fig. 5.2. In brief, the protocol contains stimuli that aim to study the discharge responses to step current pulses (Fig. 5.2a), the change in spiking behavior with time immediately after a current pulse (Fig. 5.2b), the response to a ramp current (Fig. 5.2c), the shape of the action potentials (Fig. 5.2d), the response to short depolarizing delta pulses (Fig. 5.2e), the hyperpolarization after a longer pulse, (Fig. 5.2f),
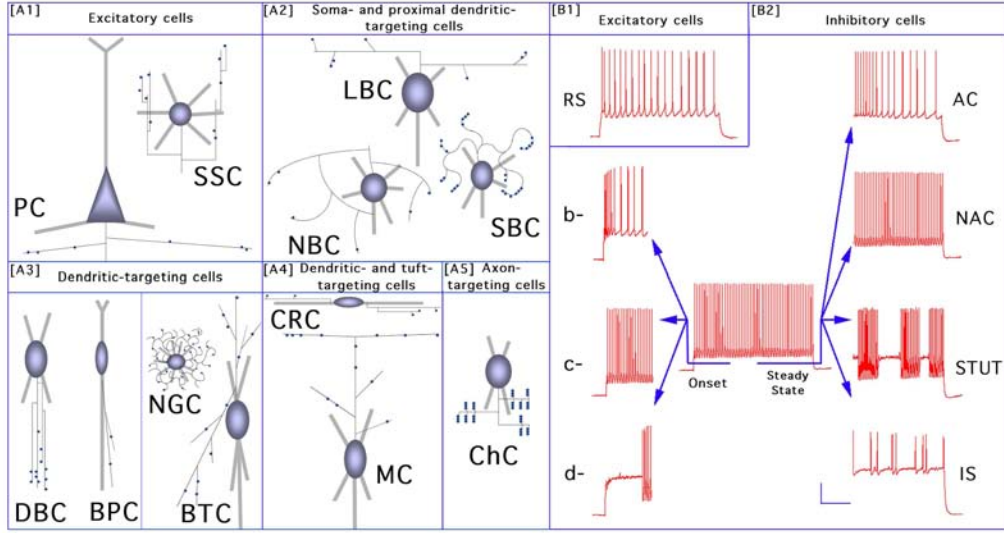
FIGURE 5.1: Anatomical and Electrophysiological Diversity of Neocortical Neurons – A: Scheme summarizing the main anatomical properties of neocortical excitatory (A1) and inhibitory (A2-5) neurons. Each neuron type labeled by 3-letter abbreviation (see text for explanation). Dendrites: thick, light gray; axon: thin, black lines; blue dots: axonal boutons. Spines omitted for clarity. Neurons oriented with pia facing upwards and white matter (WM) downwards. Note the presence of a prominent, vertical dendrite directed towards WM on some interneurons (A2-4). Inhibitory interneurons (A2-5) are mainly distinguished by the structure of their axonal arbor (see text) and typically innervate selective domains [A2: (peri-) somatic; A3,4 dendritic; A5: axonal] of their target cells. B: Representative samples of the most common discharge responses of neocortical excitatory (B1) and inhibitory (B2) neurons to standardized intrasomatic step-current injections. B1: Excitatory cells typically display regular-spiking (RS) discharge behavior. B2: Inhibitory interneurons display a vast repertoire of discharge responses, displaying either bursts (b-), delays (d-) or neither burst/delay (classical, c-) at step-onset, and accommodation (AC), non-accommodation (NAC), stuttering (STUT) or irregular spiking (IS) at steady-state. Scale bar (20 mV; 500ms) applies to all traces. Reproduced from [Toledo-Rodriguez *et al.*, 2002]
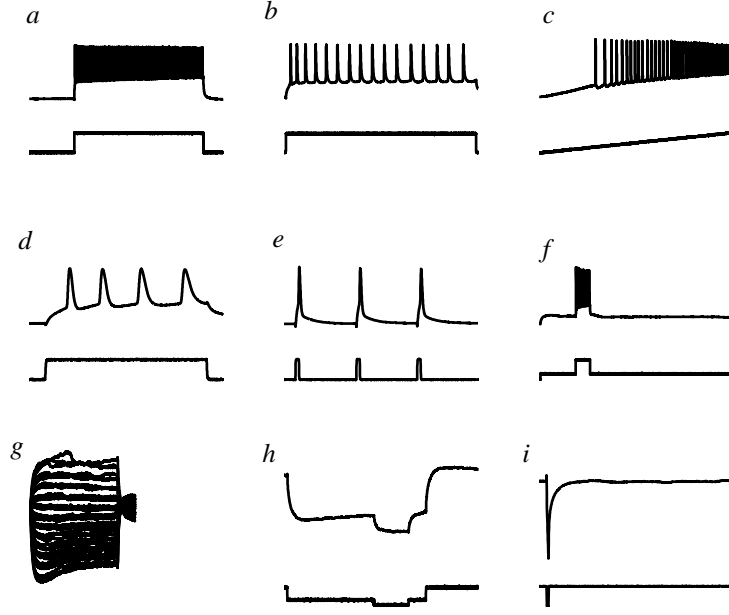
Figure 5.2: Overview of the eCode stimuli considered in this work. For description, see text

the IV characteristic (Fig. 5.2g), the response to depolarizing current steps (Fig. 5.2h) and the response to a depolarizing delta pulse (Fig. 5.2i).

The stimuli in Fig. 5.2 can be separated in three groups; each row of Fig. 5.2 forms a group. From top to bottom:

1. Super-threshold sustained current injection (steps)

2. Super-threshold pulse-like stimuli (pulses)

3. Sub-threshold stimuli (steps and pulses)

These classes of stimuli have distinct aims; the super-threshold steps serve to qualify the class of behavior, since the classification schemes of neocortical neurons are based on descriptions of the responses to these stimuli. The super-threshold pulse-like stimuli are generally of higher resolution and allow the study of quantitative aspects such as spike width, shape, rise and fall time and changes in those quantities after onset of the pulse. The sub-threshold stimuli serve to characterize the passive properties of the cell and are generally regarded as less important for the classification of the neuron ("Discharge responses to supra-threshold [sic] current injections have proven to be the most useful parameter in distinguishing subclasses of both excitatory as well as inhibitory neurons" [Toledo-Rodriguez *et al.*, 2002, p. 722]).

5.1.3 In vivo-like stimuli through conductance injection

In recent years a different approach has become more and more popular in addition to the traditional in vitro stimulation protocols. The idea is, instead of injecting pulses and ramps to characterize the neuron, to present it with stimuli that qualitatively resemble the activity it experiences in vivo. In vivo cells get inputs from thousands of excitatory and inhibitory synapses. The assumption is that this overall activity can be modeled with a random process. This activity is felt as a varying random conductance, which is
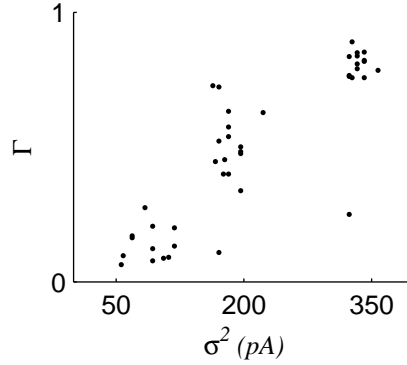
FIGURE 5.3: Intrinsic reliability of the neurons for different stimuli in the data set provided by Rauch and colleagues. Each dot represents the average Γ evaluated over the combinations of the four presentations of the identical stimulus.

modulated by the cell's own membrane potential. The total synaptic current is given by [Robinson & Kawai, 1993]:

$$I_{syn} = g_e(u - E_e) + g_i(u - E_i) \tag{5.1}$$

where the respective g's are the excitatory and inhibitory conductance, under the assumption that the contribution of individual synapses is small. The E's are the reversal potentials of the coupling. The input can then be described by an Ornstein-Uhlenbeck process [Tuckwel, 1988]. This process can either be simulated, including information about the dynamics of the synapses [Destexhe & Paré, 1999], or, as was done for the data set we use, approximated by a single equation, assuming the time courses of the excitatory AMPA and the inhibitory GABA$_A$ receptors are identical. The equation for updating the total synaptic current at each time step is given by

$$I(t + dt) = I(t) - \frac{I(t)}{\tau_I} + m_I dt + s_I \xi(t)\sqrt{dt} \tag{5.2}$$

where mean and standard deviation m_I and s_I are parameters and ξ is a zero mean unitary Gaussian random variable.

The data set we used is an extension to the one presented by Rauch *et al.* [2003] and was previously used by Jolivet *et al.* [2006b] for prediction of spike timing using threshold models.

Cortical pyramidal neurons fire irregularly on these kind of stimuli, but without long periods of spikes or silence [Mainen & Sejnowski, 1995; Stevens & Zador, 1998]. Furthermore, the reliability of the response is determined by the type of stimulus [Mainen & Sejnowski, 1995]; stimuli with low variance are unreliably reproduced, whereas highly varying stimuli are reproduced with a reliability of up to 80–90%.

The stimuli in the data set were generated in advance and each repeated four times to every cell. This allows evaluation of the intrinsic reliability as a reference for the performance of the models. See Fig. 5.3 for an overview of the coincidence factor (2.39) between spike trains from cells in the data set as a function of the variance of the input signal.

5.1.4 System identification

Bifurcation models are, as are most neuron models, nonlinear dynamical systems. When we try to represent data from real neurons with these models we therefore enter the domain of nonlinear dynamical system identification.

Nonlinear system identification is a fast-developing field of research. The amount of different techniques available is dazzling and new ones are added on a daily basis. This large variety of available techniques represents the uniqueness of nonlinear processes. Basically nonlinear systems all share one property: they hardly share any properties.

This is the reason many discussions on nonlinear system identification start by treating linear system identification, which, on the contrary, is a well established theory with clear rules and guidelines [Ljung, 1987]. It is commonplace to first attempt linear system identification before resorting to nonlinear techniques [Nelles, 2001, p. 457]. We will use linear system identification techniques for the analysis of the data set, as well as for fitting the FitzHugh-Nagumo model to subthreshold data.

The procedure of system identification can be separated into distinct steps:

1. Experiment design.

2. Choice of the model structure and complexity.

3. Choice of a loss function

4. Parameter estimation.

5. Model verification

Experiment design

The first step was only available to us in a very limited fashion. A major difficulty is that the experiments may have different goals, and that the goal of the study in this thesis (an identification task: fitting generic bifurcation models) is not entirely compatible with the original goal with which the data was collected (a classification task: correlating gene expressions to genetic profiles). Even so, considerations from nonlinear system theory some could in some cases help to improve stimulation protocols, independent of the goal of the experiment.

Choice of the model structure and complexity

The second step mainly addresses the question which model suffices for the task at hand. In our case this amounts to the decision whether the information in the experimental data can be reproduced in a satisfying way with either one of the two models available to us. It is important to mention the bias-variance trade off in this context [Weiss & Kulikowski, 1991], although this is more of an issue when models with many degrees of freedom are available (especially in the context of neural networks [Geman *et al.*, 1992]).

It is clear that the more complex a model is, the better it will be able to represent the complex data. Independently of the identification method used, it is possible to say something about the optimal model complexity for the problem at hand.

In real systems the output is inevitably distorted by noise. Neurons are certainly not an exception to this rule and hence we have a probabilistic framework in which we want to optimize the expectation of some output error. For the theoretical treatment we
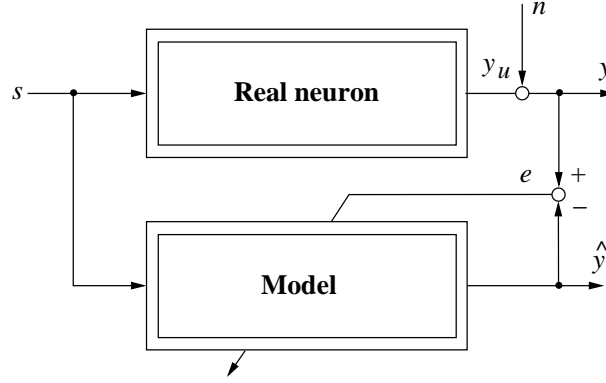
FIGURE 5.4: System identification.

assume that this is simply the difference between predicted output $\hat{y}$ and measured output $y = y_u + n$, where y_u is the real output of the neuron, which we cannot measure, and n is the noise on that output (See Fig.5.4). This means that any model, even the most complex one, can only predict the system output up to a factor equal to the noise variance. The minimum of the loss function, when the model error is zero, is therefore equal to this noise variance:

$$\text{loss function} = \text{model error} + \text{noise variance} \tag{5.3}$$

Since we cannot influence the noise variance, the model error is the term to be minimized. It can be decomposed into two parts: the *bias error* and the *variance error* [Nelles, 2001]:

$$(\text{model error})^2 = (\text{bias error})^2 + \text{variance error} \tag{5.4}$$

The bias error describes the error due to the restricted flexibility of the model. The bias error depends directly on the model complexity; if the model complexity is too low, the bias error is large. It can be reduced by increasing the model complexity, where the decrease in bias error is very fast in the beginning and then reduces, somewhat like an inverse power law. So for a too simple model, a lot can be gained by increasing even slightly the model complexity.

Increasing the model complexity will just increase the requirements on computational power, so, naively, one could simply take the most complex model ones computational resources allow. There are two reasons why this is not true.

First of all, in our case we don't want to just identify the model, we want the simplest model that still is a *good* representation of the reality, where the subjective criterion "good" of course depends on what we want to do with the model. This already implies a trade-off. But that is not the end of the story since the model error is most often dominated by the variance error.

The optimization based on the bias error supposes we can actually reach the bias error, i.e., that we can indeed find the optimal parameter values that make $\hat{y} = y$. Of course this is never the case in real applications. In practice we are dealing with noisy data of limited length. The latter feature is especially true in neuroscience, where data is noisy and it is often hard to measure traces longer than a couple of seconds from neurons and to maintain a neuron in the right conditions for longer than a couple of hours. Some authors
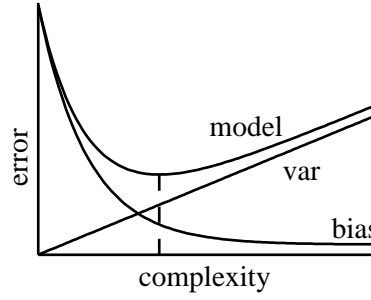
Figure 5.5: Bias-variance tradeoff. The horizontal axes displays the abstract notion of model complexity and the vertical axes the total error (between zero and unity). Dashed line indicates optimum complexity.

even argue that stationarity of the data is lost long before that (see Rauch *et al.* [2003, Fig. 1, panel C]).

When using too complex models for too short data sequences, one risks modeling the noise in the data, rather than the information. This is known as *over-fitting*. Generally, the variance error increases with the model complexity due to over-fitting and because it is more difficult to fit large numbers of parameters in a reliable way.

Putting the dependencies of the bias and variance error together one obtains a curve like the one sketched in Fig. 5.5 The optimum model complexity is a trade off between bias and variance error known as the Parsimony principle, or Ockham's razor: "*Pluralitas non est ponenda sine neccesitate* – entities should not be multiplied unnecessarily", i.e., of all the models that can describe the process (bias error), the simplest one is the best (variance error).

Choice of the loss function

When we build a model we want to make a mathematical description of reality. We want to choose the best possible description between a certain number of candidates. A questions fundamental importance is therefore: what is a "good" description? This question is made explicit by the choice of the *loss function*; a mathematical description of our idea of what a good model should be. The loss function quantifies this idea as a function of the model parameters θ and is given by $I(\theta)$ [Nelles, 2001].

The loss function forms a *loss surface* in parameter space. The goal of parameter optimization techniques is to find the global minimum of this loss surface with a minimum effort in a minimum amount of time.

Parameter estimation by optimization techniques

Optimization techniques for identification of linear systems are well developed and the state of the art is implemented in the MATLAB system identification toolbox [Ljung, 2006]. In this work we will use state space models, which are fit with the prediction error method that automatically determines the optimal model amongst the different available state-space realizations. The quality of the fit is determined as the average distance between the solutions, normalized and expressed as a percentage:

$$\mathcal{F} = 100 \left(1 - \frac{|y - \hat{y}|}{|y - \langle y \rangle|} \right) \tag{5.5}$$

where, referring to Fig. 5.4, y is the output of the system to be identified (the real neuron in our case) and $\hat{y}$ is the output of the model.

Three different approaches to parameter estimation can be distinguished:

- supervised learning

- reinforcement learning

- unsupervised learning

In both reinforcement learning and unsupervised learning no output value is known for each input. In reinforcement learning usually only general feedback about the performance of the model is available, whereas for unsupervised learning only input data is available on which statistical learning, such as automatic classification, pattern recognition and regression, is done.

Our case falls in the first category of supervised learning. Many different parameter optimization techniques are available for supervised learning, of which a great deal is designed specifically for high-order models, or models with a certain specific structure that does not correspond to the structure of our models (e.g., (recurrent) neural networks, fuzzy and neuro-fuzzy models).

The goal of supervised learning techniques is to minimize the error in the model with respect to the data. How to define this error is a user's choice, which depends on the goals of the modeling task. It can be simply the sum of squared errors between the measured and simulated outputs, or a much more complicated function. Three categories of optimization exist:

- linear optimization

- nonlinear local optimization

- nonlinear global optimization

We stress the difference between linear and nonlinear optimization techniques and linear and nonlinear models. Nonlinear optimization techniques can, and sometimes have to, be used in linear systems identification. The contrary is less common however.

Linear optimization techniques are the fastest and easiest to work with. The loss function always has a global minimum which can be found analytically and one-shot algorithms exist that arrive within a well-defined error from that minimum. For our problems, even when we use linear models, linear optimization techniques cannot be used.

When the error depends in a nonlinear way on the parameters no analytic solution exists and information about the gradient of the error surface usually has to be obtained numerically, which makes one-shot algorithms like the least-squares-type approaches, that exist for linear optimization unavailable.

All nonlinear local methods are iterative methods that evaluate the loss function in a point in parameter space and somehow try to evaluate the right direction and size of the step to take for the next iteration. When we use local optimization techniques it is for the optimization on a small number of parameters. Also, in our case, the evaluation of the loss function involves simulating the system, which is computationally costly. The best methods for these conditions are direct search methods and quasi-Newton, which are both implemented in the MATLAB linear system identification toolbox [Ljung, 2006].

Nonlinear global optimization techniques work on the entire parameter space. The goal of these techniques is to converge to the global minimum of the error surface as fast as possible without getting stuck in a local minimum. The principle approach of most techniques to try to avoid those local minima by using randomness.

The most simple global of techniques are the *random multi-start* methods. More advanced techniques include *simulated annealing*, *genetic algorithms* and *tabu search*.

Random multi-start techniques only use randomness for the choice of the initial parameter values. They then run many local algorithms ran in parallel for these different initial conditions. Random multi-start techniques are mainly used to get an initial idea of the structure of the error surface and to find initial points for other global optimization techniques.

Simulated annealing [Kirkpatrick *et al.*, 1983] tries to avoid local optima by adding a random component to the parameter updating step from a local algorithm. The disadvantage is that this randomness will deteriorate the convergence speed and precision of the final solution. To get around this in simulated annealing the randomness is decreased in time. In the beginning, when local optima have to be avoided, the random component is chosen large. As the algorithm progresses and finds the region of the global optimum, the random component decreases until finally the algorithm converges to a local optimization.

Genetic programming and evolutionary algorithms do not use gradient information at all, it simply evaluates the loss function at a lot of points in parameter space, keeping the best of these points (the *elite group*) to generate new points (*offspring*). A random component is introduced in the generation of this offspring, called *cross-over* and *mutation*, reflecting the evolution-theory on which it is based.

Tabu search is a relatively new technique that combines local and global techniques. A local search is started in many different places at the same time, much like the random multi-start methods, but now a history of the searches is kept to avoid visiting the same place in parameter space twice.

Techniques that use a single starting point, such as simulated annealing, are more suitable if the local minima are not too far from the global minima and are not too frequent. If there are many local minima, that in addition are relatively close in value (but not in distance) to the global optimum, methods with a single starting point will spend too much time in these regions; for instance the temperature decreasing scheme in simulated annealing has to be chosen very slow to avoid getting stuck in one of the local optima. In this case a method that keeps track of multiple solutions at the same time, such as a genetic algorithm is more profitable.

A good strategy to determine the shape of the loss function and the choice of the global optimization technique is to perform a random multi-start local optimization first [Nelles, 2001, p. 113]. This gives an idea of right choice of the global strategy and also helps the choice of the settings of the many fiddle parameters of these methods.

In summary: global methods are good at finding regions and local methods are good at finding points. It makes therefore sense to combine both methods. We now have two degrees of freedom in compiling the ideal optimization strategy. The first is the choice between local and global methods, and the second is the choice which parameters to optimize when. (It is not necessary – and often not possible – to optimize all parameters at the same time). Combining these two choices gives us three different strategies: subsequent optimization, nested optimization and staggered optimization [Nelles, 2001]. Subsequent optimization first performs a global optimization to get near the global optimum and then

refines the solution using local techniques. Nested optimization can be used when some parameters are easy to optimize. The global technique is performed on the partition of the parameter set θ_{hard} that is hard to optimize. For each evaluation of the loss function it optimizes the other parameters θ_{easy} to get the optimal solution at that point in the space θ_{hard}. Staggered optimization can be used if the influence of the individual parameters is close to orthogonal. Each parameter is optimized separately by using a global strategy first, if necessary, and then a local strategy.

CONSTRAINED OPTIMIZATION

The optimization techniques outlined above all work on the entire p-dimensional parameter space. Our neuron models have a considerable amount of parameters, even when the number of parameters is optimized by generalization of the models. On the other hand the models usually only work properly for a very small partition of the parameter space. Parameter values outside of this partition lead to a behavior that is inherently unable to model the experimental data and can thus be ruled out *a priori*. Very often a bounded region in parameter space can be established:

$$\mathbf{G}(\theta) < 0 \tag{5.6}$$

Obviously it would be a huge advantage to be able to incorporate these constraints into the optimization methods. For the global methods this is usually not too much of a problem. Genetic algorithms, multi start methods and simulated annealing can be stopped at the boundaries of the parameter regions. Local methods however iteratively try to find their path on the error surface and, if the surface is too irregular, can "fall off" the bounds in the parameter space. Techniques for nonlinear local optimization are mathematically much more complicated than the unconstrained methods [Vanderplaats, 1984].

The most advanced methods aim to approximate the Kuhn-Tucker equations or optimize the Lagrange multipliers that are posed by the inequalities describing the bounds [Vanderplaats, 1984]. The algorithm incorporated in the MATLAB optimization toolbox is sequential quadratic programming, which is one of the most powerful algorithms.

If the bounds are relatively easy, it is sometimes more simple and straightforward ways to incorporate constraints directly in the loss function using an extra penalty term that penalizes (severely) parameter values outside of the region of interest [Nelles, 2001]:

$$I_p(\theta, p) = I(\theta) + pP(\theta) \tag{5.7}$$

The penalty function $P(\theta)$ should be large for parameter values outside of the region of interest. The term p weights the penalty function and allows easy tuning of the method once the penalty function itself is fixed. For the choice of the penalty function two different approaches can be distinguished: the exterior and the interior approach. For an exterior approach the penalty function is quadratic, which means that the loss function increases rapidly when the parameters are outside of the bounded region, thus bending the edges of the error function such that solutions that start outside of the region will quickly converge into the region. The interior approach takes $-1/\mathbf{G}(\theta)$ as the penalty function. The loss function will therefore quickly converge to infinity when approaching the bounds of the parameter region from inside. The drawback is that outside the bounded region the penalty term becomes negative, and the optimization will converge to the boundaries and stay there, so when using the interior approach one has to be sure to start within the parameter regions and also that the optimum is not to close to a boundary of this region.
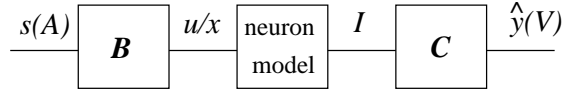
Figure 5.6: Addition of input and output interfacing to neuron models

5.2 Considerations for automated identification of bifurcation models

Some general considerations can be formulated that hold for the problem of fitting generic bifurcation models to neuronal data independent of the specific model. Also, to fit generic bifurcation models – which give a qualitative representation of reality – to real data, additional degrees of freedom have to be introduced. This section presents extensions to the FitzHugh-Nagumo and Hindmarsh-Rose models that facilitate working with electrophysiological measurements and a discussion on the choice of the loss function.

5.2.1 Generalizations for interfacing with real world quantities

Although I is always referred to as the input current and the first state variable as the membrane potential, all units in the FitzHugh-Nagumo and Hindmarsh-Rose model are dimensionless. This means there are additional, implicit, parameters in the models interfacing with the real-world quantities time, (input) current and (output) voltage. In system identification and control theory the usual terminology for the input and output scaling is B and C. These factors do not appear directly in the model, but form an interface between the model and reality. Schematically, the contents of the block "model" in Fig. 5.4 can then be filled out as shown in Fig. 5.6 where, with respect to the usual representation [Ljung, 1994] the direct path from input to output is left out, for obvious reasons.

The time scaling means an explicit definition of what the dot operators in (2.6) and (2.29) mean. We will call the degree of freedom associated to this assignment τ_s. Then the model time t_m is scaled according to:

$$\tau_s = t/t_m \quad \text{(s)}. \tag{5.8}$$

The addition of the three parameters and the interfacing with measurement signals s and model output $\hat{y}$ can be expressed for the FitzHugh-Nagumo model as:

$$\begin{cases} \dfrac{\mathrm{d}u}{\mathrm{d}t} &= \tau_s^{-1}\left(f\left(u(t)\right) - w(t) + Bs(t)\right), \\ \dfrac{\mathrm{d}w}{\mathrm{d}t} &= \phi\,\tau_s^{-1}\left(u(t) - bw(t)\right), \\ \hat{y}(t) &= Cu(t), \end{cases} \tag{5.9}$$

For the Hindmarsh-Rose model the expression is analogous. In practice the time scaling can be performed on the time vector of the measurements directly.

5.2.2 Choice of the optimization methods

Which global optimization method to use depends on several factors. Important for the choice of the global method is the initial guess of the parameters and the shape of the loss function. In the case of generic bifurcation models the link with physical parameters is

very weak and it cannot be induced in advance in which region the optimum parameters should lie. In practice it turns out that the loss surface for all situations where a global optimization method was used in this thesis was so irregular that a genetic algorithm gave the best results.

The choice of the local optimization method is less obvious and several options are available that usually perform equally well on the average, but whose performance is not necessarily equal for different problems. Much of the choice of the local method comes from the user's experience [Nelles, 2001]. One thing is clear however: due to the bifurcation structure and the non-straightforward form of the loss criteria there is no hope to obtain a least squares, or any kind of analytical expression, for the gradient of the loss function. This is a usual phenomenon in grey box models and it already rules out some of the available techniques. Another feature specific for the problem at hand is that we have a large prior knowledge on bounds and structure of the parameter space through the analytical techniques presented in Chap. 2. The disadvantage of not having gradient information is partially compensated by the great advantage of prior knowledge on the range of possible parameter values. This allows the use of a constrained optimization algorithm, which, instead of solving the optimization problem directly, focus on solving the Kuhn-Tucker equations [Nelles, 2001, p. 107] and are highly efficient.

The exact choice of the optimization technique then depends on the choice of the loss function, but limits itself to techniques that need a low number of function evaluations and no analytical gradients. The state of the art algorithms for these restrictions are Sequential Quadratic Programming, if the gradient is sufficiently regular and Simplex Search, if no analytical gradient information can be obtained or used.

5.3 Reproduction of diversity in electrical profiles

From the analytical and numerical treatment in Chap. 2 it should be clear that there are fundamental limitations in the representation of neocortical diversity, especially with the FitzHugh-Nagumo model. The Hindmarsh-Rose model should, in principle, be able to model qualitatively most of the features that are seen as characteristic in neocortical cell classes, although the intermittency in stuttering (or chattering) is difficult to reproduce.

5.3.1 Analysis of the data set

As is usual in literature, we separate the discussion between excitatory and inhibitory neurons.

Super-threshold step responses

In the data set only PCs were present and no SSCs. Surprisingly, of the twelve PCs investigated, apart from the expected and by far most common RS behavior, two showed STUT and one IS. The three different types of step responses are shown in Fig. 5.7.

Four subtypes of step responses were present amongst the inhibitory neurons in the data set. No bursting cells were identified. Figure 5.8 shows examples of each type.

Sub-threshold step responses

In the light of the discussion on the sub-threshold behavior of the FitzHugh-Nagumo model in Sect. 2.3.2 it is interesting to study the properties of the subthreshold behavior of the

FIGURE 5.7: Samples of the different classes of step responses of PCs encountered in the data set *a* RS. *b* IS. *c* STUT
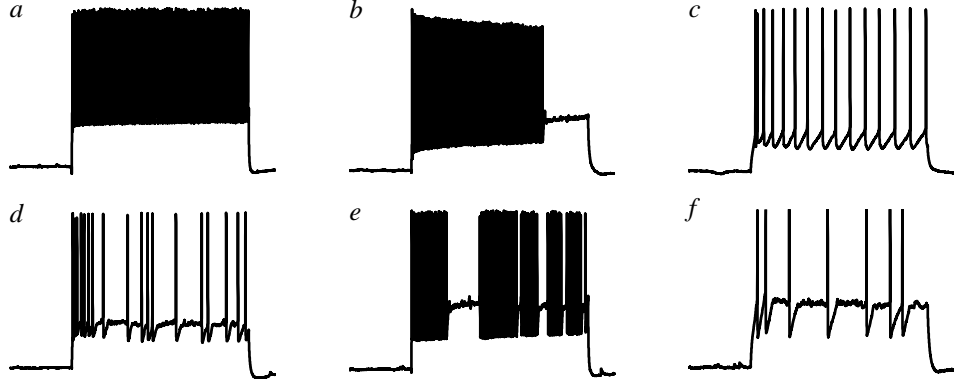

FIGURE 5.8: Samples of the different classes of step responses of inhibitory interneurons encountered in the data set *a* NAC. *b* AC. *c* AC *d* STUT *e* STUT *f* IS

neurons in the data set. Unfortunately, only simple step stimuli were available, which severely limits the possibilities for identifying linear systems from the data. However, the static gain of the system and the principal eigenvalue can usually be identified [Nelles, 2001, p. 461]. Figure 5.9 shows the results of the identification of the subthreshold step responses and IV curves in the data with linear black box models of different order. The subthreshold stimuli were each applied three times. Two of these repetitions were used for the identification and the third for validation of the fit. The fit of a first order linear black box model on the validation set of the subthreshold data is $(78.5 \pm 7.7)\%$; $(n = 51)$. The fit does not improve with increasing order. The remaining 21.5% can only partially be explained by the influence of noise (the absolute minimum of the fit determined by the bias error), but analysis of the residuals show a strong correlation for nonnegative time lag. This indicates that the residuals contain information that is not captured by the models.
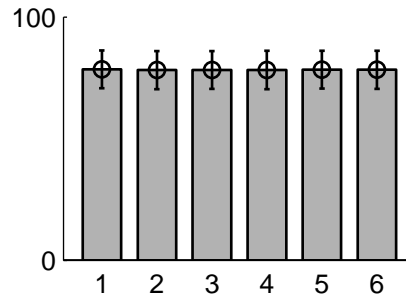

FIGURE 5.9: Linear identification of the subthreshold data for different orders of the linear model (x-axis)
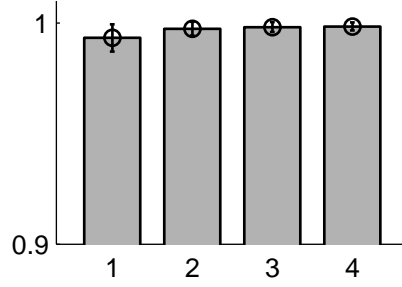
FIGURE 5.10: Curve fit of the IV curve with polynomials of different order (x axis). Note that for detail, the y-axis does not start at zero.

Two explanations are then possible: 1. the input signal is too limited in frequency content to excite all modes and does not allow the identification of higher order linear components and 2. the system has a nonlinear component.

To verify this second possibility, we look at the static IV relation of the cells. This relation is defined as the value of the membrane potential at the end of a long current step, as a function of the applied current (cf. (2.17)). The IV characteristic of all cells were fit to polynomials of increasing order using a bisquare weights scheme to account for outliers in the data. The number of points in each characteristic was 11 and, as before, the number of cells investigated $n = 51$. The R-square value of the linear fit is (0.9933 ± 0.0062) and the improvement for increasing order is within the standard deviation (Fig. 5.10). This is in accordance with expectations of a dominating linear IV characteristic for sub-threshold values of the membrane potential. In theory, even if the asymptotic behavior of the system is linear, the underlying system can still be nonlinear, if it is of dynamical order higher than one, this is however only possible if the nonlinearity in the hidden state(s) (any other state than the one measured) is canceled. The FitzHugh-Nagumo model has a linear hidden state and cannot model such a behavior. We conclude that there is a strong suspicion, but not proof, that the cells in the data set behave like linear integrate-and-fire cells sub-threshold.

OTHER RESPONSES

Cells from different classes often respond in a qualitatively similar way to the stimuli other than super threshold sustained current injection. Especially subthreshold behavior is qualitatively very similar from cell to cell, which motivates the use of super-threshold stimuli for the classification of neurons. Compare the responses in the complete protocol for a PC; an AC cell, an IS cell and a STUT cell shown in Figs. 5.11, 5.13 and 5.14, respectively.

Quantitatively there are large differences between the responses of different cells, also for sub threshold stimuli, but no apparent correlation between these quantitative differences and the classification according to discharge responses has been reported yet.

5.3.2 REPRODUCTION OF THE ELECTRICAL PROFILE WITH THE HINDMARSH-ROSE MODEL

As the very definition and classification of neocortical diversity is still in progress, it is very hard to quantify characteristic behavior of the different cell classes, even if we would
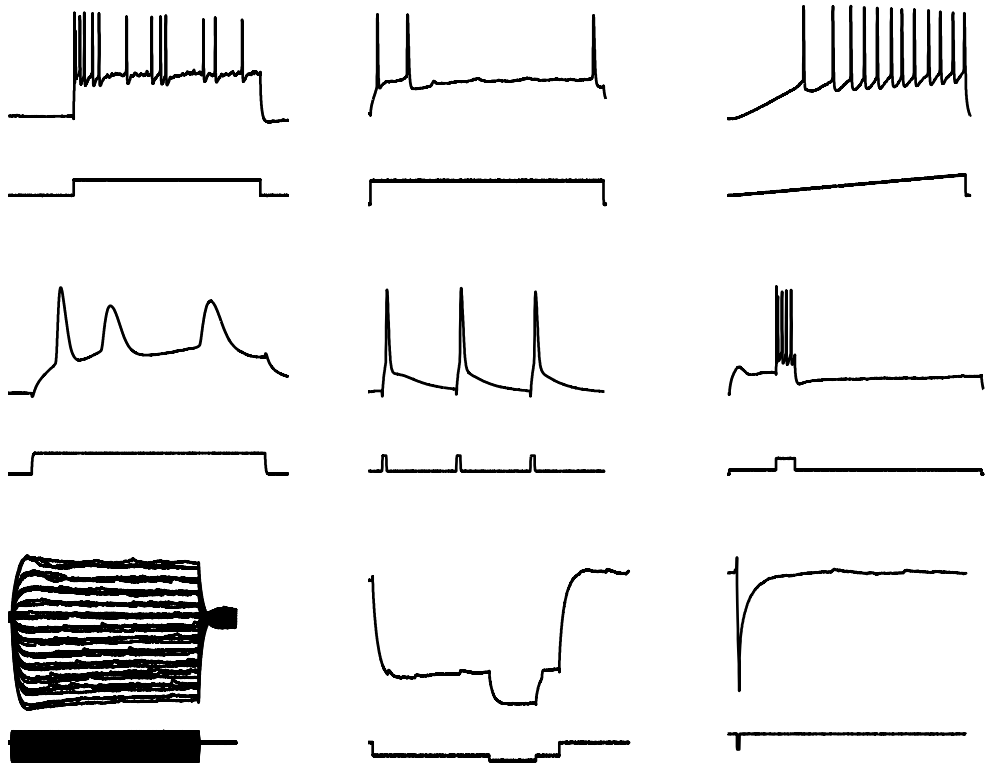
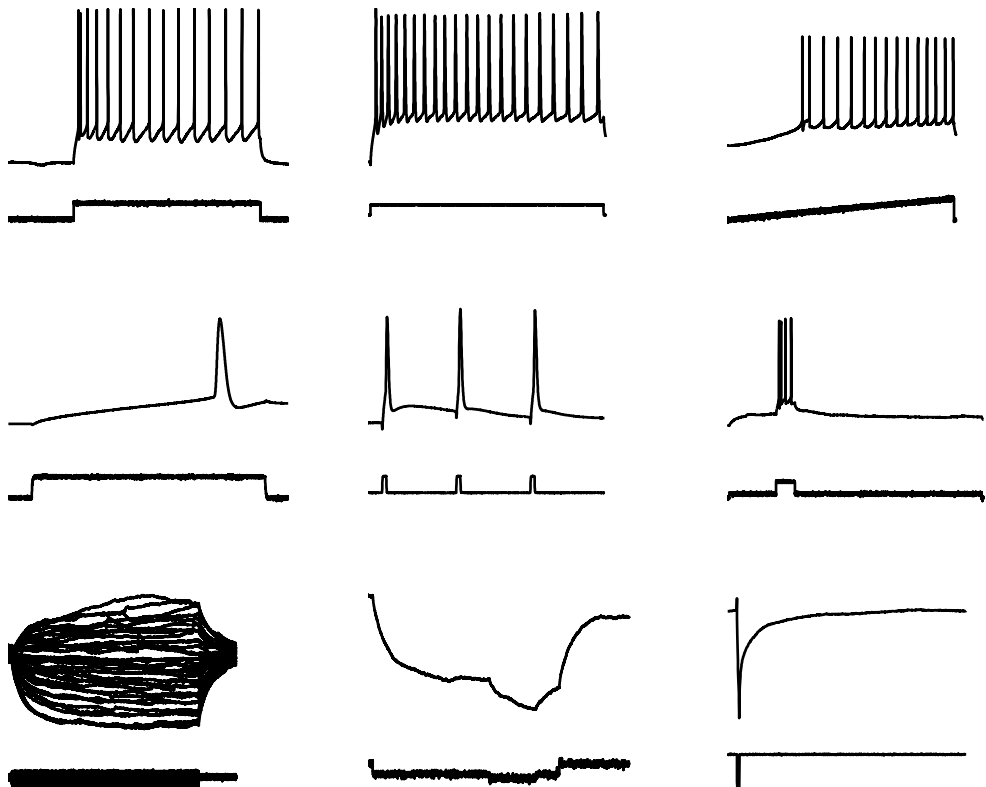Figure 5.11: Electrophysiological responses of pyramidal cell (PC).

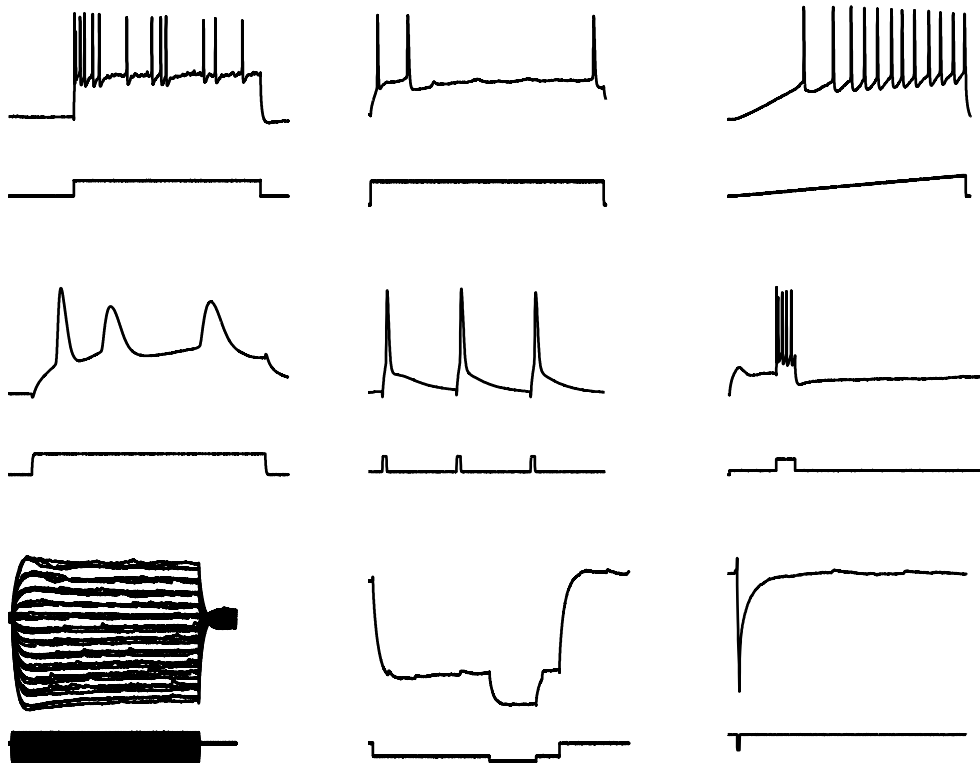Figure 5.12: Electrophysiological responses of accommodating (AC) cell.

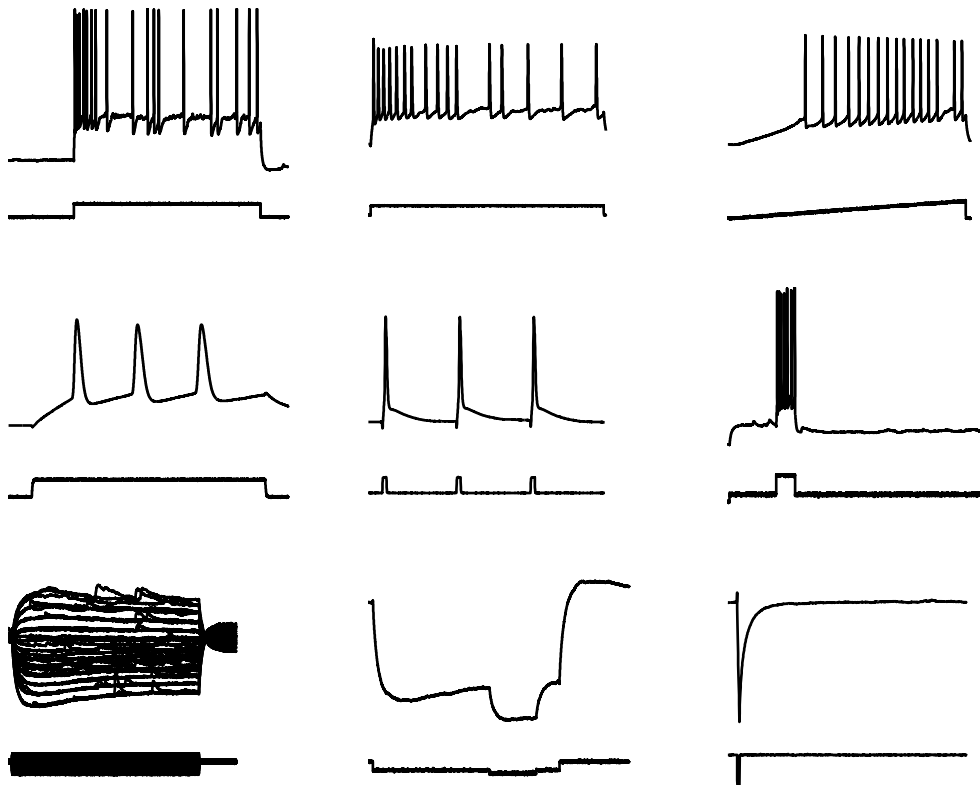Figure 5.13: Electrophysiological responses of irregularly spiking (IS) cell.

Figure 5.14: Electrophysiological responses of stuttering (STUT) cell.

agree on one specific classification scheme. This makes the choice of a quality criterion for the quality of the fit especially difficult. In literature the neocortical cell classes are characterized verbally (Sect. 5.1.1), so, until a standardized classification scheme for cell classes is proposed, we are restricted to the use of visual criteria. Simple criteria such as the spike frequency would not capture the essence of the difference in behavior outlined in Sect. 5.1.1 and would bias the fit in favor of the more simple spiking models, ignoring the detail provided by more advanced models.

We will base our classification on the scheme proposed by [Markram *et al.*, 2004], which was described in Sect. 5.1.1, and adopt the same terminology.

The theoretical limitations of the FitzHugh-Nagumo and Hindmarsh-Rose model for modeling the quantitative behavior of the discharge responses are clear from the analytical treatment in Sects. 2.3 and 2.4 respectively: the FitzHugh-Nagumo model can only reproduce simple spiking behavior and is therefore unfit to model any other than accommodating and non accommodating spiking. As shown in Sect. 5.3.1, the fitting of the FitzHugh-Nagumo model to the subthreshold responses has a theoretical upper limit equal to the quality of prediction obtained by linear models. In reality the optimal fits are far worse. Attempts to use the weakly nonlinear filtering techniques described by Jolivet *et al.* [2006b] – which give very good result for prediction of neuronal activity both for subthreshold traces and spike timing – using a class of integrate-and-fire models, failed. We refer to the discussion in Sect. 5.4 for further details.

The Hindmarsh-Rose model has both a more realistic description of subthreshold activity and a larger diversity in its possible behaviors. It is possible to reproduce many of the responses observed in the data set qualitatively [De Lange & De Feo, 2006]. Using the classification scheme from Fig. 2.17 and the analytical notions from Sect. 2.4, we fitted the model to different discharge responses by a semi-automatic procedure. The reason for the choice for this hybrid approach was that it is impossible to find quantitative criteria in literature to distinguish between the different classes of behavior. We subsequently tried to reproduce each of the types of behaviors outlined in Sect. 5.1.2; – the rows in Fig. 5.2 – individually, before comparing the quality of the resulting fit on the entire protocol.

The criteria we used for the automatic fit are summarized in table. 5.1. They were based on the 61 electrophysiological properties defined by Toledo-Rodriguez *et al.* [2004, Table 3]. Many of the criteria were however not feasible, or did not make sense for a qualitative comparison (such as height of action potentials, resting membrane potential). The choices for criteria reported here should be seen as a first investigation into the possibilities for use and adaptation of this protocol to the Hindmarsh-Rose model, rather than an exhaustive investigation. To keep the results tractable a maximum of two criteria per waveform were selected. Note that not all waves in Fig. 5.2 are used. A problem is that these quantities, although they have a physiological meaning and unit, can often not be normalized, forbidding an honest comparison. For those waves only visual considerations were used. Only heuristics can show the normalization needed for each measure, hence the iterative procedure described above.

The cells were divided in three different groups: 1. NAC, 2. AC and 3. Other and one cell was selected randomly from each group for identification. The cells that were selected were C28, a NAC, shown in Fig. 5.11; C96, an AC, shown in Fig. 5.12; and C34, an IS, shown in Fig. 5.13. We explicitly mention the cell numbers to facilitate distinction between them. Each cell was fitted to each of the three groups of stimuli (super-threshold steps, super-threshold pulses and sub-threshold; cf. Sect. 5.1.2) separately. Since the fits were partially done by hand, the parameter values were adapted blindly by slide-rulers, without

Physiological properties	Description	Type
Group 1: Discharge and ramp responses		
a. IDrest		
Frequency	Difference in number of spikes	N
Discharge type	Difference type of discharge pattern	V
b. APDrop		
Accommodation	Difference in the variability between first and last ISI	N/V
c. APThreshold		
Threshold	Difference in time of onset of excitation	N
Group 2: Spike shape and after hyper/depolarization		
d. APWaveform		
Spike width	Difference in width of the first spike	N
Drop	Difference in drop in spike width between first and second spike	N
e. ADHPrest		
Spike form	Difference spike form after delta pulse	V
f. sAHP		
Hyperpolarization	Difference in behavior shortly after burst	V
Group 3: Sub-threshold		
g. IV		
Overshoot	Difference in change in input resistance (average slope of IV characteristic)	N
h. IRhyperpol		
Dynamics	Mean square error	N
i. Delta		
Time constant	First time constant from exponential fit	N

TABLE 5.1: Criteria for the fitting of the Hindmarsh-Rose model to the in vitro protocol. In column "type", N stands for numerical, V for visual. The letters correspond to Fig. 5.2.
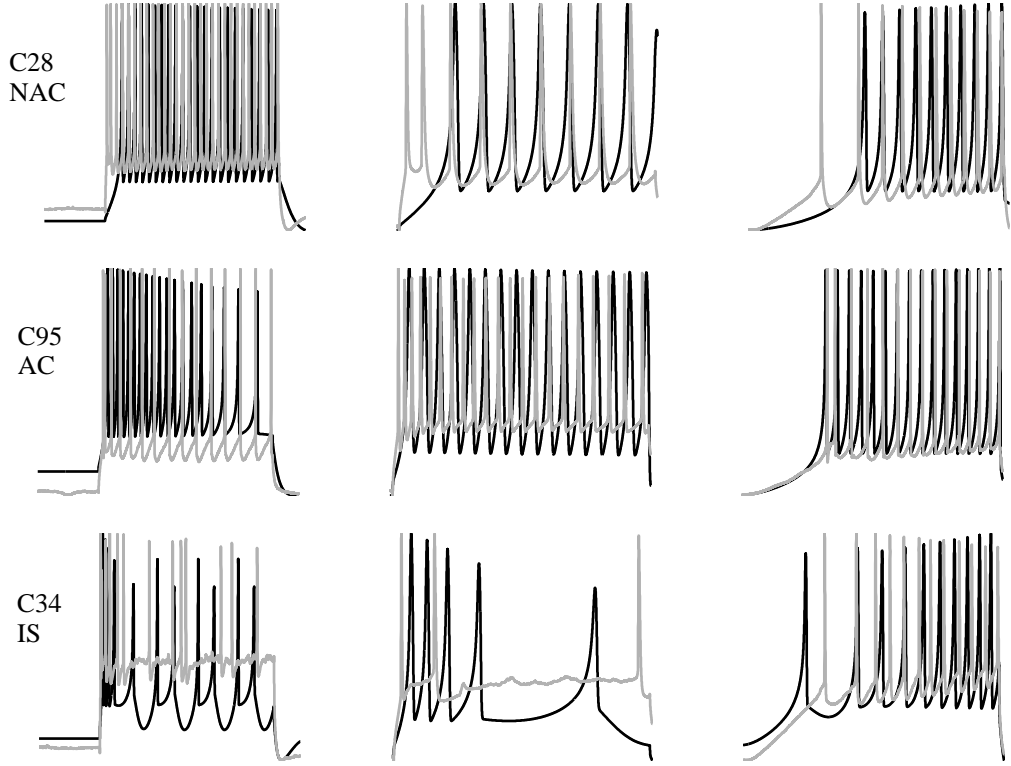
FIGURE 5.15: Results of fits of Hindmarsh-Rose model to super-threshold step and ramp currents.

information about the precise value, not to bias subsequent fits for different criteria on the same cell by prior knowledge. In addition the fits were performed in a random order. The fits shown were the second cells for each type after having gained experience and collected heuristics on the first series of three cells.

Fit on individual types of stimuli

As expected the spiking frequency of NAC cells could be faithfully mimicked by the Hindmarsh-Rose model (Fig. 5.15; left). The accommodation criterion for $IDrest$ had to be turned off since the normalization becomes ill-defined when the accommodation tends to zero. Accommodating discharge patterns can be reproduced faithfully as well as is shown in the middle row of Fig. 5.15. As can be expected in view of the mathematical limitations of the Hindmarsh-Rose model, the irregular spiking behavior is very hard to capture. Using the road map from Fig. 2.17, we were able to reproduce irregular behavior, although not similar to the one observed in the cell (bottom row in Fig. 5.15).

The spike shape is for a large part fixed in the Hindmarsh-Rose model. To approach different shape displayed in the data, unrealistic parameter values had to be taken (for very low b, the shape changes considerably), which had too large an impact on the quality of the fit on the second and the third stimulus from this group (ADHPrest and aAHP). The spike width and distance could be approximated in a satisfactory way as well as the shape of the spikes on delta pulses and the after hyperpolarization. Especially the fit on the non accommodating cell (top plot Fig. 5.16) was excellent, reproducing perfectly the hyperpolarization after the burst and the detail in the delta response.
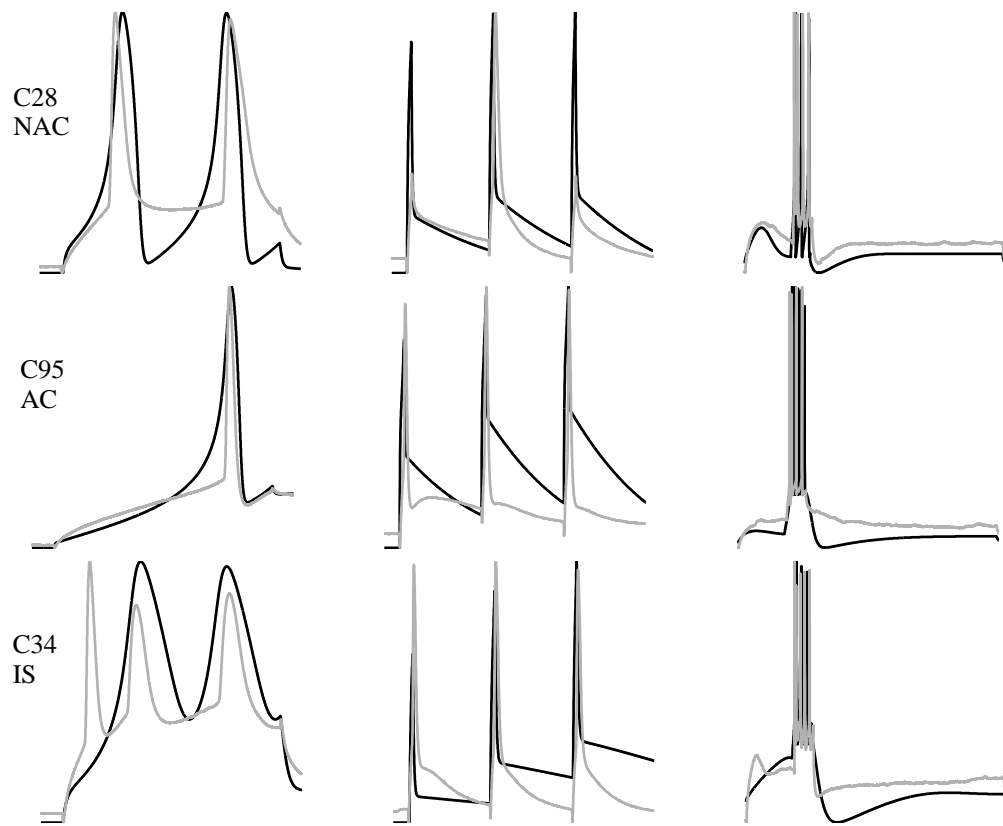
101

FIGURE 5.16: Results of fits of Hindmarsh-Rose model to super-threshold pulses.
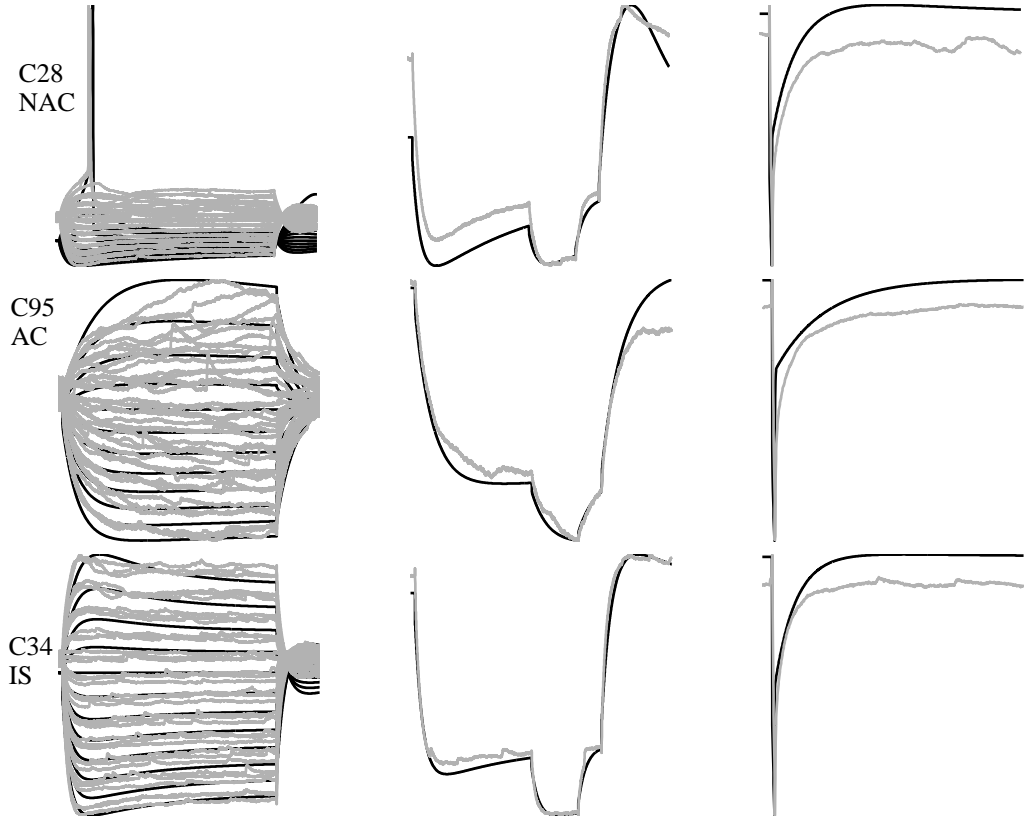
FIGURE 5.17: Results of fits of Hindmarsh-Rose model to sub-threshold steps.

The problem with the modeling of the shape of the action potential becomes apparent when comparing the fit of C95 and C34 (middle and bottom row Fig. 5.16): the fit concentrated too much on capturing exactly the timing and shape of the action potential, losing quality in the fit of the other two stimuli. This could possibly be improved by redefining the fitness criteria, or adjusting the weights of the different criteria.

In contrast to the FitzHugh-Nagumo model, for which the fits on subthreshold data failed to give any reasonable results, the Hindmarsh-Rose model is capable of representing the diversity in subthreshold dynamics very faithfully. In the fit shown in the top plot of Fig. 5.17, no specific attention was paid to reproduce the fact that the highest of the steps elicited a spike (accidently). This trace was taken out as an outlier, but included in the validation, and indeed reproduced. This could have been a coincidence however and further investigation is necessary on other cells in the data set that contain this "accident".

The results presented above show that many, but not all, of the features of the in vitro protocol can be reproduced in great detail by the Hindmarsh-Rose model. Since the fits were done on specific features at a time this does not prove that the Hindmarsh-Rose model is a good representation of neocortical neurons on the whole. Especially the quality of the fit on the subthreshold data could seem obvious, considering the general consensus that the subthreshold behavior of neurons is trivial in comparison to the complex nonlinear dynamics that govern the super-threshold behavior. To be able to assess the quality of the Hindmarsh-Rose model in representing neuronal behavior it is therefore important to

Cell	Group	parameter				
		B	s	μ	R	τ_s
	1	3	1	0.002	0.004	100
C28	2	3.6	4	0.01	0.01	150
	3	3.6	4	0.005	0.007	200
	1	3	4	0.03	0.009	150
C95	2	2.8	4	0.01	0.01	100
	3	2.8	1	0.01	0.005	200
	1	3	2	0.005	0.007	100
C35	2	3	0.005	0.005	0.007	100
	3	3.4	0.002	0.002	0.0035	100

TABLE 5.2: Parameter values for the fittings of the Hindmarsh-Rose model to three cells in the in vitro data.

look at the results of the fits on the entire protocol. It seems impossible to formulate unambiguous criteria for the fitting of the entire protocol at once, but it is possible to compare the fits presented above on the other stimuli. Not only this allows the assessment of the general quality of the predictions, in addition, the results give insight in which features are decisive for the quality of the fit and will help formulate a protocol for tuning the Hindmarsh-Rose model to specific cell-type behavior.

COMPARISON OF THE FITS ON THE ENTIRE PROFILE

The values of the fitted parameters for each cell are given in table 5.2. For brevity, we display the results for one cell; the full results for all three cells are reported in appendix A. The results shown in this section are for cell C28; the non accommodating LBC. While not identical, the results for the AC cell allow the same general conclusions, whereas results for the IS cell are harder to compare since the model is incapable of faithfully reproducing the discharge response.

The fit based on the discharge responses is not very good. The main problem is that there are too many degrees of freedom when a fit is done on the spike frequency and adaptation alone. The spike frequency is controlled both by the time scaling factor and by the input scaling factor. For a given sustained input current, there exist pareto-optimal curves of identical frequency in (τ_s, B), as sketched in Fig. 5.19. In principle, if the frequency were fit for steps of different amplitude and if the threshold were known, it should be possible to locate the exact optimal point on these curves, because the spike threshold will only depend on B. In practice it is hard to determine the spike threshold from the ramp current. It was apparently impossible to estimate the threshold correctly from the strong super threshold pulses and the ramp current. This could be explained by the difference between the dynamic and static threshold (see the discussion in Sect. 2.3.2): the ramp current will identify mostly the static excitation threshold, whereas for all other stimuli the neuron operates in transient mode.

When looking at the values in table 5.2 it seems that this caused as misfit of parameters b and s, which were identified better from the other two groups of stimuli. This shows that the choice of the type of behavior and the accommodation from discharge responses
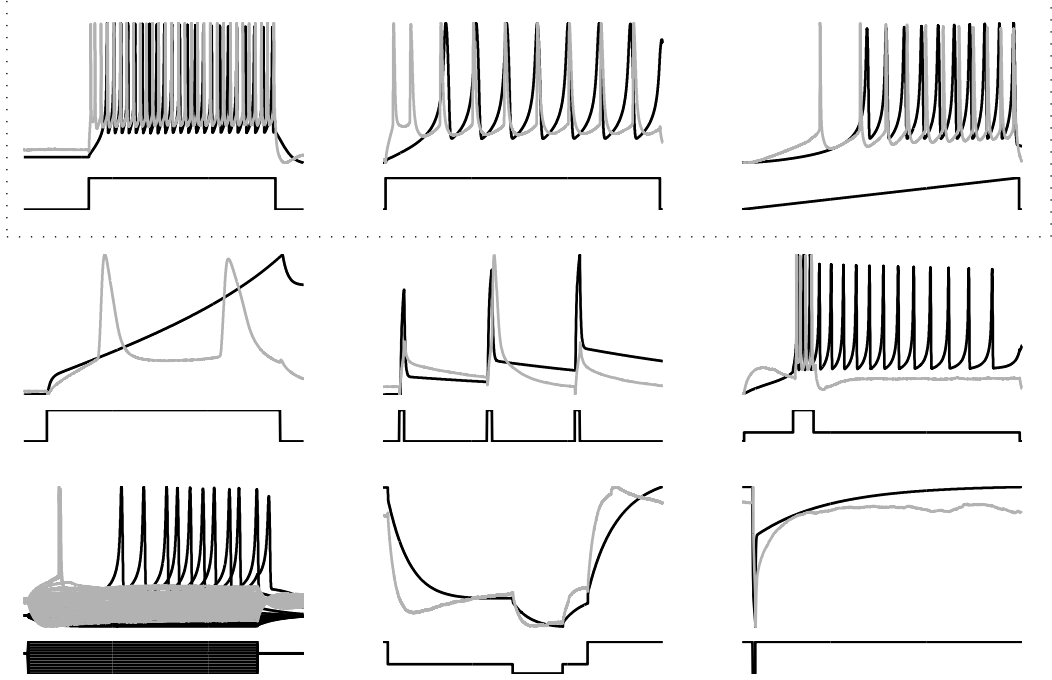
FIGURE 5.18: Results of the reproduction of the complete protocol, with fits based on super threshold discharge responses (first row; indicated by dotted rectangle).
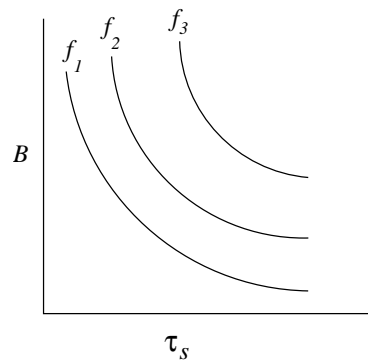

FIGURE 5.19: Sketch of curves of constant spike frequency as a function of τ_s and B for given constant I in the Hindmarsh-Rose model.
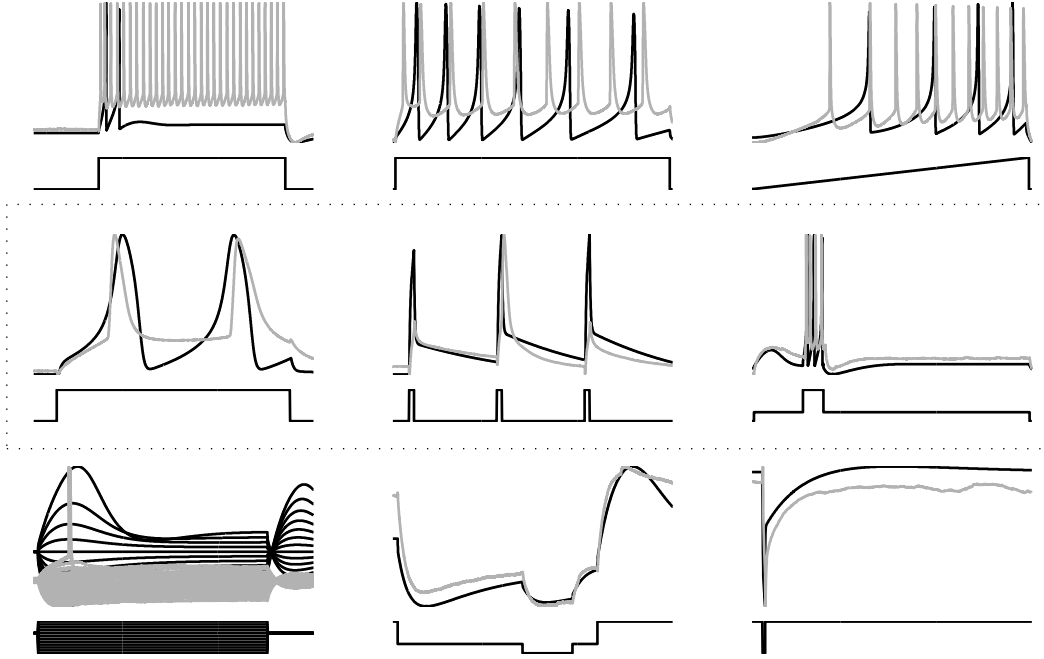
Figure 5.20: Results of the reproduction of the complete protocol, with fits based on shape of action potentials (second row; indicated by dotted rectangle).

only is a dangerous one, although to induce statistics much more cells have to be fit.

The fit that resulted from focussing on the second group of stimuli was good for the subthreshold signals. This can be expected, since both groups focus on details of dynamic behavior, rather than the more large-scale phenomena taken into consideration by the first group. The frequency of the discharge responses is underestimated which is probably due to an underestimation of the spike threshold that can also be seen from the IV characteristic in the bottom row.

Finally, the model fit on subthreshold stimuli from group 3 yielded the best results. Especially surprising is the good fit of the ramp and APDrop stimuli. The value of b is probably too high, which explains the cessation of spiking after sustained current injection and what looks like adaptation in the APDrop response.

5.3.3   Discussion

Surprisingly the fitting procedure gave the best results when fits were done based on subthreshold signals. Nevertheless, the reproduction of each individual type of criterion (discharge response, spike shape and subthreshold response) is best when the fit is directly based on these responses. Unfortunately it is not possible to combine the three fitting protocols: since some parameters influence the quality of more than one criterion (see table), it is impossible to assign a parameter, of combination of parameters to a given criterion, making fitting of the entire protocol at once feasible. However, there are still some general guidelines and principles that should be used when fitting the Hindmarsh-Rose model to in vitro data. The best results will be obtained if detailed sub-threshold responses are available. This is in contradiction with the idea of the neuron behaving like
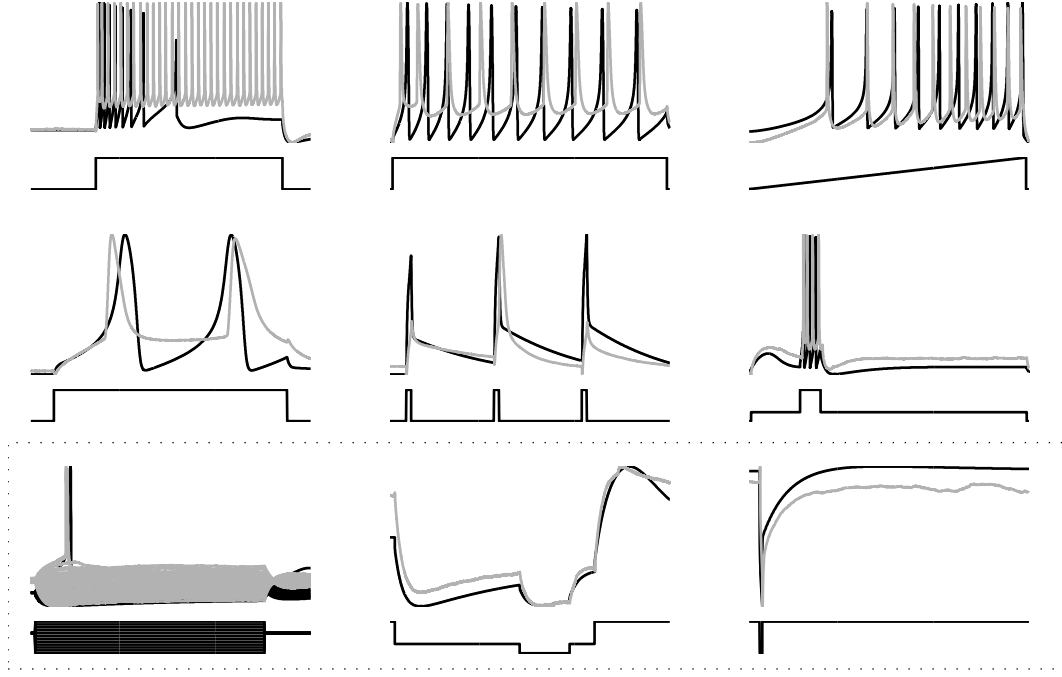
FIGURE 5.21: Results of the reproduction of the complete protocol, with fits based on sub-threshold behavior (third row; indicated by dotted rectangle).

a simple linear integrator sub-threshold, which could mean that the imperfection in the linear fits presented in Sect. 5.3.1 does in fact contain essential, nonlinear, information.

The fit results confirm the intuition that the classification on steady state behavior presented in Sect. 2.4 is not valid under the transient conditions in vitro. The values of b obtained are often well in the bursting region, but under the in vitro stimuli this bursting does not manifest itself; the cell seems to be operating in a transient mode that regularized the response. Under these stimuli, the dynamic parameters μ, s and τ_s seem decisive.

What concerns subthreshold behavior, the Hindmarsh-Rose model definitely seems to give an adequate description, better even than the higher order ARMAX models that were automatically identified on the same data. This, too, should be subject of further investigation.

5.4 REPRODUCTION OF SPIKE TIMING TO IN VIVO-LIKE STIMULI IN PYRAMIDAL NEURONS

For the fitting of the FitzHugh-Nagumo model to the data from the second data set, with only in vivo-like conductance-based stimuli, an automatic optimization method was applied. As a general introduction, we propose an automated optimization strategy for generic bifurcation models in particular and the FitzHugh-Nagumo and Hindmarsh-Rose model specifically. To show the power of the fitting strategy it is then tested on the least favorable candidate; the FitzHugh-Nagumo model.

Group	Parameter	Bifurcations	Dynamics	Scale
	a	$+$	$+/-$	$-$
G	b	$+$	$++$	$-$
	ϕ	$+$	$+$	$-$
	B	$-$	$-$	$+$
L	C	$-$	$-$	$+$
	τ_s	$-$	$-$	$+$

TABLE 5.3: Influence of different parameters of the generalized FitzHugh-Nagumo model.

5.4.1   OPTIMIZATION STRATEGY FOR GENERIC BIFURCATION MODELS

We begin the design of a brute force strategy based on the FitzHugh-Nagumo model because the derivation is more clear and straightforward due to the fewer parameters and the relative simplicity of the model. The extra considerations needed for the Hindmarsh-Rose model, partially based on the observations from Sect. 5.3 will be outlined at the end of the discussion.

The parameters of the FitzHugh-Nagumo model can be separated in two groups based on the type of influence they have on the behavior of the model (see table 5.3). The parameters of the original model – a, b and ϕ – have no influence on the scale of the in and output. On the other hand their influence on the dynamical behavior of the model is very strong. They can cause bifurcations and strong changes in the qualitative behavior. This makes their influence on the loss function very nonlinear and hard to predict.

Scaling parameters B, C^1 and τ_c have a complementary function to that of the other parameters (a separation that is not as clear for the Hindmarsh-Rose model). They do not influence the dynamics of the model at all, so their influence on the loss function is very regular. As an example one can imagine the influence of C for fixed values of the remaining parameters. All C does is to scale the output. If the loss function is a least square error on the output, the optimum as a function of C will be easy to find.

According to this separation we define two groups. The set G $= (a, b, \phi)$ are the variables that have a strongly irregular influence. Although this depends on the exact choice of the loss function, generally speaking the subspace $I(G)$ with constant B, C and τ_s of the loss surface is most probably highly irregular with many local minima and discontinuities corresponding to the bifurcations. The parameters can be optimized best with a global method. The parameters in the set L $= (B, C, \tau_s)$ have a more regular influence on the loss function, so a local method can be used to optimize them. We will use a *nested optimization* approach. For every point $G_i = (a_i, b_i, \phi_i)$ in the global optimization method the optimum values of $L_i = (B_i, C_i, \tau_{s,i})$ are determined using nonlinear local optimization.

The speed of convergence of the local optimization can be greatly improved incorporating prior knowledge into the choice of the initial values for the algorithm [Nelles, 2001, p.83]. In the case where the loss function has irregularities, this can even be decisive for convergence. For a given point in G it is possible to obtain quickly a rough estimate of good values for B,C and τ_s by inspection of the data. We review briefly the influence of each of those parameters for a fixed point in G.

---

[1]Since the quality criterion used only considered spike timing, we did not use parameter C. We decided to include it here however to keep the discussion general.

108

C. The maximum voltage is practically constant in G since the vertical position of the cubic nullcline $f(u)$ 2.8 is independent of all parameters. Some small variations may occur when ϕ is varied (cf. Fig. 2.6). A good initial guess for C is therefore the maximum voltage occurring in the training data divided by the maximum value of u in the FitzHugh-Nagumo model $u_{max} \approx 2$. The error made by assuming $u_{max} = 2$ is illustrated in the right column of Fig. 5.22.

τ_c. For fixed a, b and ϕ the dynamics are fixed and the time scale is entirely determined by the spike width. The spike width does only depend on a and b in a very weak way, but scales almost linearly with ϕ (cf. Fig. 2.6). Therefore a good initial guess would be

$$\tau_s = \frac{\phi_0}{\phi} \frac{sw_0}{sw}, \tag{5.10}$$

where sw is the spike width in the data, ϕ_0 is a reference value that gives a spike width of sw_0 (we take $\phi = 0.08$, which for the standard values of (2.7) gives $sw_0 \approx 44$). See Fig. 5.22, left column for the error of this estimator for different parameter values. Alternatively, the spike width for given a, b and ϕ can be easily determined with a very short simulation of the system at fixed $I > I_s(a, b, \phi)$ (cf. (2.19)).

B. The estimation of the scaling factor of the input current is a little harder. There is one reference value that can be reasonably easily extracted from data and that is the static spike threshold. Usually stimulation protocols include a special stimulus for detection of the threshold – a ramp, or stepping current for instance. In the case of noisy input data, the average current at the onset of spikes is a good estimate according to [Jolivet *et al.*, 2006b]. Of course one never really detects the static threshold since the equilibrium state is only asymptotically reached. This effect could possibly be accounted for by including a correcting term for the underestimation that results using the approximation of the dynamic threshold of (2.25). This approximation is only valid for $\phi << 1$; (see the discussion in Sect. 2.3). In practice a correction factor of 0.8 to (2.25) gives the best results.

So, if V_{max} is the maximum membrane potential in the training data, $\langle dt \rangle$ is the average width of the spikes in the training data and I_{th} is the estimated input current at the static threshold V_{th}, we obtain initial guesses for the parameters as follows:

$$\begin{cases} B = \left(-f(x_{1,min}) + x_{1,min} \right) / I_{th}, \\ x_{1,min} = \frac{1}{3} \left(a + 1 - \frac{\sqrt{a^2 - a + 1}}{3} \right) \end{cases} \tag{5.11}$$

$$C = \frac{V_{max}}{2} \tag{5.12}$$

$$\tau_s = \frac{\phi_0}{\phi} \frac{dt_0}{\langle dt \rangle} \tag{5.13}$$

AN ALGORITHM FOR THE NESTED OPTIMIZATION OF GENERIC BIFURCATION MODELS

The procedure outlined above does not restrict itself to the FitzHugh-Nagumo model. For any generic bifurcation model two groups of parameters can be identified that separate in a similar way the parameters in those that have a regular influence and those that determine the qualitative behavior; the bifurcation parameters. A nested optimization strategy can then be defined as follows:
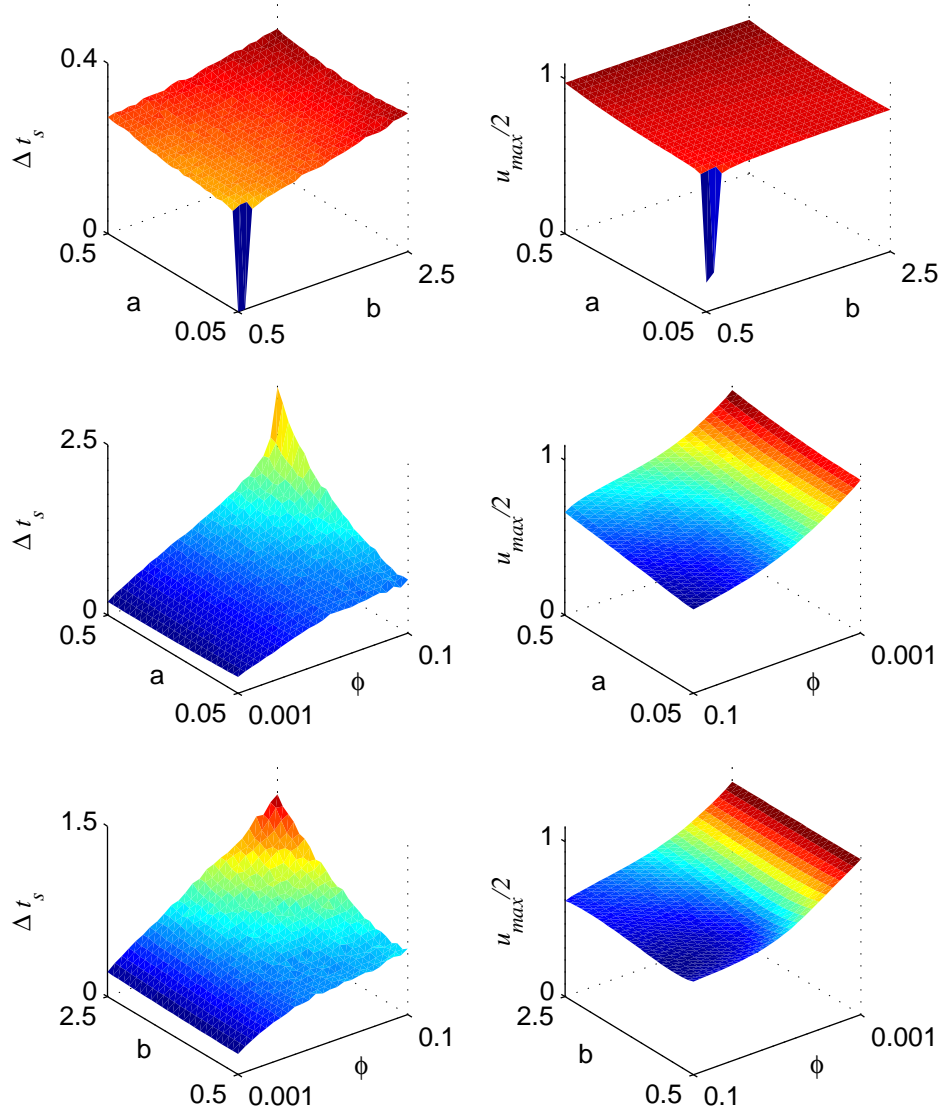
FIGURE 5.22: Dependence of the spike width and amplitude on the parameters of the generalized FitzHugh-Nagumo model. *Left:* Normalized spike width (Δt_s is the width of the spike divided by the width of a nominal spike at a, b and ϕ as in (2.7)) as a function of the three model parameters. *Right:* The maximum error in assuming $u_{max} = 2$ as a function of the three model parameters. The ϕ-axis is reverted for visual reasons

Algorithm 1: Global optimization

1. Randomly pick N points in parameter subspace G and perform local optimization with algorithm 2 on each of these points.

2. Pick an initial point (simulated annealing), or an initial ensemble of points (genetic algorithm, tabu search) and determine the optimization parameters based on the results from step 1.

3. Apply algorithm 2 to the current point, or each individual in the population.

4. Apply the update scheme of the global algorithm

5. If the result is satisfactory, stop, otherwise go to step 3.

and the sub-algorithm for local optimization:

Algorithm 2: Local optimization

For a given point in G:

1. Choose an initial point in L using (5.11), (5.12) and (5.13).

2. Perform a local optimization starting at the initial point

If no clear idea is available about the region the global parameters should lie in that restricts them to a smooth part of the loss surface, multi-start methods like a genetic algorithm or tabu search will almost always outperform simulated annealing.

Strategy for the Hindmarsh-Rose model

The strategy we propose for automated identification of the Hindmarsh-Rose model is very similar to the one presented above for the FitzHugh-Nagumo model, so we restrict ourselves to stressing the main differences and considerations.

The overall strategy of nested optimization is also the optimal way of attacking the problem of identifying the Hindmarsh-Rose model from data. The differences between the strategies for both models come mainly from the fact that the behavior of the Hindmarsh-Rose model has a closer resemblance to that of real neurons as shown in Sect. 5.3. The FitzHugh-Nagumo model can be seen as a very rough characterization of excitable behavior in general, which captures the essence, but not the exact form, of some of the features of real neurons. This means that there are more possibilities for an educated guess of the initial parameter range based on available data as well as a more pronounced loss surface. Also, it can be expected from the examples given in Chap. 2 that the optimum solution for the Hindmarsh-Rose model is in general much better than that of the FitzHugh-Nagumo model.

The subset of the parameters that are locally optimized does not change, since the same scaling extensions are used for both models. The global parameters that are of importance are the bifurcation parameter b, the slow parameter μ and s, the adaptation.

In the Hindmarsh-Rose model the spike width does not depend on the slow parameter. The width of the spike corresponds to the right part of the limit cycle of the fast subsystem 2.30, in contrast to the FitzHugh-Nagumo model, where the spike width is governed by the movement over the right branch of the slow manifold $f(u)$ (cf. (2.8)). Therefore the
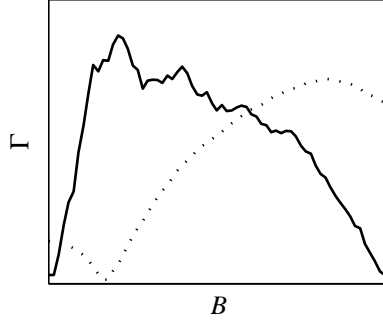
FIGURE 5.23: The influence of parameter B on the coincidence factor Γ

time-scaling parameter can directly be estimated from the data and can remain fixed after one cycle of optimization, which reduces the dimension of the parameter space L by one. A drawback is that the initial estimate for the two other local parameters is much harder to establish. The spike threshold (border of the blue area in Fig. 2.17) does not show a straightforward relation to the global parameters and the height of spikes and bursts is not constant, but depends on the exact form an position of the limit cycle, which is, by the way, a situation that corresponds better to reality than the fixed spike height in the FitzHugh-Nagumo model.

Summarizing: we take $G = (b, \mu, s)$ and $L = (B, C)$, and apply algorithms 1 and 2.

5.4.2 METHODS

As a criterion for the quality of the prediction the coincidence factor (2.39) between the data and the model spike trains was evaluated. The procedure of assessing the quality of the fit from the prediction was identical to the one used by Jolivet *et al.* [2006b]. Optimization techniques aim to minimize the loss function, so

$$I(\theta) = 1 - \Gamma(\theta) \tag{5.14}$$

To decide on the local optimization algorithm, tests of random points in parameter space were done for speed of convergence and structure of the local loss surface. The loss curve for fixed τ_s is shown in Fig. 5.23. The irregularities come partially from the structure of Γ, which shows quantization – on changes of B, Γ will show jumps as coincidences appear and disappear – and a stochastic nature.

A solution to this problem is to take the spike rate as a local optimization criterion. Since B and *tau* are directly related to the spike rate, for good fits, the optimum of Γ should coincide with the optimum of the spike rate; a perfect prediction also means an identical number of spikes. This is shown by the dotted line in Fig. 5.23, which represents the absolute difference in number of spikes between the model and the data. In this case the fit is not optimal ($\Gamma = 0.35$), so the two optima do not exactly coincide. To avoid getting stuck in the flat part when the model has no spikes and the difference is constant, we introduced a penalty term, which activates when the number of spikes in the model is zero.

The initial parameters of the global algorithm were chosen randomly within the bounds (2.16), imposing a minimum of 0.1 on b to guarantee excitability of the model (see Sect. 2.3). The local parameters were estimated using (5.11) and (5.13). Parameter
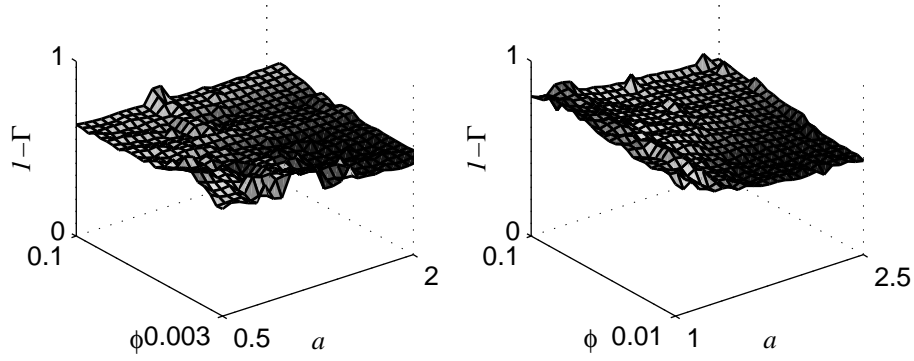
FIGURE 5.24: The loss surface for global parameters a and ϕ in the FitzHugh-Nagumo model. *Left*: $b = 0.9$. *Right*: $b = 0.3$.

C was not used, since for the comparison of spike timing, the scale of the output is not relevant.

The population of the genetic algorithm was set at 20, with a stopping criterion at 50 generations, a rank scaling function with stochastic uniform selection.

5.4.3 RESULTS

First a multi start local optimization was performed on a grid of global parameter space to assess the shape of the loss function and to identify interesting regions and possible problems.

The loss surface $(1-\Gamma)$ obtained from a local optimization of points in a 25x25 grid on parameter space (a, ϕ) for the FitzHugh-Nagumo model fitted on a random cell is shown in Fig. 5.24. Simulations were done for two different values of b. As expected the loss surface is very irregular, but in addition it is flat. This indicates that the exact choice of a and ϕ, within the bounds (2.16) is not decisive for the quality of the prediction.

We randomly picked one trace in the "high standard deviation" (i.e., high reliability) range of the protocol. The four repetitions of these trace were then divided in three for training and one for validation. The results of the best individual for all four cells in the data set are reported in table 5.4. The figure $\Gamma n \rightarrow f$ is the performance of the model on the validation data ('f' for FitzHugh-Nagumo; 'n' for neuron) and $\Gamma n \rightarrow n$ is the intrinsic reliability of the cell: the average coincidence factor between the training data and the validation data. Reminding the definition of the coincidence factor (2.39),

	Cell 1	Cell 2	Cell 3	Cell 4
$\Gamma_{n \rightarrow f}$	0.5023	0.4155	0.4523	0.4628
$\Gamma_{n \rightarrow n}$	0.8635	0.8432	0.9084	0.7733
$\Gamma_{n \rightarrow f} / \Gamma n \rightarrow n$	0.5817	0.4928	0.4979	0.5985

TABLE 5.4: Coincidence factor of best individual in the final population for each of the different cells.

the threshold for statistical significance is at zero. The average ratio between $\Gamma_{n \rightarrow n}$ and $\Gamma_{n \rightarrow n}$ is (0.542 ± 0.055). One should be careful however in comparing this figure with the (0.69 ± 0.07) obtained by Jolivet *et al.* [2006b], since the fits were not done on all stimuli
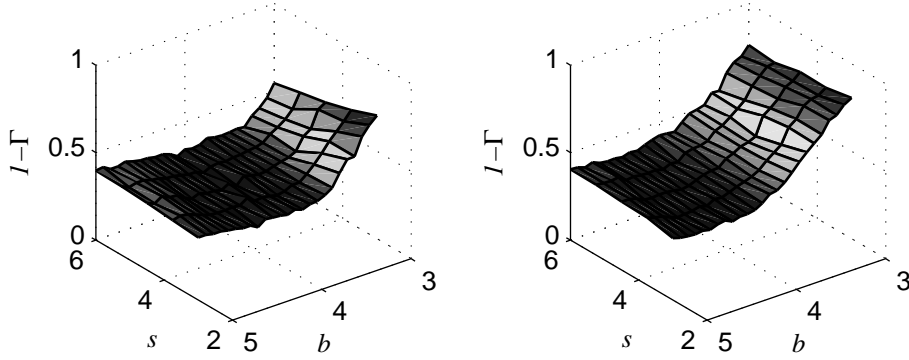
FIGURE 5.25: The loss surface for global parameters b and s in the Hindmarsh-Rose model. *Left:* $\mu = 1e - 3$. *Right:* $\mu = 1e - 2$.

and they are too few to perform statistics. Instead, these results should be seen as an indication that, although the performance of the FitzHugh-Nagumo model on the *in vitro* data is not acceptable, it can indeed reproduce features of the spike timing of pyramidal cells under conductance based current injection.

Table 5.5 reports the final parameter values for the best individual for all of the cells. Note that there is little difference between the optimal parameter values, which supports the claim that the global optimum was indeed found and that the performance reported in table 5.4 is the optimum performance of the FitzHugh-Nagumo model.

	Cell 1	Cell 2	Cell 3	Cell 4
a	2.1806	2.6044	2.4273	2.5985
μ	0.0073	0.0362	0.0316	0.0112
b	1.7689	2.1439	1.8450	2.0342

TABLE 5.5: Parameter values for the best individual in each of the different cells.

For completeness we end by reporting result of a preliminary study on the use of the Hindmarsh-Rose model to predict spike timing in this data set. The results of the multi-start local optimization for points in parameter space (b, s) for different values of μ are reported in Fig. 5.25. The results confirm the general results of this chapter and are in agreement with those for the FitzHugh-Nagumo model: the fitting of the time and input scale are more important than the exact choice of the qualitative parameters, as long as the latter remain in the correct region. It is interesting to see that the drop off in the loss surface occurs exactly at the transition to the bursting region. The flat region lies at approximately $\Gamma = 0.7$. Only one cell was fitted up to now and the optimum value of Γ on the validation data, that was obtained using a genetic algorithm on (b, μ, s) and a local optimization on the spike rate on B (τ_s was fixed on the basis of the spike width analogous to (5.13)), was $\Gamma_{n \to h} = 0.7948$, which is very close indeed to the intrinsic reliability of the cell itself. The fit seems mostly independent of the exact choice of b, but is best for values of b in the spiking region. Fit values were: $b = 3.2$, $\mu = 0.1$, $s = 1.6$, $B = 2.08$, the values of b and s corresponds well to a regular spiking pyramidal cell. The value of μ is very high with those found for the other data set, which could be explained by the fact that the cells in this data set were much faster (average spike width around $0.4\,\text{ms}$. Figure 5.26 shows a comparison between membrane potential of the cell and that of the fitted model.
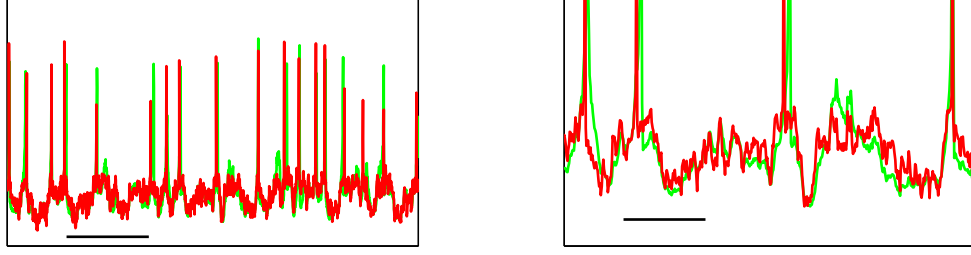
FIGURE 5.26: Comparison between the output of a neocortical pyramidal cell (red) and that of a Hindmarsh-Rose neuron on presentation of an in vivo-like input signal. *Left*: scale bar 80 ms, *Right*: scale bar 10 ms

It is interesting to see that the subthreshold fit is not perfect, but the model succeeds nevertheless in predicting the timing of all spikes in the figure with high precision. The differences in height of the spikes are due to undersampling.

5.4.4 Discussion

The results on the FitzHugh-Nagumo model are not as good as those reported for integrate-and-fire models, which are faster in simulation. The problem of the FitzHugh-Nagumo model is that the dynamics are used for the spiking mechanism and therefore the sub-threshold representation is unrealistic: the model lacks the necessary degrees of freedom to represent the complete subthreshold dynamics of the neurons. To use the spike-timing as a criterion the spike width of the model should not differ much from the spike width in the data. In the studies with threshold models, major attention is paid to the initial fit of a correct spike template to capture the refractory period. When this restriction is applied on the FitzHugh-Nagumo model, and therefore τ_s is fixed for given μ, what is left is a single degree of freedom in the dynamics (μ).

The Hindmarsh-Rose model has been shown in Sect. 5.3 to be able to model with great detail the subthreshold responses of neocortical neurons in general. Since the response patterns of neocortical interneurons are considered more complex and diverse than those of the pyramidal cells considered in this study, the Hindmarsh-Rose model should be able to perform well on this data, which is confirmed by preliminary studies.

The fact that in both cases the fit seems largely independent of the global parameters could imply that the spike timing in pyramidal cells is robust to fluctuations in environment parameters and morphology. The preliminary results on the Hindmarsh-Rose model that proved to be capable of reproducing detail in the discharge patterns of neocortical cells imply that this is not just a particularity of this model, but could lead to more general conclusions about neuronal behavior, however more research is needed to reach definite conclusions on this subject.

Also, these results could explain the failure to find a structure in the optimal fit parameters found in Sect. 5.3 and support the suspicion that there is more importance in the subthreshold characteristics.

In both cases a local simplex search optimization algorithm was used with the spike frequency as optimization criterion. Initial guesses for the parameters were made based on spike width and estimation of the spike threshold from the data.

Steady state response	Choice of parameter
Regular Spiking	$b > 3.2$
Irregular Spiking	$3 < b < 3.2$
Regular Bursting	$2.5 < b < 3$; higher for less spikes per burst
Irregular Bursting	$3.8 < b < 3$; $\mu > 0.05$
Onset	**Choice of parameter**
Strongly accommodating	$s > 3$ and $\mu > 0.005$
Weakly accommodating	$1.5 < s < 3$
Non-accommodating	$0.5 < s < 1.5$
Burst	$\mu > 0.02$

Table 5.6: Indications for the choice of model parameters in the Hindmarsh-Rose model

5.5 Guidelines for the choice of parameters in the Hindmarsh-Rose model

Based on the experience gathered with the fitting of different types of cells we distinguish the following steps that can be used as guidelines when attempting to reproduce neuronal behavior with the Hindmarsh-Rose model:

1. *Determine the type of discharge response desired*
   The qualitative aspects of the discharge behavior are determined by b and s. Educated guesses of initial values based on the type of discharge responses can be formulated as follows, provided that the data are long enough to reveal the steady state response. Table 5.6 summarizes indications for the values of the different parameters.

   The exact choice for the value of b depends on μ though, see the road maps in Fig. 2.16. The results in Sect. 5.1.3 indicate that the exact choice is not important if the goal is to reproduce subthreshold behavior and spike timing.

2. *Determine τ_s, B and μ based on the subthreshold responses*
   This step seems to be decisive for a good fit, both for the in vitro stimuli and for the conductance based ones. The problem of the absence of scale in the bifurcation models then turns into flexibility, since the scale can conveniently be automated using local search algorithms that quickly find optimal solutions based on the mean square error between the signals. Also, the formulae presented for initial guesses of the parameters are of relevance, since they influence strongly the speed and reliability of the optimization algorithms.

3. *Tweak the parameters to get optimal spike form reproduction*
   This is the most difficult step. No real indications can be given, except perhaps that μ, s do not influence the shape of the spike and b has a strong influence. In view of the results in Fig. 5.16 and Fig. 5.15, top row, it is not realistic to concentrate too much on the exact reproduction of the initial spike. The Hindmarsh-Rose model seems to have difficulty in reproducing the variety in onset behaviors.

Note that these guidelines are not exact ones, it was impossible to deduce exact relations between parameters and specific features of neocortical behavior for the cells that we studied. The number of parameters is so large, and their interaction so complex that fine

tuning is always necessary and experience with the different parameters is probably an important factor. The most successful way to apply the guidelines is iteratively. Every subsequent step will give information about the quality of the choices made in the previous one, which can be improved accordingly in the next iteration.

CONCLUSIONS

To ultimately understand how neurons communicate it is necessary to study the properties of the way they interact through synapses. We considered the approach of studying properties of this interaction through analytical and simulation methods from nonlinear dynamics and bifurcation theory. The model we used for a synapse was a very simple threshold model – fast threshold modulation (FTM) – that provides a pulse coupling [Somers & Kopell, 1993] and the neurons were represented by two models of the generic bifurcation type: a spiking model (the FitzHugh-Nagumo model [FitzHugh, 1961; Nagumo *et al.*, 1962]), and a bursting model (the Hindmarsh-Rose model [Hindmarsh & Rose, 1984]). We studied two phenomena of neuronal cooperation – coincidence detection and synchronization – for this simple pulse coupling.

Generic bifurcation models have the advantage, when compared to threshold models, of more complex dynamics. To test if these more complex dynamics can indeed model more features of real neurons, they were compared to electrophysiological measurements from real neocortical neurons. Two data sets were used. The first contained measurements on different types of neocortical neurons using a standard stimulation protocol and the second contained measurements on neocortical pyramidal neurons, using a conductance based protocol to simulate in vivo conditions.

6.1 SUMMARY OF THE RESULTS

The principle conclusions and accomplishments were:

- The FitzHugh-Nagumo model features a dynamic spike threshold, which helps provide robustness to noise and parameter fluctuations in synchronization and coincidence detection setups.

- The Hindmarsh-Rose model has a very complex, intriguing, bifurcation structure. When employed in chaotic mode synchronization through pulse coupling is robust to parameter fluctuations. This is a phenomenon that resembles closely the qualitative resonance observed in linearly coupled networks [De Feo, 2004a,b].

- In large scale networks of FTM-coupled bursting neurons, the stability of the complete synchronous solution, when it exists, is independent from the network topology and depends uniquely on the number of inputs to each neuron.

- The combination of standard techniques from nonlinear system identification, heuristics and a priori knowledge from neuroscience permit the quick identification of model parameters from measurement data.

- The FitzHugh-Nagumo model is not able to model the intrinsic diversity of neocortical neurons, but can be used as a fairly good predictor of spike timing in pyramidal cells.

- The Hindmarsh-Rose model can model much of the specific dynamical features present in neocortical neurons. Models identified purely on sub-threshold data also predict qualitative features of super-threshold stimuli.

The FitzHugh-Nagumo model was used as a paradigm for spiking behavior in neurons. From the bifurcation structure of the model [Kostova *et al.*, 2004; Rocsoreanu *et al.*, 2000] and using simple tools from dynamical system analysis, we presented formulae for the behavior of the model in the context of neuronal modeling as a function of the parameters.

In a study on the master-slave synchronization properties under pulse-coupling, it was shown how a quiescent FitzHugh-Nagumo neuron can react to incoming spike trains and simple spikes from the master system, also for sub-threshold stimulations; which is a situation that is common in real neurons, but not modeled by, for instance, the integrate-and-fire model.

Based on the observations from the study of the master-slave interaction, we presented a setup for a coincidence detector consisting of a FitzHugh-Nagumo neuron that receives input from two other FitzHugh-Nagumo neurons through pulse coupling. The coincidence detector is robust to fluctuations in the coupling strength and shows noise-enhanced threshold detection, known as stochastic resonance. In a case study on a model of a coincidence detector in the barn owl's auditory system [Carr & Konishi, 1990; Gerstner *et al.*, 2000] we showed that the FitzHugh-Nagumo model exhibits the same behavior as a simple integrate-and-fire unit.

The Hindmarsh-Rose model can exhibit more complex stationary behavior than only periodic movement; it is capable of producing bursting solutions for a wide range of parameters as well as chaos for a specific region in parameter space. The bifurcation structure of the Hindmarsh-Rose model that was revealed by exhaustive numerical simulation and numerical continuation in combination with analytical considerations, is very similar to that of a similar bursting model for a food chain [Kuznetsov *et al.*, 2001].

We showed a possible direct application of these complex dynamics in basic network configurations. Synchrony between Hindmarsh-Rose models coupled through pulse-coupling is more robust to parameter fluctuations when the neuron receiving the coupling is in chaotic mode than when it is in regular mode. This phenomenon has been reported in linear coupled dynamical systems by De Feo [2004a] and baptized *qualitative resonance*, but has not been reported in pulse coupled setups previously. There remain however some differences between qualitative resonance as observed and defined in linearly coupled systems and the phenomenon reported in this work, which deserve further investigation.

Full, stable synchronization in pulse coupled networks of dynamical systems, (meaning that the norm on the solutions of all systems converges asymptotically to zero) is only possible when the systems in the network all receive an equal amount of inputs. Such regular networks of pulse coupled Hindmarsh-Rose neurons have a rule for the conditions of full synchronization that contrasts strongly with that of linear systems. Whereas for linear systems the lowest value of the coupling for which stable synchronization occurs

increases quadratically with the number of elements in the network, the conditions in pulse-coupled networks only depend on the number of inputs each cell receives. Although this analytical result is only valid for networks in which each cell receives an equal amount of coupling, it implies that synchronization conditions in general are very different under pulse coupling than they are under linear coupling. Since the coupling synapses provide is of the pulse type, this could have important implications on the synchronization properties of neural networks.

The electrical behavior of neurons has two clearly separated regimes for two ranges of membrane potentials. These ranges are separated by what has become known as the "threshold", although strictly speaking the transition is continuous. For values of the membrane potential below threshold, the behavior is weakly nonlinear and far enough below threshold it can be faithfully reproduced by a two-dimensional linear dynamical system. In sharp contrast is the highly nonlinear behavior for membrane potentials above threshold, which needs a strong nonlinearity.

   The FitzHugh-Nagumo neuron model is a two-dimensional nonlinear neuron model. The modeling of the super-threshold behavior requires two-dimensions and this seems to severely limit its possibilities to faithfully represent the sub-threshold dynamics. The FitzHugh-Nagumo model therefore performs poor when compared to even simple integrate-and-fire models when it concerns reproduction of the exact timing of spikes in pyramidal neurons. The main advantage of the FitzHugh-Nagumo model with respect to integrate-and-fire models is the natural presence of a dynamic threshold. Features such as robustness to fluctuations in parameter values can not be reproduced by models with a fixed threshold and the smooth onset of spiking is considered more realistic than the all or nothing behavior exhibited by models with a sharp threshold.

The Hindmarsh-Rose model gives a good representation of the subthreshold dynamics of various types of in vitro measurements. The fact that models fitted only on subthreshold stimuli also gave acceptable similarities in the response on super-threshold stimuli indicates that there are possibilities to classify neocortical neurons based on subthreshold responses. These claims have to be verified since the subthreshold signals used in the stimulation protocol were not rich enough to optimally identify the neuron models.

   There are preliminary indications that the Hindmarsh-Rose model outperforms threshold models when it concerns the prediction of spike timing in neocortical pyramidal neurons [Jolivet *et al.*, 2006b], which could imply that details in neuronal behavior not captured by those models are of significance even for spike timing reproduction under conductance based stimulations.

6.2   RECOMMENDATIONS FOR FUTURE WORK

Much of the work presented in this thesis is explorative and the results of all of the studies should be verified and explored further. Especially the research on the representation of neocortical cell classes by generic bifurcation models can be continued in many directions.

   The continuation analysis of the Hindmarsh-Rose model should be completed to unravel the complete structure and organizing principled of the model. Also the bifurcation analysis could be extended to other parameters, although results in this work indicate that they are of less spectacular influence. An interesting project would be to do a bifurcation analysis of a more complex, realistic, neuron model and try to find out how the two relate

and whether a comparison of both gives indications to possible features that are missed by the Hindmarsh-Rose model.

The properties of synchronization in networks of dynamic systems in general and of pulse coupled networks specifically is an active subject of research at LANOS. The phenomenon of qualitative resonance under pulse coupling is another important subject that needs further investigation. When the network structure is irregular, complete full synchronization is not possible anymore, but clusters of synchronized cells might occur. This is already an active topic of research at LANOS.

In moving toward more realistic situations, new features that have not been addressed in this work are the introduction of heterogeneity in both parameter values and synaptic coupling (mix of excitatory and inhibitory as for instance done by Kopell & Ermentrout [2004]) and of time varying coupling strength, which would model synaptic plasticity.

To move forward in the identification of model parameters from experimental data, a structured identification procedure for bifurcation models should be developed. Also, more precise measures are needed to classify different neocortical cell types. This would need a cooperative effort between experimental and computational neuroscientists.

Once such a procedure has been developed, one could study the possible clustering of parameters of the models for different types of neurons. In combination with fast, online identification procedures, neocortical neurons could then be automatically classified.

The observation that subthreshold data might contain information about the cell class should be verified by presenting the neuron with richer sub-threshold stimuli. Considerations from system identification theory can play an important role in the choice of excitation signals.

The Hindmarsh-Rose model could also be of practical use to experimental neuroscientists. The tool that was designed to test the in-vitro protocol on the Hindmarsh-Rose model is so fast (up to ten times real time) that it could be inverted to serve as a dry run for tests of new in vitro stimuli. Especially in combination with the parameter maps presented in this work this could be a powerful tool.
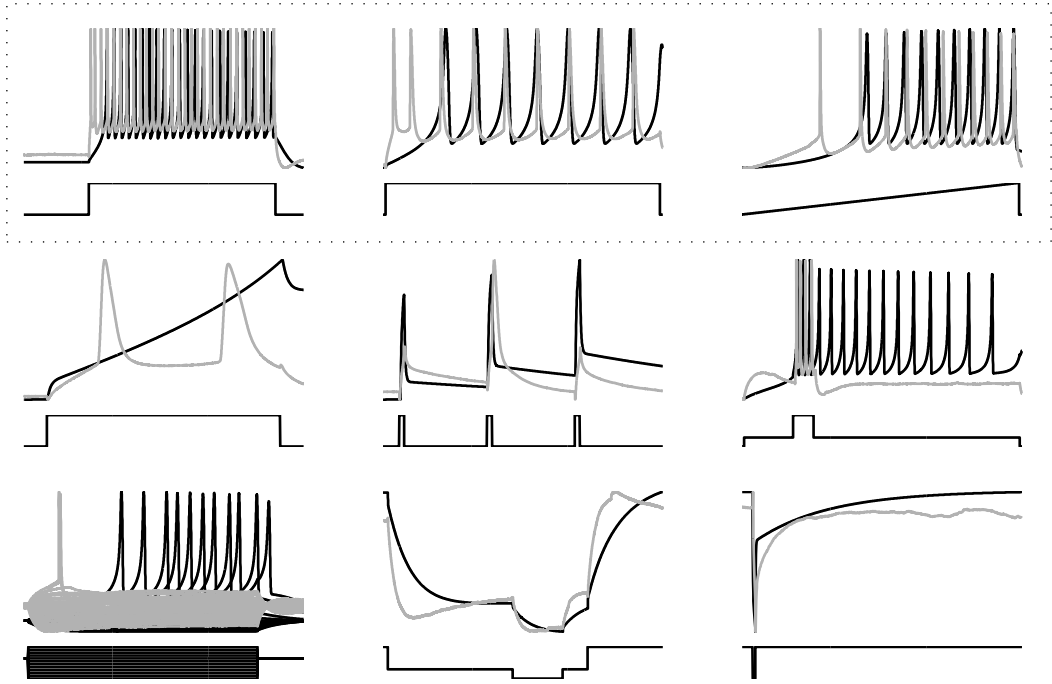
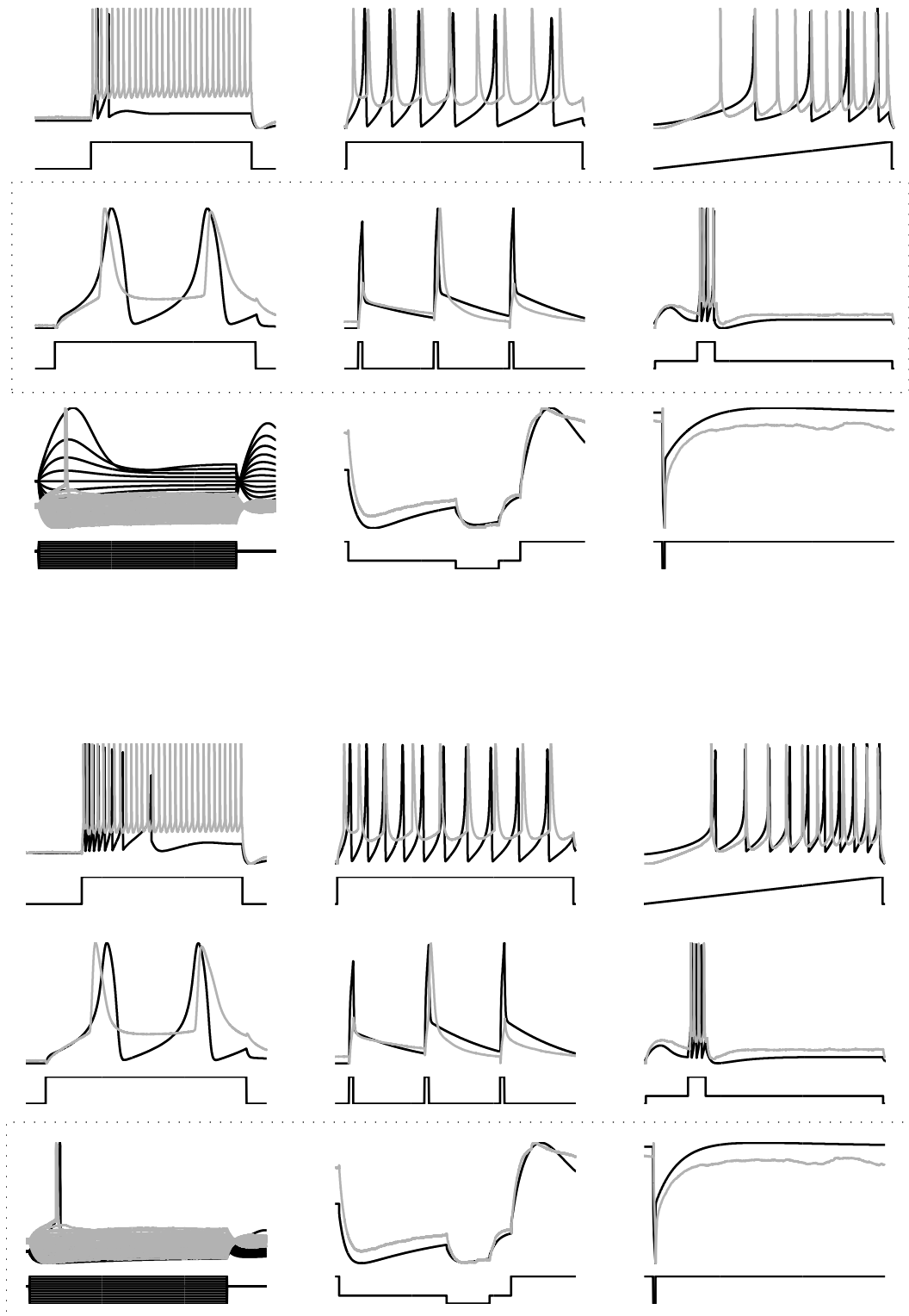# REPRODUCTION OF THE IN VITRO RESPONSES OF THREE NEOCORTICAL CELLS

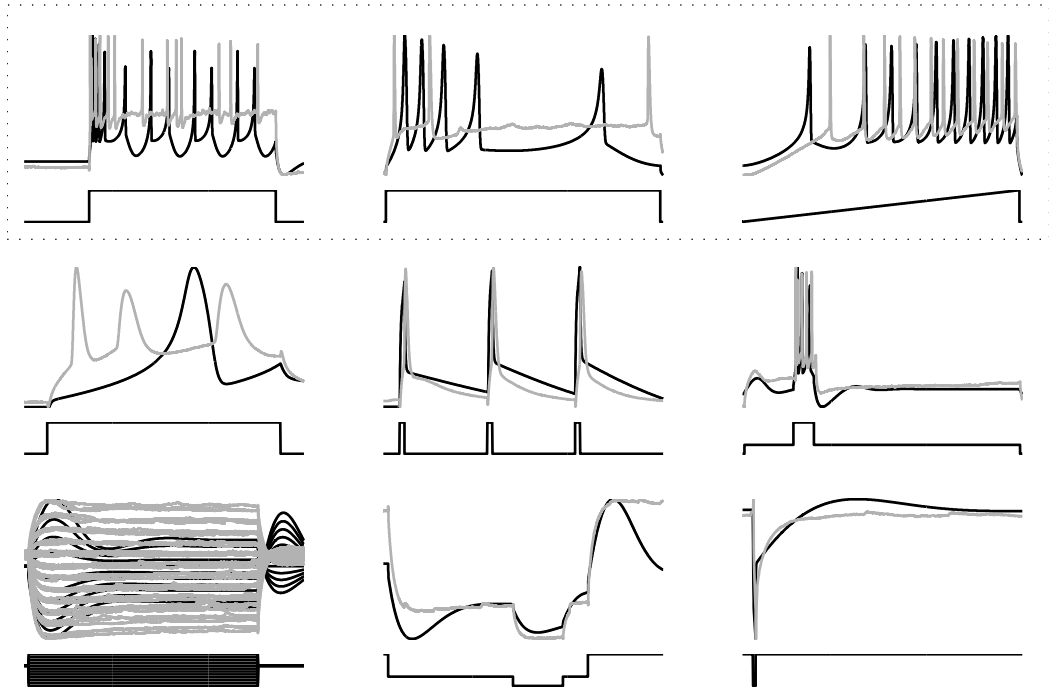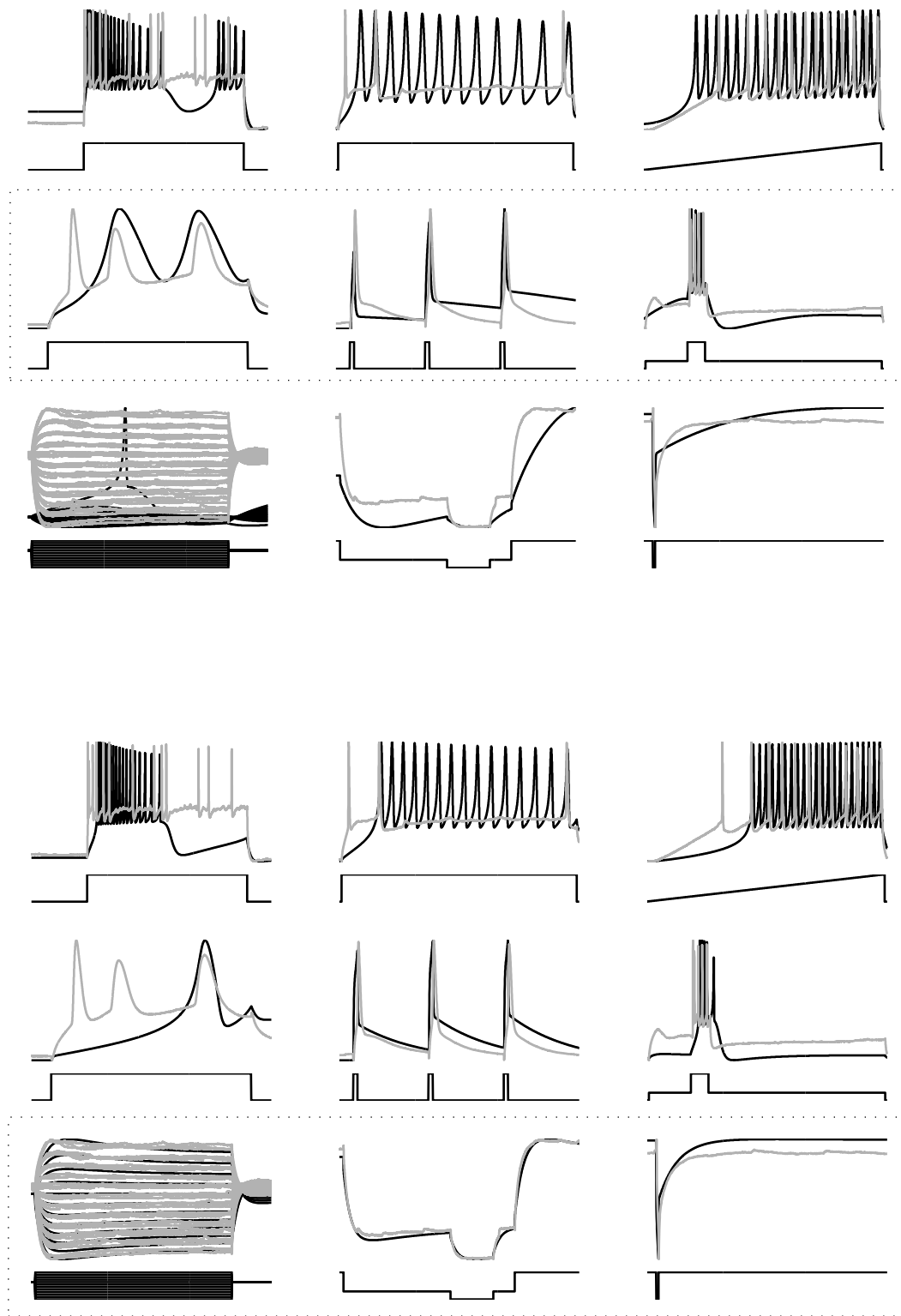## A.1 NON ACCOMMODATING PYRAMIDAL CELL C28
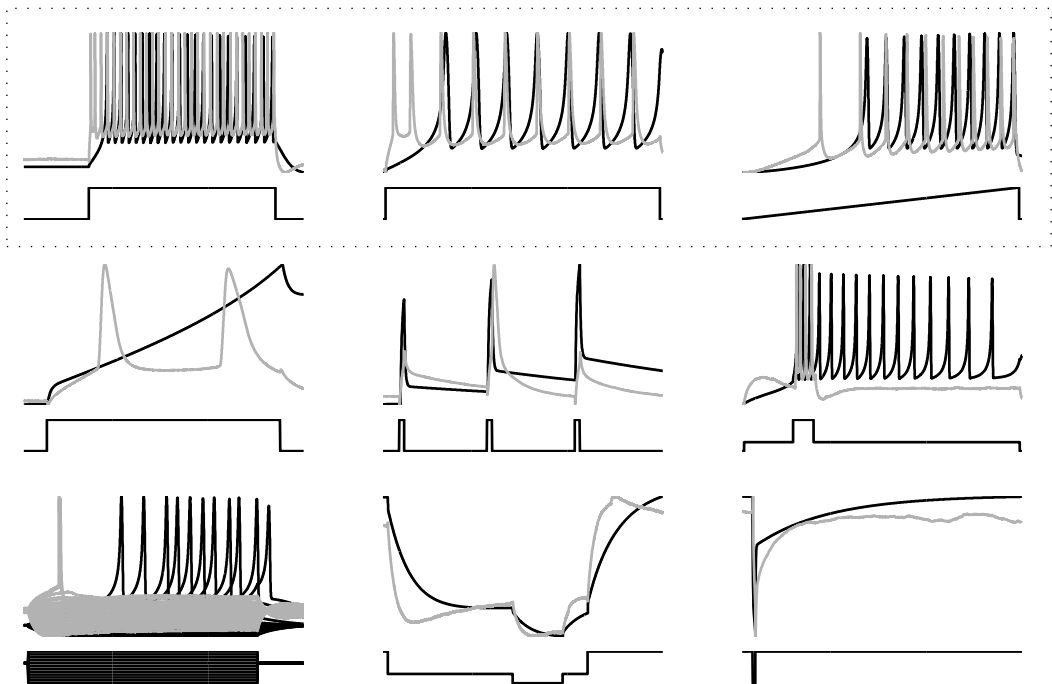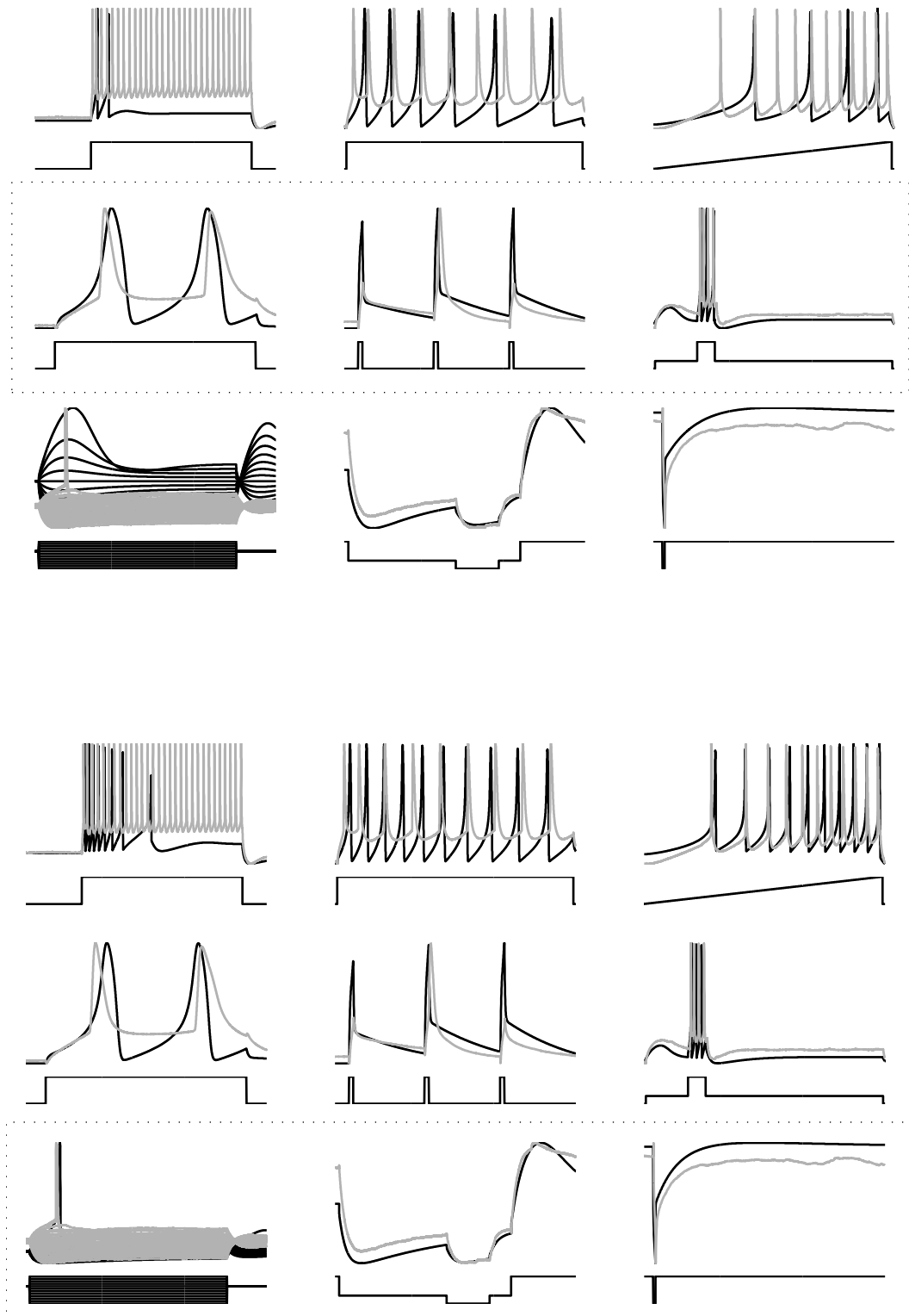
A.2 Accommodating Martinotti cell C95

A.3 Irregularly spiking large basket cell C34

Bibliography

ABARBANEL, H.D.I., RABINOVICH, M.I., SELVERSTON, A., BAZHENOV, M.V., HUERTA, R., & SUSHIK, M.M. 1996. Synchronization in neural assemblies. *Physics-uspehi*, **39**(4), 337–362.

ABBOTT, L.F., & VAN VREESWIJK, C. 1993. Asynchronous states in a network of pulse-coupled oscillators. *Physical Review E*, **48**, 1483–1490.

ARBIB, M.A. (ed). 2002. *The handbook of brain theory and neural networks.* 2nd edn. MIT Press.

BAIER, N.U. 2005. *Approximately periodic time series and nonlinear structures.* Ph.D. thesis, Ecole Polytechnique Fédérale de Lausanne.

BARGAS, J., & GALARRAGA, E. 2002. *Ion channels: keys to neuronal specialization. In:* Arbib [2002]. Pages 496–501.

BAUTIN, NN. 1984. *Behavior of dynamic systems near the boundary of the stability region (in Russian).* Gostekhizdat, Moscow.

BELYKH, I. 2002. *Hindmarsh-Rose model and its individual dynamics.* Personal communication.

BELYKH, I., DE LANGE, E., & HASLER, M. 2005a. Synchronization in pulse-coupled networks of bursting neurons. *Pages 699–702 of: Proceedings of the international symposium on nonlinear theory and its applications.*

BELYKH, I., DE LANGE, E., & HASLER, M. 2005b. Synchronization of bursting neurons: What matters in the network topology. *Physical review letters*, **94**(18), 8101.

BELYKH, I.V., BELYKH, V.N., NEVIDIN, K.V., & HASLER, M. 2003. Persistent clusters in lattices of coupled nonidentical chaotic systems. *Chaos*, **13**, 165–178.

BELYKH, V.N., BELYKH, I.V., & HASLER, M. 1998. Connection graph stability method for synchronized coupled chaotic systems. *Physica D*, **195**, 159–187.

BELYKH, V.N., BELYKH, I.V., COLDING-JØRGENSEN, M., & MOSEKILDE, E. 2000. Homoclinic bifurcations leading to the emergence of bursting oscillations in cell models. *The european physical journal E*, **3**, 205–219.

BERGLUND, N., & GENTZ, B. 2003. Geometric singular perturbation theory for stochastic differential equations. *Journal of differential equations*, **19**, 1–54.

BEYN, W.-J., CHAMPNEYS, A., DOEDEL, E., GOVAERTS, W., & KUZNETSOV, Y.A. 2002. *Numerical continuation, and computation of normal forms. In:* Fiedler [2002]. Pages 149–220.

BEZZI, P, GUNDERSEN, V, GALBETE, J, SEIFERT, G, STEINH AUSER, C, PILATI, E, & VOLTERRA, A. 2004. Astrocytes contain a vesicular compartment that is competent for regulated exocytosis of glutamate. *Nature neuroscience*, **7**, 613–620.

BRETTE, R., & GERSTNER, W. 2005. Adaptive exponential integrate-and-fire model as an effective description of neuronal activity. *Journal of neurophysiology*, **94**, 3637–3642.

CALITOIU, DRAGOS. 2006. New measures for describing the synchronization of bursting neurons. *Pages 75–76 of: Proceedings of the EPFL-Latsis symposium 2006*.

CARR, C.E., & KONISHI, M. 1990. A circuit for detection of the interaural time differences in the brain stem of the barn owl. *Journal of neuroscience*, **10**, 3227–3248.

CHAMPNEYS, AR, KUZNETSOV, YuA, & SANDSTEDE, B. 1996. A numerical toolbox for homoclinic bifurcation analysis. *International journal of bifurcations and chaos*, **6**, 867–887.

CHECHIK, G. 2003. Spike time dependent plasticity and relevant information maximization. *Neural computation*, **15**, 1481–1510.

CONNORS, B.W., & GUTNICK, M.J. 1990. Intrinsic firing patterns of diverse neocortical neurons. *Trends in neuroscience*, **17**, 3894–3906.

DE FEO, O. 2001. *Modelling diversity by strange attractors with application to temporal pattern recognition*. Ph.D. thesis, Ecole polytechnique fédérale de Lausanne.

DE FEO, O. 2004a. Qualitative resonance of Shil'nikov-like strange attractors, part I: Experimental evidence. *International journal of bifurcation and chaos*, **14**(3), 893–912.

DE FEO, O. 2004b. Qualitative resonance of Shil'nikov-like strange attractors, part II: Mathematical analysis. *International journal of bifurcation and chaos*, **14**(3), 873–891.

DE FEO, O. 2005a. Transforming subharmonic chaos to homoclinic chaos suitable for pattern recognition. *International journal of bifurcations and chaos*, **15**(10), 3345–3357.

DE FEO, O. 2005b. Tuning chaos synchronization and anti-synchronization for applications in temporal pattern recognition. *International journal of bifurcations and chaos*, **15**(12), 3905–3921.

DE FEO, O., MAGGIO, G. M., & KENNEDY, M. P. 2000. The colpitts oscillator: Families of periodic solutions and their bifurcations. *International journal of bifurcation and chaos*, **10**(5), 935–958.

DE LANGE, E., & BELYKH, I. 2003. Phase locking and coincidence detection in threshold coupled neural oscillators. *Pages 65–68 of: Proceedings of the 11th workshop on nonlinear dynamics of electronic systems*.

DE LANGE, E., & DE FEO, O. 2006. Mapping electrophysiological diversity of neocortical neurons on a simple mathematical diversity. *Pages 103–104 of: Proceedings of the 2006 EPFL-Latsis symposium*.

DEFELIPE, J. 1993. Neocortical diversity: Chemical heterogeneity revealed by colocalization studies of classic neurotransmitters, neuropeptides, calcium binding proteines, and cell surface molecules. *Cerebral cortex*, **3**, 273–289.

DESTEXHE, A, & PARÉ, A. 1999. Impact of network activity on the integrative properties of neocortical pyramidal neurons in vivo. *Journal of neurophysiology*, **81**, 1531–1547.

DESTEXHE, A., CONTRERAS, D., STERIADE, M., SEJNOWSKI, T.J., & HUGUENARD, J.R. 1996. In vivo, in vitro and computational analysis of dendritic calcium currents in thalamic reticular neurons. *Journal of neuroscience*, **16**, 169–185.

DESTEXHE, A, RUDOLPH, M, FELLOUS, J-M., & T, SEJNOWSKI. 2001. Fluctuating synaptic conductances recreate in vivo-like activity in neocortical neurons. *Neuroscience*, **107**, 13–24.

DHAMALA, M., JIRSA, V.K., & DING, M. 2004. Enhancement of neural synchrony by time delay. *Physical review lettters*, **92**, 074104.

DOEDEL, E.J., PAFFENROTH, R.C., CHAMPNEYS, A.R., FAIRGRIEVE, T.F., KUZNETSOV, YU.A., SANDSTEDE, B., & WANG, X. 2001. *Auto 2000: Continuation and bifurcation software for ordinary differential equations (with homcont)*. Tech. rept. Caltech.

ERMENTROUT, G. B., & KOPELL, N. 1986. Parabolic bursting in an excitable system coupled with a slow oscillation. *SIAM journal on applied mathematics*, **46**, 233–253.

ERMENTROUT, G.B. 1996. Type I membranes, phase resetting curves, and synchrony. *Neural computation*, **8**, 979–1001.

FAURE, P., & KORN, H. 1997. A nonrandom dynamic component in the synaptic noise of a central neuron. *Proceedings of the national academy of sciences of the United States of America*, **94**, 6506–6511.

FELLIN, T, PASCUAL, O, GOBBO, S, POZZAN, T, HAYDON, P, & CARMIGNOTO, G. 2004. Neuronal synchrony mediated by astrocytic glutamate through activation of extrasynaptic NMDA receptors. *Neuron*, **43**, 729–743.

FENG, J (ed). 2004. *Computational neuroscience: A comprehensive approach*. Chapman and Hall/CRC.

FENG, JIANFENG. 2001. Is the integrate-and-fire model good enough? – a review. *Neural networks*, **14**, 955—75.

FIEDLER, B. (ed). 2002. *Handbook of dynamical systems, volume 2*. Elsevier.

FIEDLER, B., IOOSS, G., & KOPELL, N. (eds). 2000. *Handbook of dynamical systems, volume 3: Toward applications*. Elsevier.

FITZHUGH, R. 1960. Thresholds and plateaus in the Hodgkin-Huxley nerve equations. *Journal of general physiology*, **43**, 867.

FITZHUGH, R. 1961. Impulses and physiological states in theoretical models of nerve membrane. *Biophysical journal*, **1**, 445–466.

FOURCAUD-TROCME, N., HANSEL, D., VAN VREESWIJK, C., & BRUNEL, N. 2003. How spike generation mechanisms determine the neuronal response to fluctuating inputs. *Journal of neuroscience*, **23**, 11628–11640.

GAMMAITONI, L., HÄNGGI, P., JUNG, P., & MARCHESONI, F. 1998. Stochastic resonance. *Reviews of modern physics*, **70**(1), 223–287.

GEMAN, S., BIENENSTOCK, E., & DOURSAT, R. 1992. Neural networks and the bias/variance dilemma. *Neural computation*, **4**(1), 1–58.

GERSTNER, W., KEMPTER, R., VAN HEMMEN, J.L., & WAGNER, H. 1996a. A neuronal learning rule for sub-millisecond temporal coding. *Nature*, **383**, 76–78.

GERSTNER, W, VAN HEMMEN, JL, & COWAN, J. 1996b. What matters in neuronal locking? *Neural computation*, **8**, 1653–1676.

GERSTNER, W., KEMPTER, R., & VAN HEMMEN, J.L. 2000. *Hebbian lerning of pulse timing in the barn owl auditory system. In:* Fiedler *et al.* [2000]. Chap. 14, pages 353–377.

GERSTNER, WULFRAM, & KISTLER, WERNER. 2002. *Spiking neuron models.* 1st edn. Cambridge, UK: Cambridge University Press.

GIBSON, J., & CONNORS, B. 2002. *Neocortex: Chemical and electrical synapses. In:* Arbib [2002]. Pages 725–729.

GOLOMB, D, & RINZEL, J. 1993. Dynamics of globally coupled inhibitory neurons with heterogeneity. *Physical review E*, **48**, 4810–4814.

GRADSTEIN, I.S. 1953. Application of A.M. Lyapunov's theory of stability to the theory of differential equations with small coefficients in the derivatives. *Matematicheskii sbornik, novaya seriya*, **32**(74), 263–286.

GUPTA, A., WANG, Y., & MARKRAM, H. 2000. Organizing principles for a diversity of GABAergic interneurons and synapses in the neocortex. *Science*, **287**(5451), 273–278.

HANSEL, D, & MATO, G. 2003. Asynchronous states and the emergence of synchrony in large networks of interacting excitatory and inhibitory neurons. *Neural computation*, **15**, 1–56.

HARSCH, A, & ROBINSON, H. 2000. Postsynaptic variability of firing in rat cortical neurons: the roles of input synchronization and synaptic NMDA receptor conductance. *Journal of neuroscience*, **20**, 6181–6192.

HILLE, B. 2001. *Ionic channels of excitable membranes.* 3rd edn. Sinauer.

HINDMARSH, J.L., & ROSE, R.M. 1984. A model of neuronal bursting using three coupled first order differential equations. *Proceedings of the royal society London, series B*, **221**(1222), 87–102.

HODGKIN, A.L., & HUXLEY, A.F. 1952. A quantitative description of membrane current and its application to conduction and excitation in nerve. *Journal of physiology (London)*, **117**(4), 500–544.

HOPFIELD, J.J. 1984. Neurons with graded response have collective computational properties like those of two state neurons. *Proceedings of National Academic Science*, **81**, 3088–3092.

HOPFIELD, J.J., & BRODY, C.D. 2001. What is a moment? transient synchrony as a collective mechanism for spatiotemporal integration. *Proceedings of the national academy of sciences of the United States of America*, **98**, 1282–1287.

HOPPENSTEAD, F.C., & IZHIKEVICH, E.M. 1997. *Weakly connected neural networks.* Springer-Verlag.

IZHIKEVICH, E.M. 2000a. Neural excitability, spiking and bursting. *International journal of bifurcation and chaos*, **10**(6), 1171–1266.

IZHIKEVICH, E.M. 2000b. Phase equations for relaxation oscillators. *SIAM journal on applied mathematics*, **60**(5), 1789–1804.

IZHIKEVICH, E.M. 2001a. Resonate-and-fire neurons. *Neural networks*, **14**, 883–894.

IZHIKEVICH, E.M. 2001b. Synchronization of elliptic bursters. *Sirev*, **43**, 315–344.

IZHIKEVICH, E.M. 2003. Simple model of spiking neurons. *IEEE transactions on neural networks*, **14**, 1569–1572.

IZHIKEVICH, E.M. 2004. Which model to use for cortical spiking neurons? *IEEE transactions on neural networks*, **15**, 1063–1070.

JEFFRESS, L.A. 1948. A place theory of sound localisation. *Journal of comparative physiology and psychology*, **41**, 35–39.

JOHNSTON, D, & WU, M-S. 1995. *Foundations of cellular neurophysiology.* MIT Press.

JOLIVET, R. 2005. *Effective minimal threshold models of neuronal activity.* Ph.D. thesis, Ecole Polytechnique Fédérale de Lausanne.

JOLIVET, R., RAUCH, A., LÜSCHER, H.-R., & GERSTNER, W. 2006a. *Integrate-and-fire models with adaptation are good enough. In:* Weiss *et al.* [2006]. Pages 595–602.

JOLIVET, R., RAUCH, A., LÜSCHER, H.-R., & GERSTNER, W. 2006b. Predicting spike timing of neocortical pyramidal neurons by simple threshold models. *Journal of computational neuroscience*, **21**(1), 35–49.

KAWAGUCHI, Y, & KUBOTA, Y. 1997. GABAergic cell subtypes and their synaptic connections in rat frontal cortex. *Cerebral cortex*, **7**, 476–486.

KEMPTER, R., GERSTNER, W., VAN HEMMEN, J.L., & WAGNER, H. 1998. Extracting oscillations: Neuronal coincidence detection with noisy periodic spike input. *Neural computation*, **10**, 1987–2017.

KIRKPATRICK, S, C, GELATI, & VECCHI, M. 1983. Optimization by simulated annealing. *Science*, **220**, 671–680.

KISTLER, W., GERSTNER, W., & VAN HEMMEN, J. 1997. Reduction of Hodgkin-Huxley equations to a single-variable threshold model. *Neural computation*, **9**, 1015–1045.

KNIGHT, B. 1972. Dynamics of encoding in a population of neurons. *Journal of general physiology*, **59**, 734–766.

KNUDSEN, E.I., BLASDEL, G.G., & KONISHI, M. 1979. Sound localization by the barn owl (Tyto alba) measured with the search coil technique. *Journal of comparative physiology*, **133**, 1–11.

KOCH, C. 1999. *Biophysics of computation: Information processing in single neurons.* Oxford University Press: New York.

KOCH, C, & ZADOR, A. 1993. The function of dendritic spines: devices subserving biochemical, rather than electrical compartimentalization. *Journal of neuroscience*, **13**, 413–422.

KONISHI, M. 1992. The neural algorithm for sound localization in the owl. *Harvey lectures*, 47–64.

KONISHI, M. 1993. Listening with two ears. *Scientific american*, **268**, 66–73.

KOPELL, N., & ERMENTROUT, B. 2004. Chemical and electrical synapses perform complementary roles in the synchronization of interneuronal networks. *Proceedings of the national academy of sciences of the United States of America*, **101**(43), 15482–15487.

KOPELL, N., & SOMERS, D. 1995. Anti-phase solutions in relaxation oscillators coupled through excitatory interactions. *Journal of mathematical biology*, **33**(3), 261–280.

KOSTOVA, T., RAVINDRAN, R., & SCHONBEK, M. 2004. Fitzhugh-Nagumo revisited: Types of bifurcations, periodical forcing and stability regions by a Lyapunov functional. *International journal of bifurcation and chaos*, **14**, 913–925.

KUZNETSOV, Y., DE FEO, O., & RINALDI, S. 2001. Belyakov homoclinic bifurcations in a tritriphic food chain model. *SIAM journal of applied mathematics*, **62**(2), 462–487.

KUZNETSOV, Y.A. 1995. *Elements of applied bifurcation theory.* Springer Verlag, Berlin.

LAPIQUE, L. 1907. Recherches quantitatives sur l'excitation électrique des nerfs traitée comme une polarisation. *Journal de physiologie et de pathologie générale*, **9**, 620–635.

LEWIS, P.A.W, & SHEDLER, G.S. 1978. *Simulation of nonhomogeneous Poisson processes by thinning.* Tech. rept. IBM Research Report RJ 2286.

LINKENS, D.A. 1979. The method of harmonic balance applied to coupled asymmetrical van der pol oscillators for intestinal modelling. *Bulletin of mathematical biology*, **41**, 573–589.

LJUNG, L. 1987. *System identification: Theory for the user.* 1st edn. Prentice Hall, Englewood Cliffs.

LJUNG, L. 1994. *Modeling of dynamic systems.* Prentice Hall.

LJUNG, L. 2006. *Matlab system identification toolbox, version 6.0.* The Mathworks, Inc.

LLINÁS. 1988. The intrinsic electrophysiological properties of mammalian neurons: insights into the central nervous system function. *Science*, **242**, 1654–1664.

MAINEN, Z.F., & SEJNOWSKI, T.J. 1995. Reliability of spike timing in neocortical neurons. *Science*, **268**, 1503–1506.

Markram, H., Lubke, J., Frotscher, M., & Sakmann, B. 1997. Regulation of synaptic efficacy by coincidence of postsynaptic APs and EPSPs. *Science*, **275**, 213–215.

Markram, H., Toledo-Rodriguez, M., Wang, Y., Gupta, A., Silberberg, G., & Wu, C. 2004. Interneurons of the neocortical inhibitory system. *Nature reviews neuroscience*, **5**, 793–807.

Markram, H., Toledo, M., Siberberg, G., Holzer, R., & Goodman, P. 2005. *eCode: standard stimulus protocol, standard parameter definition, standard software.* Tech. rept. EPFL. v0.1.

McCormick, D.A., Connors, B.W., Lighthall, J.W., & Prince, D.A. 1985. Comparative electrophysiology of pyramidal and sparsely spiny neurons of the neocortex. *Journal of neurophysiology*, **54**, 782–806.

Mehra, RK. 1974. Optimal input signals for parameter estimation in dynamic systems—survey and new results. *IEEE transactions on automatic control*, **19**, 753–768.

Moehlis, J. 2006. Canards for a reduction of the Hodgkin-Huxley equations. *Journal of mathematical biology*, **52**, 141–153.

Morris, C., & Lecar, H. 1981. Voltage oscillations in the barnacle giant muscle fiber. *Biophysics journal*, **35**(1), 193–213.

Nagumo, J.S., Arimoto, S., & Yoshizawa, S. 1962. An active pulse transmission line simulating nerve axon. *Pages 2061–2070 of: Proceedings of the institution of electronic and radio engineers.*

Nelles, Oliver. 2001. *Nonlinear system identification.* Springer-Verlag Berlin Heidelberg.

Ott, Edward. 1993. *Chaos in dynamical systems.* Cambridge university press.

Pecora, L.M. 1998. Synchronization conditions and desynchronizing patterns in coupled limit-cycle and chaotic systems. *Physical review E*, **58**, 347–360.

Pecora, L.M., & Carroll, T.L. 1998. Master stability functions for synchronized coupled systems. *Physical review letters*, **80**, 2109–2112.

Peters, A., & Jones, E.G. 1984. *Cerebral cortex, vol. I: Cellular components of the cerebral cortex.* Plenum Press, New York.

Pikovsky, A., Rosenblum, M., & Kurths, J. 2001. *Synchronization: A universal concept in nonlinear sciences.* 1st edn. Cambridge, UK: Cambridge University Press.

Prinz, A, Abbott, L, & Marder, E. 2004. The dynamic clamp comes of age. *Trends in neurosciences*, **27**, 218–224.

Rabinovich, MI, Varona, P, & Abarbanel, HDI. 2000. Nonlinear cooperative dynamics of living neurons. *International journal of bifurcation and chaos*, **10**, 913–933.

RAUCH, A., LA CAMERA, G., LÜSCHER, H.R., SENN, W., & FUSI, S. 2003. Neocortical pyramidal cells respond as integrate-and-fire neurons to in vivo-like input currents. *Journal of neurophysiology*, **90**, 1598–1612.

REYES, R.A., RUBEL, E.W., & SPAIN, W.J. 1994. Membrane properties underlying the firing of neurons in the avian cochlear nucleus. *Journal of neuroscience*, **14**, 5352–5364.

RICHARDSON, M.J., BRUNEL, N, & HAKIM, V. 2003. From subthreshold to firing-rate resonance. *Journal of neurophysiology*, **89**, 2538.

ROBINSON, H.P.C. 2004. *The biophysical basis of firing variability in cortical neurons. In:* Feng [2004].

ROBINSON, H.P.C., & KAWAI, N. 1993. Injection of digitally synthesized synpatic conductance transients to measure the integrative properties of neurons. *Journal of neuroscience methods*, **49**, 157–165.

ROCSOREANU, C., GEORGESCU, A., & GIURGITEANU, N. 2000. *The FitzHugh-Nagumo model: Bifurcation and dynamics.* Kluwer Academic Publishers, Boston.

RUBIN, J, & TERMAN, D. 2002a. *Geometric singular perturbation analysis of neuronal dynamics. In:* Fiedler [2002]. Chap. 3.

RUBIN, J, & TERMAN, D. 2002b. Synchronized bursts and loss of synchrony among heterogeneous conditional oscillators. *SIAM journal of applied dynamical systems*, **1**, 146–174.

RUBIN, J.E., & TERMAN, D. 2000a. Analysis of clustered firing patterns in synaptically coupled networks of oscillators. *Journal of mathematical biology*, **41**(6), 513–545.

RUBIN, J.E., & TERMAN, D. 2000b. Geometric analysis of population rhythms in synaptically coupled neuronal networks. *Neural computation*, **12**(3), 597–645.

SHAMPINE, L.F., & REICHELT, M.W. 2005. *The MATLAB ODE suite.* The Mathworks, Inc.

SHERMAN, A. 1994. Anti-phase, asymmetric and aperiodic oscillations in excitable cells— I. Coupled bursters. *Bulletin of mathematical Biology*, **56**, 811–835.

SOFTKY, W., & KOCH, C. 1993. The highly irregular firing pattern of cortical cells is inconsistent with temporal integration of random EPSPs. *Journal of neuroscience*, **13**, 334–350.

SOMERS, D., & KOPELL, N. 1993. Rapid synchronization through fast threshold modulation. *Biological cybernetics*, **68**(68), 393–407.

STEIN, R.B. 1967. Some models of neuronal variability. *Biophysics journal*, **7**, 37–68.

STERIADE, M. 2004. Neocortical cell classes are flexible entities. *Nature reviews neuroscience*, **5**, 121–134.

STEVENS, C, & ZADOR, A. 1998. Input synchrony and the irregular firing of cortical neurons. *Nature neuroscience*, **1**, 210–217.

STOOP, R., SCHINDLER, K., & BUNIMOVICH, L.A. 2000. Neocortical networks of pyramidal neurons: from local locking and chaos to macroscopic chaos and synchronization. *Nonlinearity*, **13**, 1515–1529.

STROGATZ, SH. 2001. Exploring complex networks. *Nature*, **410**, 268–276.

STROGATZ, STEVEN. 1994. *Nonlinear dynamics and chaos: with applications to physics, biology, chemistry and engineering.* Addison-Wesley, Reading, MA.

TERMAN, D. 1991. Chaotic spikes arising from a model of bursting in excitable membranes. *SIAM journal on applied mathematics*, **51**, 1418–1450.

TERMAN, D. 1992. The transition from bursting to continuous spiking in excitable membrane models. *Journal of nonlinear science*, **2**, 133–182.

TIHONOV, A.N. 1952. Systems of differential equations containing small parameters in the derivatives. *Matematicheskii sbornik, novaya seriya*, **31**, 575–586.

TOLEDO-RODRIGUEZ, M., GUPTA, A., WANG, Y., WU, C.Z., & MARKRAM, H. 2002. *Neocortex: Basic neuron types. In:* Arbib [2002]. Pages 791–725.

TOLEDO-RODRIGUEZ, M., BLUMENFELD, B., WU, C., LUO, J., ATTALI, B., GOODMAN, P., & MARKRAM, H. 2004. Correlation maps allow neuronal electrical properties to be predicted from single-cell gene expression profiles in rat neocortex. *Cerebral Cortex*, **14**(12), 1310–1327.

TRACHTENBERG, J.T., CHEN, B.E., KNOTT, G.W., FENG, G., SANES, J.R., WELKER, E., & SVOBODA, K. 2002. Long-term in vivo imaging of experience-dependent synaptic plasticity in adult cortex. *Nature*, **420**, 788–794.

TUCKWEL, H. 1988. *Introduction to theoretical neurobiology: Volume 1, Linear cable theory and dendritic structure.* Cambridge University Press.

VAN DER POL, B. 1928a. Le battement du cœur considéré comme oscillation de relaxation et un modèle électrique du cœur. *Onde electrique*, **7**, 365–392.

VAN DER POL, B. 1928b. On relaxation oscillators. *Philosophical magazine*, **2**, 978.

van VREESWIJK, C., & HANSEL, D. 2001. Patterns of synchrony in neural networks with spike adaptation. *Neural computation*, **13**, 959.

VANDERPLAATS, G.N. 1984. *Numerical optimization techniques for engineering design.* McGraw-Hill, New-York.

WANG, X.J. 1993. Genesis of bursting oscillations in the Hindmarsh-Rose model and homoclinicity to a chaotic saddle. *Physica D*, **62**, 263–274.

WEISS, S.M., & KULIKOWSKI, C.A. 1991. *Computer systems that learn.* Kaufmann Publishers, San Francisco.

WEISS, Y., SCHÖLKOPF, B., & PLATT, J. (eds). 2006. *Advances in neural information processing systems 18.* MIT Press, Cambridge.

WHITE, J.A., RUBINSTEIN, J.T., & KAY, A.R. 2001. Channel noise in neurons. *Trends in neuroscience*, **23**, 131–139.

WILSON, H.R. 1999. Simplified dynamics of human and mammalian neocortical neurons. *Journal of theoretical biology*, **200**, 375–388.

ZWILLINGER, D. 1998. *Handbook of differential equations.* third edn. Academic Press. Pages 501–503.

Curriculum Vitae

Enno de Lange was born August 21, 1977 in Amsterdam, the Netherlands. In 2002 he obtained his Ir. (MS) title in Electrical Engineering from the Delft University of Technology with a graduation project on structured design of low-distortion linear feedback amplifiers, which he partially performed at the laboratory of nonlinear systems (LANOS) at the Ecole Polytechnique Fédérale de Lausanne (EPFL).

He then continued his research at LANOS as a PhD student, taking up an interest in neuroscience and working on synchronization properties of pulse-coupled neural networks and analysis of neuron models, combining analytical and numerical techniques. He was also a teaching assistant at three different courses given by the sections of computer science and communication science.

Besides Dutch, his native language, Enno is fluent in English, French, German and Spanish.